Check for updates

Copper and Copper-Based Bimetallic Catalysts for Carbon Dioxide Electroreduction

Mulatu Kassie Birhanu, Meng-Che Tsai, Amaha Woldu Kahsay, Chun-Tse Chen, Tamene Simachew Zeleke, Kassa Belay Ibrahim, Chen-Jui Huang, Wei-Nien Su,* and Bing-Joe Hwang*

Among many alternatives, CO_2 electroreduction (CO_2ER) is an emerging technology to alleviate its level in the atmosphere and simultaneously to produce essential products containing high energy density using various electrocatalysts. Cu-based mono- and bimetallics are electrocatalysts of concerns in this work due to the material's abundance and versatility. Intrinsic factors affecting the CO_2ER are first analyzed, whereby understanding and characterizing the surface features of electrocatalysts are addressed. An X-ray absorption spectroscopy-based methodology is discussed to determine electronic and structural properties of electrocatalyst surface which allows the prediction of reaction mechanism and establishing the correlation with reduction products. The selectivity and faradaic efficiency of products highly depend on the quality of surface modification. Preparation and modification of electrocatalyst surfaces through various techniques are critical to increase the number of activity sites and the corresponding site activity. Mechanisms of CO_2ER are complicate and thus are discussed in accordance with main products of interests. The authors try to concisely compile the most interesting, recent, and reasonable ideas that are agreeable to experimental results. Finally, this review provides an outlook for designing better Cu and Cu-based bimetallic catalysts to obtain selective products through CO_2ER.

development of power plants, industries and consumption of fossil fuels, which are the major and direct causes of global warming, rising sea levels, and more erratic weather patterns that are threatening environmental issues.[2–7]

Currently, various efforts are performed to develop and promote green (renewable) energy sources; although until now majority of energy consumption is obtained from nonrenewable sources specifically fossil fuels that contribute the increment of carbon dioxide level in the atmosphere in addition to other causes such as deforestation of plants and natural sources of CO_2.[3,8–11] For this reason, controlling and minimization of its emission using different methods such as electrochemical, biochemical, photochemical, thermochemical and hydrothermal reduction of CO_2 to convert into various essential compounds and simultaneously energy generating are one of crucial tasks to solve the challenge.[7,8,12–18]

1. Introduction

1.1. Background

Electrochemical conversion of CO_2 into essential chemicals and the reverse reaction of combustion offer a promising and emergent method for adjustment of the Earth's carbon balance.[1,2] Currently, CO_2 level reaches an approximate concentration of 410 ppm ($\approx$0.04% by volume) so far, and the natural balance is gradually disrupting. The emission is arise specially from the

1.2. Summary of Previously Published Articles

In previous review articles about electrocatalytic reduction of CO_2 they have addressed different views, ideas and interests, which depend on the contribution to forward in the era of research discipline. Some of review articles have provided generic principles and reduction mechanisms including extrinsic factors like electrolyte solutions and environmental conditions that can affect the reduction efficiency. Others have forwarded a summary of review specific to transition

M. K. Birhanu, M.-C. Tsai, A. W. Kahsay, C.-T. Chen, T. S. Zeleke,
C.-J. Huang, B.-J. Hwang
Department of Chemical Engineering
National Taiwan University of Science and Technology
Taipei 106, Taiwan
E-mail: bjh@mail.ntust.edu.tw

The ORCID identification number(s) for the author(s) of this article can be found under https://doi.org/10.1002/admi.201800919.

K. B. Ibrahim, W.-N. Su
Department of Applied Science and Technology
National Taiwan University of Science and Technology
Taipei 106, Taiwan
E-mail: wsu@mail.ntust.edu.tw

B.-J. Hwang
National Synchrotron Radiation Research Center
Hsin-chu 30076, Taiwan

**ADVANCED
SCIENCE NEWS**

www.advancedsciencenews.com

**ADVANCED
MATERIALS
INTERFACES**

www.advmatinterfaces.de

metal, metal derived oxides, chalcogenides, etc., through electrocatalytic or photochemical reduction of CO_2. Singh et al.[19] has broadly summarized the effects of membrane constituent, catalyst type, electrolyte solutions and operating conditions on the activity of solar based electrochemical reduction of CO_2. Zhu et al.[17] have referred to wide range of heterogeneous metal-based electrocatalysts and reviewed their general features that include description of basic principles, fundamental parameters, types of transition metal electrocatalysts and types of reduction products. Regrettably, limited explanation about site activities and number of active sites are given. Merino-Garcia et al.[20] have studied specifically about membrane reactors for the purpose of electroreduction of CO_2 to review and summarize effects of cation or anion exchange membranes in reduction efficiency and amount of products. Interestingly, Zhao et al.[21] have discussed briefly opportunities and limitations in the process of CO_2 reduction by Au and Ag based electrocatalysts with comparison of bulk metals, nanoparticles and atomic level nanoclustsers in catalytic activity and stability. He et al.[22] have prepared a concise mini-review regarding transition metal alloys such as Sn–Pd, Sn–Ag, Pd–Pt, Au–Pd, Ag–Zn, Au–Cu, Ni–Ga, etc., for electrochemical reduction process without indicating principles and basic reduction mechanisms of CO_2.

Therefore, by identifying the gaps from previous reviews such as limitations of detailed reduction mechanisms, lack of identification of site activity and number of active sites, absence of reviews about Cu related electrocatalysts in the reduction phenomenon, etc.; this article is specifically focused on CO_2ER using Cu and Cu based electrocatalysts especially on analyzing intrinsic parameters and their tuning effects in site number and site activity of CO_2ER. Additionally, unique electronic and structural property of Cu and its derivative electrocatalysts enabling the formation of wide range of products is another motivation behind this work.

Electrochemical conversion method of CO_2 has notable advantages because it is not affected by geology, amount of sunlight, or weather, as such it can performed at ambient conditions.[3,8,13,17,18,23,24] A desirable electrocatalyst for CO_2 reduction should have a low overpotential for catalysts and to derive a large turnover frequency (TOF), and at the same time the catalyst should be stable and selective.[1] This process can be regarded as a convenient way of storing energy and to convert CO_2 into CO, formate, methane, ethylene, ethanol, methanol, n-propanol, allyl alcohol, acetaldehyde, propionaldehyde, acetate, ethylene glycol, glycolaldehyde, hydroxyacetone, acetone, glyoxal, and other products. Electrochemical reduction is an interesting and promising way especially when the process is performed at reasonable cost of electrocatalyst and activity with high selectivity and efficiency.[15–17,25]

Mostly, CO, formate, hydrocarbons, and alcohols are the main reduction products through electrolytic reduction of CO_2. Hydrogen evolution reaction (HER) is commonly observed in the reduction process, and considered as a side reaction. Among these products, CO is one of the prominent yields from the electrochemical reduction of CO_2 obtained by selective electrocatalysis. The reason why CO is the desired product is that it can be further reduced into its derivatives such as formate, ethanol, methanol and simple hydrocarbons (CH_4 and C_2H_4) through the reduction process. It is selectively produced from reduction of CO_2 using transition metal catalysts such as

Mulatu Kassie Birhanu is a Ph.D. student in chemical engineering at National Taiwan University of Science and Technology (NTUST), Taipei, Taiwan. Currently, his research area is electrochemical reduction of CO_2 to convert into valuable products using Au and Cu nanoparticle as electrocatalyst. He received his M.Sc. degree in analytical chemistry in 2011 from Bahir Dar University, Bahir Dar, Ethiopia.
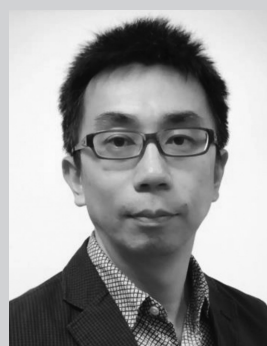
Wei-Nien Su is an associate professor of the Graduate Institute of Applied Science and Technology at National Taiwan University of Science and Technology (NTUST), Taipei, Taiwan. He is the secretary of the chemical society of Taiwan. His research interests are materials synthesis and characterization of nanocatalysts for various electrochemical activities. He is involved in various research programs. He received his Ph.D. degree from the Wolfson School, Loughborough University (UK) and in chemical engineering from Universität Stuttgart (Germany).

Bing-Joe Hwang studied chemical engineering and received his Ph.D. degree in 1987 at the National Cheng Kung University, Taiwan. Since 2006, he has served as chair professor at National Taiwan University of Science and Technology (NTUST). His research work has spanned a wide range of subjects from electrochemistry to spectroscopy, interfacial phenomena, materials science, and theoretical chemistry. He has established both experimental and computational strategies for the development of new materials and understanding interfacial phenomena. His work has led to a better understanding of electrochemical reaction mechanisms and to an improved ability to predict the properties of potential new materials for batteries, fuel cells, CO_2 reduction, and biosensors.

Au, Ag, Pd, and Zn. Eventually, CO and other reduced gases can be detected and determined using chromatogarphic and spectroscopic techniques in laboratory scale, but electrolytic

**ADVANCED
SCIENCE NEWS**
www.advancedsciencenews.com

**ADVANCED
MATERIALS
INTERFACES**
www.advmatinterfaces.de

reduction of CO_2 and separation of each product in production or factory scale have not implemented due to plenty of challenges.[7,26–28] The separation techniques of each product from reaction mixture face a challenge, which is discussed briefly together with other limitations of CO_2ER in Section 1.3 of this article.

Various types of catalysts have been utilized for the reduction of CO_2 such as metal oxides, chalcogenide, organometallic complexes, metals, organic compounds, semiconductors, bimetallics, and others.[29] Commonly, Cu is the most preferable electrocatalyst in different forms of morphology, structure and shape, which is controlled during preparation of the metal and its modification technique to obtain the required properties. Currently, bimetallic electrocatalysts are promising and emerging due to their efficient and effective reduction activity arising from synergistic, strain and alloying effects of atoms that results in better selectivity, stability, activity and less energy consumption.
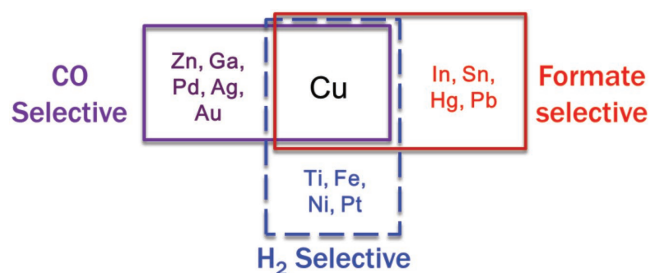
The development of bimetallic electrocatalysts is shown in timeline scheme in **Figure 1**, which is drawn based on the results of many research findings. As we have observed from the timeline scheme, since 1991 researchers have been strived to improve the effectiveness and efficiency of CO_2 reduction by adding various contributions starting from compositions of metal foils to single atom electrocatalyst. However, the number of publications of CO_2ER increased in sluggish rate in between 1998–2012. Afterward the rate of publication is very high and continuing

using sophisticated instruments and analytical tools for characterization of electrocatalysts. Majority of studies have been focused on transition metals, which can be traced back to the work in 1985 by Hori and Suzuki who reported methane and ethylene as the major yields of CO_2 reduction on copper electrode.[22,35–37]

Based on the types of reduction yields, metal catalysts are categorized into different major groups in the reduction process and denoted as, CO selective, formate selective, HER (side reaction in CO_2ER) favorable electrocatalyst and hydrocarbon (CH_4 and C_2H_4) are significantly and uniquely formed together with other products on Cu electrocatalyst as it is revealed in **Figure 2**. It is clear that H_2 is not the reduction product of CO_2 rather it is the competing side reaction arises from water or aqueous media that occurs during reduction of CO_2. Bimetallics can catalyze CO_2 more selectively into CO, formate, etc., than monocatalysts due to the synergistic effects between atoms. Among all electrocatalysts Cu is a unique metal that is able to catalyze CO_2 into wide range of reduction products including hydrocarbons, formate, CO, hydrocarbons, alcohols and many others products.[4,14,33,38–41] However, the above grouping does not mean that those metal catalysts generates only the indicated product rather it is expected that other reduction products in small amount are formed in addition to the dominancy of the selected product. Electrocatalysts, selective to formate, are associated with lower current density, while those precious metals selective to CO able to generate higher current density.[8,17,29]
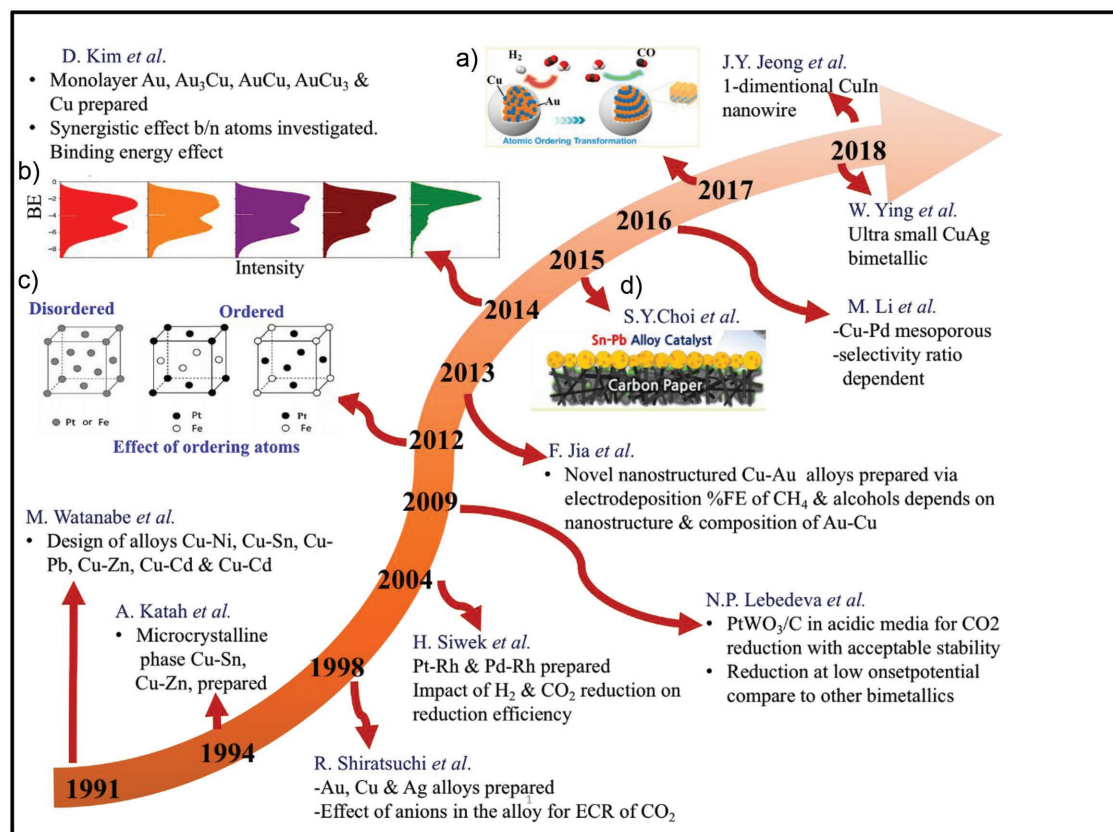
Figure 1. The timeline scheme for the development of selected Cu-based bimetallic electrocatalysts applicable in CO_2ER since 1991 until 2018. a) Reproduced with permission.[34] Copyright 2017, American Chemical Society. b) Reproduced with permission.[8] Copyright 2014, Springer Nature. c) Reproduced with permission.[31g] Copyright 2012, Elsevier Ltd. d) Reproduced with permission.[31a] Copyright 2016, American Chemical Society.

**ADVANCED
SCIENCE NEWS**
www.advancedsciencenews.com

**ADVANCED
MATERIALS
INTERFACES**
www.advmatinterfaces.de

Figure 2. Brief scheme categories for CO and formate selective electrocatalysts in CO_2ER, and identification of transition metals favorable for HER, which is considered as a side reaction.

The trends of catalysts generating different products of CO_2 reduction are suggesting various reaction mechanisms with different surface affinities of intermediates and final products. The catalytic activity of metals depends not only on their intrinsic atomic chemical properties, but also on their surface characteristics such as roughness and surface area to volume ratios. Roughness and surface area affects the plane edges exposed at the surface where CO_2 adsorption is dominant, and its binding strength significantly affect the type and amount of products.[28,39,42–46]

1.3. Concise Overviews of CO_2ER

The striving and development of high promising catalysts or electrodes needs a basic understanding of electrode materials to describe what kind of influence on reaction mechanisms are conducted, such as adsorption of reactants, intermediates and products on the electrode surface during reduction process. Early studies of CO_2ER were concentrated on bulk composite

electrocatalysts. However, nanosized metal electrocatalysts are much promising than bulk or foil metals in various aspects such as columbic efficiency, catalytic activity, selectivity of products and others phenomena. That is the reason why recent electrocatalyst activity is focused on nanocatalysts. Majority of electrocatalysts for CO_2ER are classified into metallic, nonmetallic, and molecular catalysts regardless of product types of the reduction.[15,24–26,41,47] However, this review article is concentrated on metal-based electrocatalysts, specifically on Cu and Cu-based materials for conversion of CO_2 electocatalytically.

Commonly, electroreduction process has been performed in a divided cell containing the anode and cathode compartments. To separate the two electrode (anode and cathode) compartments, an ion exchange membrane is important to prevent the flow of electrons by allowing passage of protons, which avoids further oxidation of species formed from electrochemical reduction of CO_2 at cathode.[17,26]

At cathode both CO_2 reduction together with hydrogen evolution reaction (HER) are conducted on the surface of electrocatalysts in electrolyte solution. The schematic reactor configuration and reaction mechanisms of CO_2ER are shown in **Figure 3**.

In electrochemical reduction process of CO_2, there are three crucial steps conducted, which are mentioned below.

a. Adsorption of CO_2 on the electrode surface.
b. Charge transfer reaction with harmonization of H^+/e^- into CO_2 to form intermediates.
c. Desorption or removal of products on the active sites of electrocatalyst during electroreduction of CO_2.[48,49]
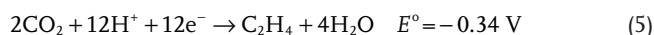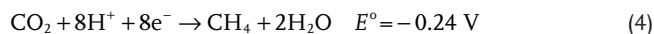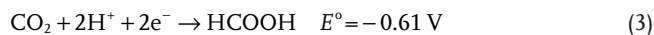
CO_2 is thermodynamically stable and for that matter additional energy is required to break the strong bonds of CO_2 during reduction reaction using catalysts to lower the activation energy. More precisely, the Gibbs free energy of the relevant reaction can be controlled by changing the potential. Since CO_2
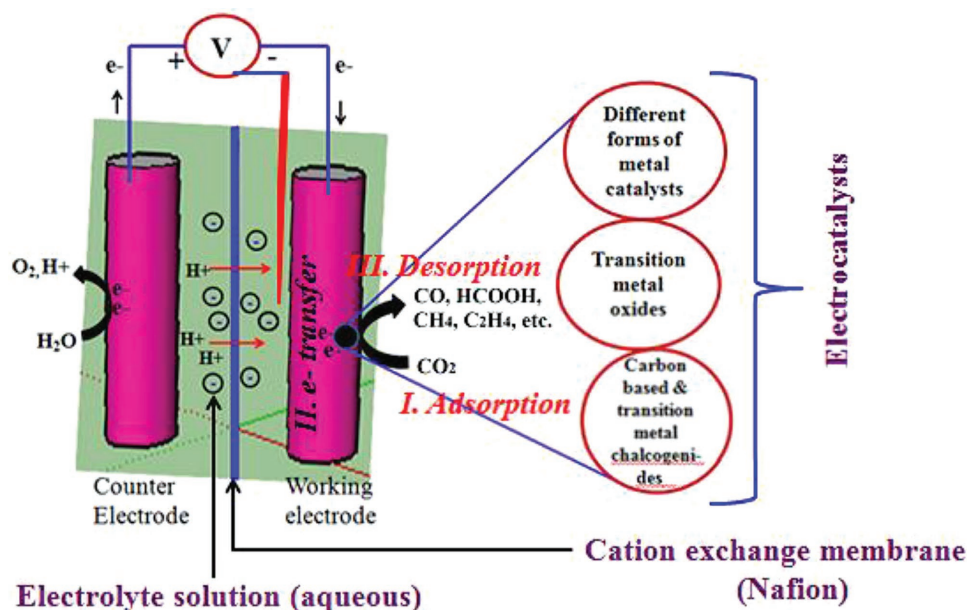
Figure 3. Demonstration for principles of CO_2ER on electrocatalysts (working electrode) and the role of anode and cathode in the reduction system in aqueous media.

reduction is endergonic or endothermic (absorption of energy with positive free energy) and the applied potential for different products is mostly in negative potential range. The following chemical equations are describing reduction potentials (vs standard hydrogen electrode) of CO_2 at room temperature, atmospheric pressure and pH 7 for each product formation via two or more electron transfers as listed in Equations (1)–(7)[17,50]

$$CO_2 + 2H^+ + 2e^- \rightarrow CO + H_2O \quad E^\circ = -0.52 \text{ V} \tag{1}$$

$$CO_2 + 4H^+ + 4e^- \rightarrow HCHO + H_2O \quad E^\circ = -0.51 \text{ V} \tag{2}$$

$$CO_2 + 2H^+ + 2e^- \rightarrow HCOOH \quad E^\circ = -0.61 \text{ V} \tag{3}$$

$$CO_2 + 8H^+ + 8e^- \rightarrow CH_4 + 2H_2O \quad E^\circ = -0.24 \text{ V} \tag{4}$$

$$2CO_2 + 12H^+ + 12e^- \rightarrow C_2H_4 + 4H_2O \quad E^\circ = -0.34 \text{ V} \tag{5}$$

$$CO_2 + 6H^+ + 6e^- \rightarrow CH_3OH + H_2O \quad E^\circ = -0.38 \text{ V} \tag{6}$$

$$2H^+ + 2e^- \rightarrow H_2 \quad E^\circ = -0.42 \text{ V} \tag{7}$$
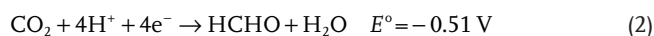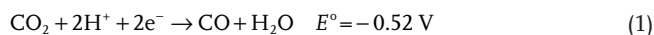
Low stability of copper electrocatalyst is not uncommon in electrocatalytic reaction and this can be also a cause for less faradaic efficiency in catalytic activity. In other way, it is possible to say poor product selectivity and less stability are typical limitations of Cu for practical applications. Therefore, clear understanding of the catalytic mechanism using Cu is an important step for future design of efficient and selective catalysts for CO_2 reduction by minimizing such challenges.[11,17,51–53] The above challenges will be described with more details in the next section of this article, including other difficulties faced in the process of CO_2ER.

1.4. Challenges of CO_2ER

In addition to the competitive reaction of HER, there are also other challenges during the electrochemical reduction process of CO_2. The following scenarios mentioned are among the drawbacks or limitations occurring in the reduction processes that causes for low faradaic efficiency and poor selectivity of the electrode towards the required product.[16]

The first limitation is slow kinetics of CO_2 reduction because of its high stability and also low solubility in water. Low solubility of CO_2 in water limits the amount of CO_2 in the electrolyte solution that retards the mass transfer capability and it becomes an obstacle for large scale and efficient electrochemical reduction of CO_2. However, to reduce this barrier high pressurized CO_2, high gas-liquid interfacial area, and electrolytes with high CO_2 affinity can effectively increase solubility of CO_2 in the solution, which enhances the conversion rate and faradaic efficiency of products.[26,33,38] Second, CO_2ER requires high overpotential due to the high energy barriers of CO_2 reduction; this implies that low energy efficiency of the reduction process with responses of low current density and

consequently low faradaic efficiency. The consequence of utilizing high overpotential would be also a cause for the competitive formation of HER in the reduction process, because at high potential, HER is much dominant than CO_2ER. The third limitation is poisoning or deactivation of electrocatalysts by excessive adsorptions of intermediate species, side products and impurities, which leads to a significant damage of catalysts and then shortens its life time.[16,17,33,54]

The forth limitation, in case of mixtures (gases and liquid) of reduction products, identification, determination and separation of each products in the mixture is a difficult task due to the existence of products in different physical states. Mostly, gas chromatography is an appropriate analytical tool to quantify and separate gaseous products, while high performance liquid chromatography and NMR spectroscopy are suitable for determination of liquid products in laboratory scale level. However, the separation technique needs special configuration of reactor and high technical skills and these requirements make the process costly. Additionally, separation of reduction products in large/production scale has not been implemented yet. The product analysis in a production process could pose a challenge.

Finally, the exact reaction steps and mechanism of CO_2ER is not clearly known and it is not well understood why carbonates and bicarbonates from electrolyte solution cannot be reduced on the catalyst surface. The possible cause for limited understanding of reduction mechanism might be due to the formation of various types of products and multiple transfers of electrons and protons. Formations of multiple products are because of carbon can harmonize various valence states resulting complexity of C−C coupling chemical reactions with different reaction mechanisms and paths that challenges to understand detailed mechanisms of CO_2 reduction.[17,29,55,56] All these mysteries of CO_2 reduction lead to poor understanding of the factors that influence the selectivity of catalysts and hinder development of this application. Therefore, to minimize these limitations and challenges, tuning and optimizing of parameters during preparation of electrocatalyst and reduction process is an inevitable task. This is an interesting scenario for future researchers to establish a promising and an emerging technology to know precisely each reaction mechanisms in CO_2ER.

2. Intrinsic Factors of CO_2ER on Cu-Based Electrocatalysts

2.1. Active Sites of Electrocatalysts in CO_2ER

Prior to mentioning intrinsic effects of CO_2ER, well understanding of site activity and number active sites is important. Activity of electrocatalysts is directly linked to number of active sites present on the surface in which their number depends on the modification type and intensity. It is obvious that large amount of actives sites have better catalytic activity.

Electrocatalysts alter their structure during reaction conditions in which the restructuring can be induced by physical parameters (temperature, pressure, potential, etc.) including adsorbates and reactants. These established structures with minimized thermodynamic energy in reaction conditions are responsible for the detected catalytic properties of CO_2

reduction. Alteration of atomic arrangement, composition and oxidation state of electrocatalyst is a crucial step to understand structure-reactivity correlations to design efficient catalysts. Development of improved and enhanced electrocatalyst with tremendous activity and selectivity with analyzing active sites is still a long time objective/goal to realize the real application of CO_2ER. Commonly researchers are mixing up the terms catalytic activity and activity site in catalysis process, even though they are different scientific meanings, which is related as follows

Catalytic activity = Site activity ± number of active sites

Number of active site can be enhanced by increasing the surface area of electrocatalysts. To increase the surface area its modification by the principle of surface engineering via different techniques would be applicable. For example, surface modification of bulk metal surface, which is initially weak activity in CO_2 reduction makes in to a high surface area nanoparticle, nanowire, nanocrystal, etc., that shows better performance in the reduction activity. This is because after modification significant number of active sites is created due to the creation of large surface area. Active sites of metal nanoparticles might have different roles for the formation of product types during CO_2ER. Researchers proposed that edge sites can speed up the formation of CO, however, the corner site of nanoparticle has a tendency for HER. Identification or quantification of active site is one important step to accomplish the overall catalytic activity effectively and efficiently.

Identification of active sites of an electrocatalyst is a great challenge without clear and defined electrocatalyst structure. Currently, the invention of atomic and electronic characterizations of nanoclusters of electrocatalysts offers huge opportunities for the investigation of single atom as an active site.[1,49,57] Single atom active sites, which are distributed atomically on active metal centers, have shown the highest atom efficiency and an outstanding selectivity in various catalytic reactions. This is because single active site has unique electronic properties, which leads for the expectation to have a huge potential to enhance the performance of CO_2ER. The presence of high surface energy in single atom is one challenge to establish stable single atom catalyst. Understanding of these catalysts and additional design of advanced and new single atom catalysts of CO_2 reduction might be faced challenges like the difficulty to find electronic structure of single atom catalysts.[1,58,59] Nowadays, the rapid development of technologies for characterization of electronic and structural properties of atoms is expected to be a good opportunity for the application of single atom electrocatalysts specially for CO_2 reduction.

It is expected that the following intrinsic factors would affect the catalytic activity and number of active sites on electrocatalysts for CO_2ER. Many researchers could not differentiate the factors that contribute to increase number of actives sites, but in general they revealed some parameters are enhancing the overall catalytic ability of electrocatalysts. In addition to intrinsic factors extrinsic parameters such as temperature, types and amount of electrolyte solution, concentration of CO_2 and pH of solution, types of anion or cation exchange membrane, electrochemical cell or reactor design have also an effect

in catalytic activity and product selectivity of CO_2ER. However, in this review we focus on intrinsic factors appear on Cu and its bimetallic electrocatalysts. We believe that almost all intrinsic factors (binding strength between the catalyst and intermediate, catalyst surface area, particle size of electrocatalyst, morphology, composition, etc.) have significant contribution in increasing active sites and catalytic activity.
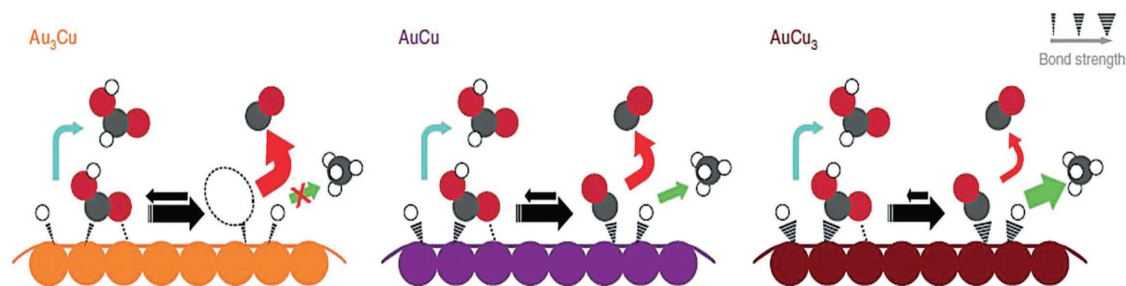
2.2. Binding Strength of CO_2 and Intermediates

Among plenty of intrinsic factors, binding ability of reaction intermediates with Cu-based electrocatalyst has a huge impact on electrochemical reduction of CO_2. Reaction activity and product selectivity of CO_2 reduction significantly depend on the binding strength of the key intermediates (CO*, COOH*, CHO*, COH*, etc.) and CO_2 itself. For example, formate and CO are the most favorable reduction product if there is no strong interaction between the surface and reduction intermediates because the C−O bond does not dissociate in case of weak binding strength.[17,38,59,60] Those electrocatalysts that can bind CO strongly yields limited amounts of product (CO and HCOOH) because there is a high possibility of the surface poisoned by the adsorption of CO or other intermediates formed during the electrochemical reduction process. For this reason, hydrogen generated from the competing water reduction becomes the main product in addition to the final reduction products of CO_2ER, i.e., hydrocarbons, alcohols, etc. In other way, metals that weakly bind CO produces significant amount CO and there is no chance to produce alcohols and hydrocarbons from further reduction of CO because it can easily desorbs from the surface before further reduction.[17,38,59,61] Therefore, binding strength between electrocatalyst surface and reduction intermediates has a great role in types and quantity of reduction product.

Yang et al. studied in advance electroreduction of CO_2 using Au, Cu, AuCu, $AuCu_3$, and Au_3Cu and they reported that the highest catalytic activity was obtained on Au_3Cu with better faradaic efficiency, current density, and TOF of CO.[8,49] **Figure 4** illustrates the binding ability and interactions of electrocatalysts and CO_2 to understand the mechanisms how the intermediates including (CO and COOH) are able to interact and optimize binding ability of each reduction species with the active surface of each composition of electrocatalysts. The figure depicts that the binding ability of each atom (C, O, and H) from CO_2 and reaction intermediates with Au_3Cu is weak, which is an important scenario to decrease HER and enhance the required reduction activity by preventing from further reduction.[8,34,62] For this reason, preparation of alloys in different types such as core-shell, ordered and other forms of arrangement is an important influence for tuning of binding strength in CO_2ER.

2.3. Electrochemical Surface Area (ECSA)

ECSA is one of the crucial parameters that influence results of CO_2ER on the surface of Cu and its derivate electrocatalyst. ECSA mainly depends on the textural structure and morphology of the catalyst surface where the active sites for electro-catalytic

ADVANCED
SCIENCE NEWS
www.advancedsciencenews.com

ADVANCED
MATERIALS
INTERFACES
www.advmatinterfaces.de

Figure 4. Illustrations of binding strength of CO_2, hydrogen, CO, formate, and hydrocarbons on Au_3Cu, AuCu, $AuCu_3$ surfaces in CO_2ER. Gray, red, and white colors refer to C, O, and H, respectively. The right corner stroke indicates the binding strength of each species to the surfaces. Dotted lines tell additional attraction between intermediates and the surface. Red, blue, and green arrows indicate the formation of CO, formate and hydrocarbons respectively by considering the thickness of the arrow that also shows production capacity. Reproduced with permission.[8] Copyright 2014, Springer Nature.

activity are present. It is known that activity of an electrocatalyst is expressed as; the product of site activity and number of active sites on that catalyst. If the catalyst has a porous or hollow structure surface, the ECSA expected to be high and lead to high catalytic activity of the reduction. Mathematically, the ECSA can be described as Equation (8)

$$ECSA = R_f \times A_s \qquad (8)$$

where A_s is a specific surface area of the smooth surface electrode; R_f is roughness factor estimated from the ratio of double-layer capacitance (C_{dl}) for the working electrode. C_{dl} is determined by evaluating the capacitive current related with double-layer charging at various scanning rates of cyclic voltammetry in electrochemical analysis.[26,49,63]

2.4. Size of Nanocatalysts

Changing the size of Cu-based nanocatalysts (nanoparticles, nanowires, nanocube, nanosheet, etc.) has a great contribution for alteration of active sites in number or/and activity manner, which has an overall effect in selectivity and performance of CO_2ER. Tuning of chemisorption (a type of adsorption), which indicates a chemical reaction between the adsorbate and the surface is important to enhance selectivity and catalytic activity. Size effect has been implemented to control and analyze the catalytic activity and selectivity of metal nanoparticles, but the mechanism behind still requires further investigation. The alteration of chemisorption is studied by varying the size of electrocatalyst species, which affects the active site area of the reduction activity.[56,64–66] Change of particle sizes has also a great impact on the electrochemical reduction of CO_2 including the type of reduction products and corresponding faradaic efficiencies, although a very limited number of studies are performed for size dependent CO_2 reduction.[49,64,67,68]

A new insight and interesting work performed by Strasser et al. precisely revealed the effect of size of nanoparticles in electrochemical reduction of CO_2.[69] They prepared Au nanoparticles in between 1 and 8 nm using inverse micelle encapsulation method. The linear sweep voltammetry (LSV) peak (**Figure 5**a,b) shows an outstanding increment of current density when the particle size is small, i.e., the current generated using the smallest nanoparticle (1.1 ± 1 nm) is almost 100 times higher than that is generated

using the largest Au NPs (7.7 ± 2.3 nm). Generally, the faradaic efficiency of H_2 is enhanced with the decrease of sizes of NPs although the enhanced level between small and large particle size is not proportional as we observed the variation/enhancement in current density between those particle sizes. For smaller particle sizes, the amount HER generated was significantly higher than CO, whereas the faradaic selectivity of CO greatly increased for large Au nanoparticles (Figure 5c,d).

In other words, the mole ratio of H_2 to CO (H_2/CO) increased with decreasing particle sizes, indicates that HER is dominant for smaller particle sizes (Figure 5e).[49,69] It is expected and believed that the effect of particle size which is observed on Au electrocatalysts also applicable on Cu-based electrocatalyst surfaces.

Strasser et al.[64] studied the effect of catalytic particle size on CO production from electroreduction of CO_2 on Cu nanoparticles (NPs) as shown in **Figure 6**. They investigated variation of particle size of Cu NPs in between 2–15 nm showed a significant impact on selectivity and faradaic efficiency, as depicted in Figure 6a. Smaller particle size reveals an increase in the formation of H_2 and CO compared to production of hydrocarbons (CH_4 and C_2H_4) (Figure 6b).[64] According to the investigation, if hydrocarbons are the preferred products of CO_2 reduction on Cu surface, it is important to avoid using very small nanocatalysts due to weak production of hydrocarbons. According to Figure 6c, the smallest Cu NP catalyst (1.9 nm) showed a significant increment in faradaic efficiency with a current density of −48 mA cm^{-2}, while the 2.3 nm Cu NP catalyst also showed a 50% rise in activity compared to Cu foil electrode (Figure 6d).[64,69]

Strasser et al. continued their investigation by establishing spherical Cu nanoparticle model for good clarification of size effect of nanoparticles (**Figure 7**).[64] It is agreed that size variation of NPs significantly originates from size-dependent atomic coordination of surface metal particles and its electronic structure. Figure 7a illustrates the surface arrangement of small grain size at the left side and large grain size to the right sides of NPs corresponding to the catalysts represented as S_2 and S_4 with particle sizes 2.3 and 6.7 nm respectively in which their corresponding current density is reported previously in Figure 6c.

Based on the model, the number of nearest neighbor atoms on the surface is denoted as the coordination number (CN) that is obtained and valued between CN of 5 and 11. The color coding confirms the location of individual CN on the surface of Cu nanoparticle. The red and blue representing CN 9 and CN 8 associates with Cu (111) and Cu (100) respectively, while those green
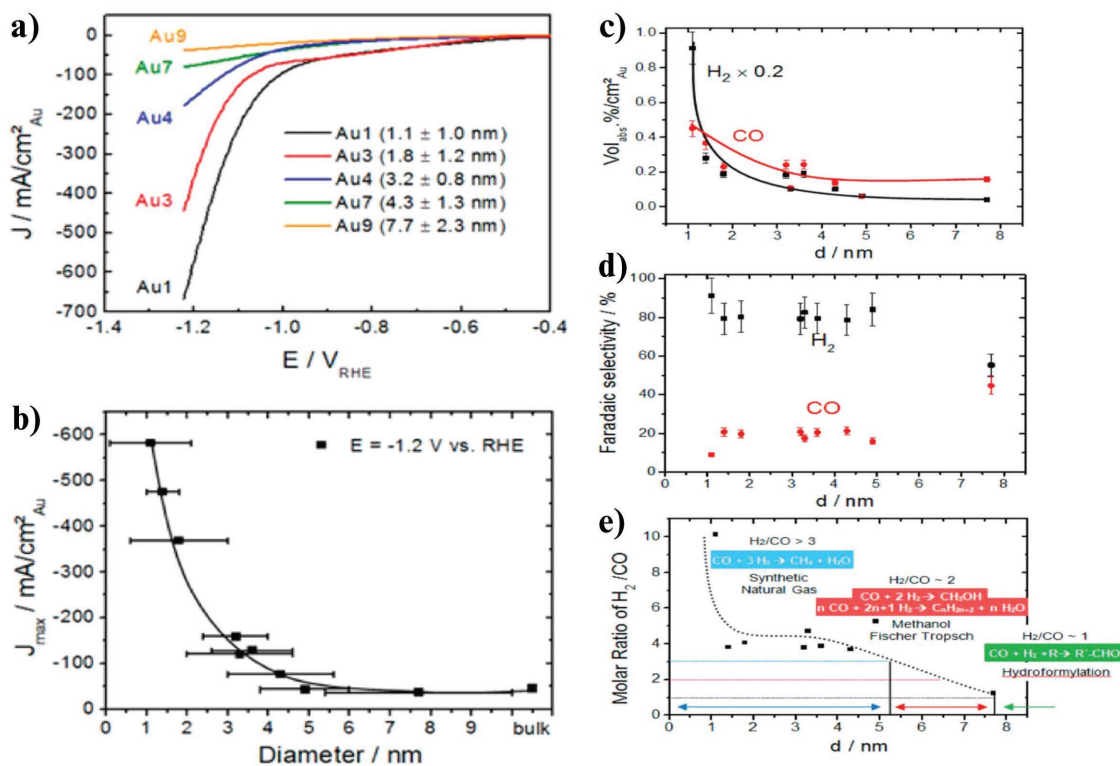
Figure 5. CO_2ER on different sizes of Au nanoparticles: a) LSV in 0.1 M $KHCO_3$ at 5 mV s^{-1}, b) current density variation, c) CO and H_2 production, d) FE of CO and H_2, e) molar ratio of H_2 to CO generated. Reproduced with permission.[69] Copyright 2014, American Chemical Society.
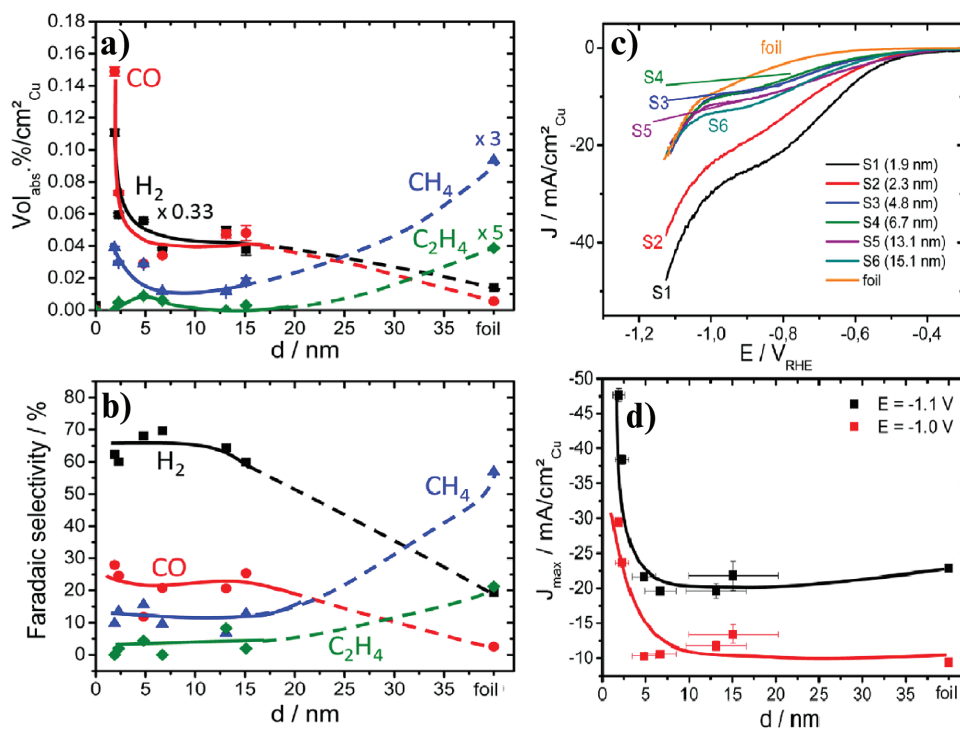
Figure 6. CO_2 reduction based on different sizes of Cu NPs. a) Production and composition distribution of gaseous products, b) size dependence Faradic selectivity of different products at −1.1 V versus RHE, c) LSV of CO_2 reduction performed at 5 mV s^{-1}, d) current density at −1.0 V and −1.1 V versus RHE. Reproduced with permission.[64] Copyright 2014, American Chemical Society.
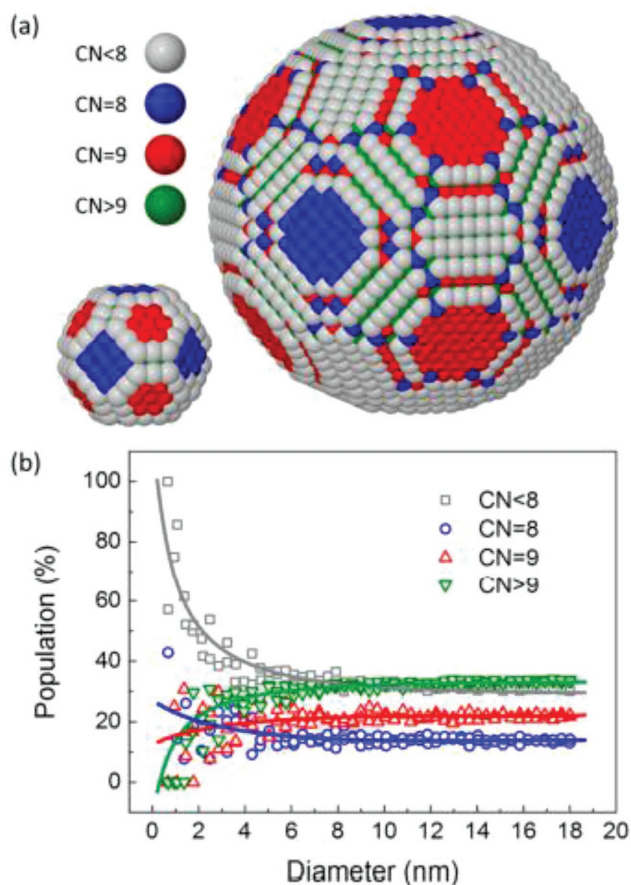
Figure 7. a) Spherical models of 2.2 and 2.9 nm diameter of Cu NPs with color coded surfaces to the neighboring atom, which is described as coordination number of CN < 8 (gray), CN = 8 (blue), CN = 9 (red), CN > 9 (green), b) the relative population of atoms on Cu surface atoms at known CN with respect to diameter of particle size. Reproduced with permission.[64] Copyright 2014, American Chemical Society.

containing CN 10 and 11 representing Cu (211) and Cu (110), respectively. High CN indicates large particle size, which leads to low current density due to less number of active sites because it surrounds by many atoms compared to low CN particles.

The ratio or proportions of atoms at the edge, corner and on the surface site are influenced by the grain size of nanoparticles. Atoms at the corner or edge directions are expected to contain less coordination number, leading to having higher surface energy. Generally, the electrochemical activity of metal foils is much lower than that of the corresponding nanoparticles due to significant reduction of active surface area in case of metal foils.[64] According to trends of Gibbs free energy customized with calculations of density functional theory (DFT) the production of essential intermediates from adsorption of CO_2 are significantly preferable on edge and corner sites than on terrace direction or positions of nanoparticles. However, formation of H* intermediate, which is used to facilitate HER is almost the same in all sites and edges.[56] Therefore, formation of CO* and HCOOH* is highly tuned by size of nanoparticles for the formation of main final products such as formate, CO, alcohols and hydrocarbons in which types of reduction products are depend on binding strength between electrocatalyst and intermediates.[56,64,65]

The catalytic activity is exhibited and enhanced by the number of active sites existing on the surface of electrocatalyst, which are created by surface modification techniques such as oxidation, doping foreign metal, alloying (causes for synergistic effect), surface etching and others. Therefore, modification of electrocatalyst alters the surface morphology (rough vs smooth), increases surface area, and affects electronic together with geometric nature of electrocatalysts. All these variations have its own contribution for the increment of active sites, leading to enhance the overall catalytic activity of the catalyst in CO_2ER on Cu surface. Smaller number of CN results in a significant catalytic activity enhancement, which arises from increment of individual population originated from size variation of Cu nanoparticles (Figure 7b).[68,70]

We can suggest that variation of product types is due to variation of particle size, which is related to the binding ability of electrocatalyst to the surface. Smaller particle size tends to have smaller coordination number to the surrounding atom and leads to have high surface area to expose itself in the catalysis environment. Therefore, as the tuning of binding strength between reduction intermediates and electrocatalyst has a great role in selectivity, variation and distribution of products in CO_2ER.
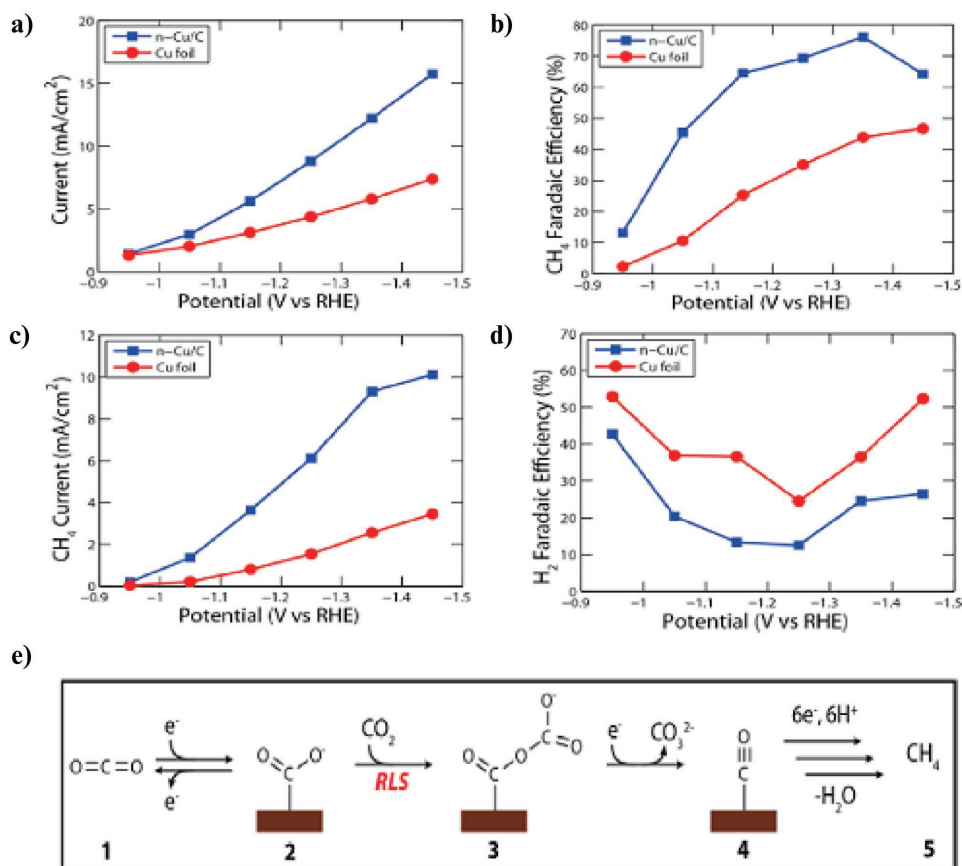
Bell et al.[71] have investigated the significant differences of electrochemical performance on Cu-NPs versus Cu-foil for reduction of CO_2 to produce methane The current density and faradaic efficiency of CH_4 on copper nanoparticle (n-Cu/C) is twice higher than copper foil within the same potential domain (**Figure 8**a,b). The partial current density of CH_4 is four times higher compared to Cu-foil at −1.35 V versus RHE (Figure 8C). In contrast, the faradaic efficiency of H_2 is higher in case of Cu-foil than nanoparticles, indicating decreasing the size of nanocatalysts decreases the undesired product (competitive reduction like HER) in the reduction process of CO_2 (Figure 8D).[71]

From Bell's we can perceived that the size of nanoparticle or nanocatalyst has a potential effect in the selectivity of products in addition to the huge contribution for the enhancement of CO_2ER on Cu and Cu-based derivative catalysts. Generally, in Figure 8 the increased faradaic efficiency, selectivity, total and partial current density of Cu NPs than Cu foil is probably due to structural, morphological, and electronic variations between the two species related to creation of more actives sites on Cu NPs than its foil. In Bell's research, the reaction mechanism is starting from adsorption of CO_2 for production of CH_4 via formation of CO* as an intermediates, which is proposed and shown at Figure 8e. In this mechanism, CO_2 reacts in a single electron transfer pre-equilibrium step to form a radical 2, which is considered as an adsorbed CO_2 on the electrode surface. The rate-limiting step is shown at the transformation of COO^- into $(COO^-)_2$ through dimerization of another COO^- on COO^- and to establish a new bond between oxygen and carbon.[71–73]

2.5. Structure of Catalyst Surface

a. Ordered—Disordered Effect

Yang et al. and Ma et al.[5,34,74] have studied independently the effect of ordered, disordered, phase-separated and intermediate ordered arrangement of individual atoms on product
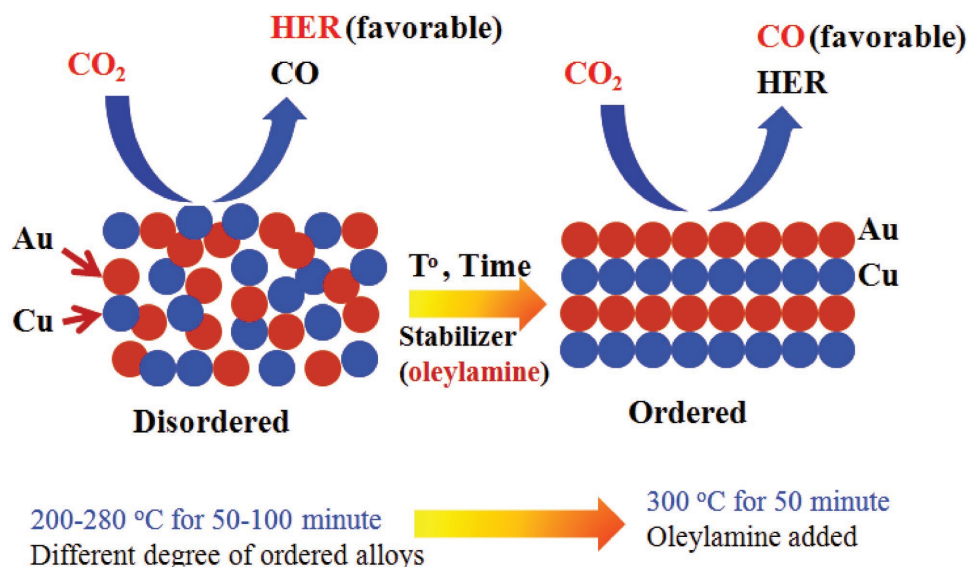
**ADVANCED
SCIENCE NEWS**
www.advancedsciencenews.com

**ADVANCED
MATERIALS
INTERFACES**
www.advmatinterfaces.de

Figure 8. a) Faradaic efficiency of Cu NPs versus Cu foil, b) FE of CH_4 on Cu NPs and Cu foil, c) current density of CH_4 on Cu NPs versus Cu foil, d) FE of H_2 on Cu NPs versus Cu foil in CO_2 reduction within the potential domain. e) Simple reaction mechanism of CO_2 reduction to produce CH_4 on Cu surfaces including rate-determining step. Reproduced with permission.[71] Copyright 2014, American Chemical Society.

selectivity and FE of CO_2 reduction using CuAu bimetallic electrocatalysts. Ma et al. have investigated product distribution and effect of morphological/structural changes of CuPd electrocatalyst for electrocatalytic reduction process.[5] They compared reduction products of CO_2 between disordered, ordered and phase-separated CuPd catalysts, which are prepared by changing different parameters during fabrication of nanoparticles. The ordered CuPd electrocatalyst confirms the highest selectivity for C1 products such as CO and CH_4 with obtaining faradaic efficiency greater than 80%. The phase-separated CuPd and Cu_3Pd assure higher selectivity (>60%) for C_2 chemicals (C_2H_4, C_2H_5OH) than $CuPd_3$ and ordered CuPd. Based on these results they suggest that the probability of dimerization of C1 intermediate and products are significant on surfaces with neighboring Cu atoms.[5]

Generally, studies revealed that the level of order of each atom in Cu–M bimetallic electrocatalyst, which is controlled by stabilizing agent, altering temperature and time during preparation of nanoparticles. Ordering degree of nanoparticles of an alloy has a significant impact on catalytic activity, stability and selectivity because alloying extents are different for different degree of ordering. For example, ordered-disordered schematic animations for AuCu bimetallic systems are illustrated and shown in **Figure 9**, indicating HER (side reaction) is the favorite reaction and leads formation of H_2 on AuCu in case of

disordered arrangement, while CO is the dominant product of CO_2 reduction on ordered AuCu.

Specifically, Yang et al. have studied the disordered-to-order transformation of individual AuCu nanoparticles using oleylamine as stabilizing agent and variation of time and temperature as a transformation parameters, with detailed electronic and structural investigations of ordered AuCu NPs, as shown in X-ray diffraction (XRD) pattern (**Figure 10**a) and transmission electron microscopy (TEM).[34] The current density generated by ordered AuCu is higher than the disordered and intermediate or partially ordered on AuCu bimetallic during catalytic reduction process. This scenario results in better selectivity of CO over HER competing reaction from aqueous media. Detailed characterizations of copper based bimetallic using XAS are discussed in section 3 of this review. Therefore, the investigations of Yang et al. revealed that the performance of electrochemical activity of ordered, semi-ordered and disordered AuCu nanoparticles by keeping each metal compositions fixed and equal number of moles of atoms on the electrocatalyst. Interestingly, they confirmed that the disordered AuCu (1:1 atomic ratio) is less active catalyst, which mainly generates hydrogen gas, while the ordered one is a better selective catalyst towards reduction of CO_2 to CO by decreasing production of H_2 evolution (Figure 10b). TEM image (Figure 10c) clearly shows the image of ordered, intermediate ordered and

**ADVANCED
SCIENCE NEWS**

www.advancedsciencenews.com

**ADVANCED
MATERIALS
INTERFACES**

www.advmatinterfaces.de

Figure 9. Illustrations of AuCu bimetallic electrocatalysts and the favorable products in CO_2ER cause by disordered and ordered atomic arrangements of bimetallic atoms.

disordered nanoparticles of AuCu considering the degree of ordering between each nanoparticle. Furthermore, DFT calculations suggested that the enhanced CO_2 reduction activities for ordered AuCu intermetallic NPs originates from the formation of compressively strained Au over layers that causes enhancement of catalytic activity and selectivity.[34] Mathematically, the degree of ordering, i.e., denoted as S can be expressed using Equation (9)[34]

$$S = \frac{\chi_A - F_A}{1 - F_A} \qquad (9)$$

where S is degree of ordering, χ_A is fractions of sites A occupied by the "right" atoms, F_A is fraction of atom A in the bimetallic. If any significant deviation from sharp long-range order causes

the super lattice lines to be weaker, so in that condition S could be detected experimentally by comparing the ratio of integrated intensity of a fundamental and super lattice line (which are determined from normalized XRD peaks by Gaussian fitting of each face) using Lorentz polarizability, structure, and multiplicity factor.[34]

b. Morphology of the Surface and Crystal Orientation

Currently, studies have reported the significance of surface morphology (rough and smooth) of copper based electrocatalysts and it showed that rough Cu surface catalysts could enhance the performance and selectivity towards production of hydrocarbon (CH_4 and C_2H_4) than the smooth surface for
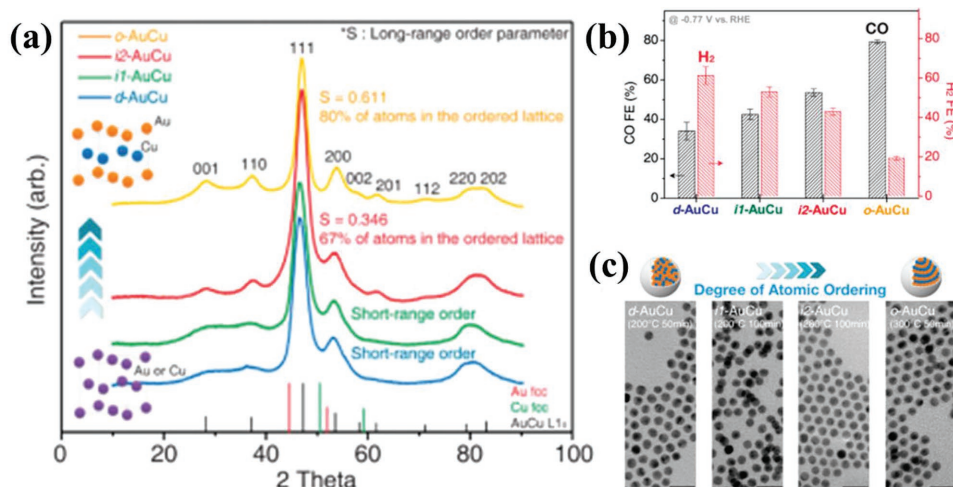
Figure 10. a) XRD pattern of ordered, intermediate ordered and disordered AuCu bimetallic nanoparticle, (b) FE of H_2 and CO on ordered, disordered and intermediate ordered AuCu in CO_2. c) TEM of ordered, intermediate ordered, and disordered. Reproduced with permission.[34] Copyright 2017, American Chemical Society.

**ADVANCED
SCIENCE NEWS**

www.advancedsciencenews.com

**ADVANCED
MATERIALS
INTERFACES**

www.advmatinterfaces.de

electrochemical reduction of CO_2.[41,45,75] This might be the number of active sites increase on rough surface compared to the smooth one. Product selectivity also depends on single crystal copper orientations among which Cu (111) is preferable for the formation of methane as the primary hydrocarbon product, whereas Cu (100) and Cu (200) crystal planes are favorable for the formation of ethylene.[76,77] According to experimental studies when the roughness degree of copper surface is very high, formate is the main instead of hydrocarbons.[77] In contrast, other studies reported Cu mesocrystals with Cu (111) as the dominant Cu crystal orientation and confirmed C_2H_4 is the main product.[76] These discrepancies show that it requires further investigation to understand detailed reaction mechanisms via crystal orientation for reduction applications.[64,75,78,79] Morphology of copper plays a significant role for good selectivity and enhancing faradaic efficiency of hydrocarbons by establishing different crystal facets containing small coordinated active sites like edges, steps and defects.[77,79,80] Modification of electrocatalyst surface is very important for creation of high energy facets, which becomes and considered as an efficient way of enhancing the catalytic activity, selectivity and stability of catalysts.

Wang et al.[74] have studied etching effect of copper surface for creation of high energy facets nanocrystals for electrochemical reduction of CO_2 and make a relationship between facet surface energy of Cu and its work function (**Figure 11**). According to their intensive investigation, from the three basic face structures of Cu, i.e., Cu (100), Cu (111), and Cu (110); Cu(110) has the least work function and the highest surface energy. The existence of high energy Cu (110) facets makes the etched Cu nanocrystals active catalysts for CO_2 reductions. This idea suggests that forming high energy facets on the surface of electrocatalyst refers a promising technique for enhancing their catalytic activity. Solvent used for etching on the surface of an electrocatalyst, type of etchant species and the addition of capping agent have some effects for the quality of etching process, which results in variation of selectivity and activity of CO_2ER. According to the study, the etched copper nanocrystal that creates high energy rich facet, i.e., Cu (110), which is more stable and selective towards CH_4, C_2H_4, C_2H_6, and C_3H_8 than the original Cu (100) in the reduction process of CO_2. The selectivity of CO on Cu (100) is greater than Cu (110), however, the overall catalytic activity of Cu (110) is significantly better than Cu (100).[74,81]

Considering all the above research ideas related to crystal orientation and surface modification, it is agreed that the etching based technology and other modification methods could be useful for the preparation of nanocrystals with high energy facets or better active sites. Advanced techniques in modification of electrocatalyst surfaces not only enhance activity and selectivity for CO_2ER, but also allow for better exploring the reaction mechanism.

2.6. Composition

Numerous structural factors and properties have a great impact in electrocatalytic performance of Cu-based catalysts. In addition to structural factors, material composition has also a significant effect in CO_2ER due to its influence on reduction rate, activity and selectivity of products. It is known the that surface and bulk compositions of Cu–M are different, and can be evaluated by using XAS analysis.[82,83]

By changing the compositions of the alloy, it is possible to alter the degree of filling of the d band electrons and one can observe the effects for catalytic reduction of CO_2. Suppose in case of Cu–M alloy the substitution of Cu atoms to M metal lattice adds extra electrons to the lattice because Cu has a filled 3d band if M has an incompletely filled d band as it is proposed by electron band theory. This issue makes the Cu–M composition more active in catalysis than monocatalyst M. This might be one reason for enhanced catalytic activity of Cu-based alloys. In case of pure alloy only electronic factor is harmonized or involved for the enhancement of electrocatalytic reduction of CO_2. In "rigid" model of electronic structure of an alloy there is a single d band with no differentiation between atoms with regard to chemical bonding properties, which is considered as electronic properties. For bimetallic clusters, if one reaction needs a surface site consisting of a number of neighbor active metals while another requires a site consisting of only one active metal atom, the previous will be prone to include inactive foreign metal atoms on the surface of composition, when compared to the latter one. This indicates there is another property that can also affect or enhance the catalysis process in addition
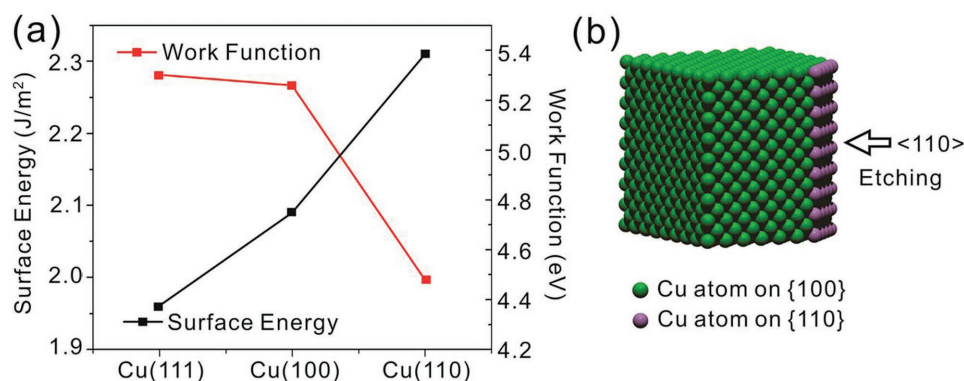
Figure 11. a) The three facets of copper expressed in terms of surface energy and work function, b) illustrations of etching effect on Cu (110) that hides low energy Cu (100) and activates the high energy Cu (110). Reproduced with permission.[74] Copyright 2016, American Chemical Society.

to electronic properties. That new property is called geometric property, which is originated from bimetallics in which Cu based electrocatalysts are applicable in this manner for CO_2ER to enhance selectivity and activity.[17,83] This issue is an interesting scenario and can be considered as one of the most promising field of study for future researchers.

According to Yang et al.[8] study bimetallics prepared in ordered monolayer are considered as a well-defined platform task and forwards to easily understand their fundamental catalytic activity including the reaction mechanism of CO_2. Therefore, the synthesis of monolayer composition of bimetallic or monometallic electrocatalyst rather than its bulk is an advanced and promising strategy to understand the reaction mechanism, and to identify reduction products during CO_2ER.[8] For example, the selectivity and activity of AuCu and Au_3Cu bimetallic are not the same since the electronic and geometric effects caused by two compositions are different (even if the overall metal loading is equal), and result in different types of products and faradaic efficiency in CO_2ER.[8,17,34]

In Takanabe and co-workers' study, CuIn exhibits better selectivity of CO formation and retard HER from CO_2 reduction than individual Cu or In electrocatalyst.[84] Referring the above ideas, we advise for future researchers to ensure whether the stability, selectivity and other performance of a bimetallic electrocatalyst might or might not be negatively affected, though the bimetallic one is expected to have higher activity.

Composition effect in terms of doped catalysts is related to the binding ability between the intermediate and the electrocatalyst surface, i.e., doping of an electrocatalyst with other foreign metal can modify the binding site or the active site of an electrocatalyst. In addition to the tuning of binding sites, doping species can enhance the active sites of an electrocatalyst, which increases activity and selectivity of reduction products. For

example doping nitrogen atom in to carbon based material performed by ammonia plasma treatment and the carbonization of nitrogen containing polymer are common activities. DFT studies reveal that metal doped porphyrin like graphene catalysts are good electrocatalysts for CO_2ER.[85] Studies showed that Rh, Co, and Ir functionalized graphene can reduce further CO into methanol with less overpotential than metal electrocatalysts.[82,86]

As a summary of composition we proposed a schematic diagram (**Figure 12**) without DFT calculations for CO_2ER on different compositions of Au and Cu nanoparticles (Au, Cu, AuCu, and $AuCu_3$) in which the binding strength of intermediates, adsorption ability of CO_2 and hydrogen into the surface of electrocatalysts and desorption ability of reduction products. The existence of different physical and chemical properties on the surface of each composition is arising from the electronic nature of Au, Cu, and synergistic (electronic and geometric) effect of bimetallics, i.e., AuCu and $AuCu_3$. Bimetallic composition of electrocatalysts can also determine its surface nature because the same compositions might have different surface property due to various distributions of atoms in the core and shell part of electrocatalyst that originates from alloying extent. Therefore, alteration of composition affects the surface of electrocatalysts and this leads to influence on the binding property between reduction intermediates and atoms on the electrocatalyst.

When the composition of Cu is dominant it is expected that the binding strength of hydrogen is higher and leads to the formation of hydrocarbons and alcohols, which are obtained from further reduction of CO and COOH. However, in the bimetallic electrocatalyst when the amount of Au is relatively higher than Cu, the binding strength of hydrogen, intermediates and CO_2 is weak that results easily desorption of significant amount of
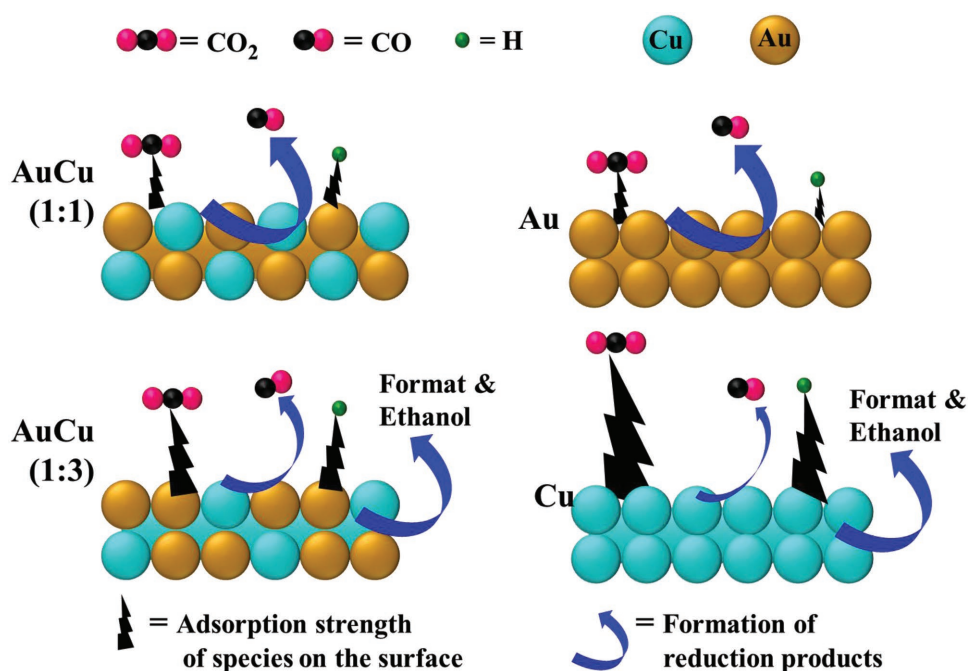
Figure 12. Schematic demonstrations for binding strength of reaction intermediates and desorption status of reduction products from the surfaces of each electrocatalyst composition.

**ADVANCED
SCIENCE NEWS**
www.advancedsciencenews.com

**ADVANCED
MATERIALS
INTERFACES**
www.advmatinterfaces.de

CO and COOH without further reduction. Therefore, we can conclude that the composition of electrocatalyst attributes the tuning of binding energy, which causes the variation of selectivity, activity and stability of the surface in CO_2ER due to the establishment of different or unequal number of active sites arises from synergistic effect, alloying extent, etc., which have different roles in the reduction activity.

3. Characterizations of Cu and Its Bimetallic for CO_2ER

3.1. General Description

Bimetallic nanoparticles are significantly dispersed species collected from atoms of two different metal elements. Formation of bimetallic nanoparticles is an important entities for the application of catalysis because it has high surface area and dispersion (ratio of atoms in the surface to total atoms in bimetallics) tendency.[87] Bimetallic physicochemical properties depend on atomic distribution or extent of alloying, segregation of atoms on the surface, homogeneity, structure and shape of nanoparticle. These entire phenomena have a significant impact on catalytic activity, selectivity and stability of nanoparticles of an alloy. Knowing the relationship between structure of electrocatalysts and the catalytic activity helps to understand the reaction mechanisms of catalysis due to the fact that catalysis is a highly surface sensitive scenario.[35,36]

Among them, XAS involving X-ray absorption near edge structure (XANES) and extended X-ray absorption fine structure (EXAFS) are considered as preferable and advanced characterization techniques of bimetallic and monometallic Cu-based electrocatalysts. Qualitative information such as electronic properties, oxidation state, d-band occupancy, fractional d-electron density and structural properties of each atom in the alloy can be depicted by XANES, while detailed information about the local atomic environment and absorbing atom due to the scattering and backscattering of neighbor elements can be revealed by EXAFS. The amplitude of EXAFS is proportional and refers to the number of nearby atoms, and the change of phase with the wavelength of photoelectron, which depends on the distance between the backscattering and the emitter atoms. EXAFS is also very essential to create structural models and to determine the sizes of nanoparticles of the alloy due to its high sensitivity to particle size and segregation of surface composition. However, it is insensitive to size of big particles larger than 10 nm and surface segregation of bulk metal alloy.[36,88,89]

Operando and in situ characterization methods are significantly useful in exposing or observing catalyst restructuring scenario as they can provide physical and chemical information under the reaction situations. In a certain phenomenon the reconstructed catalysts are subject to additional structural variation when the catalytic conditions stop. For this reason, operando characterization is an important task to detect an actual catalytically active species during CO_2ER.[57,90] In situ XAS characterization of electrocatalysts is also important to avoid undesired reaction or unnecessary transformation of catalysts through oxidation or reduction, which could have occurred due to exposure of atmospheric air during ex situ catalysis.

Therefore, EXAFS and XANES analyses of bimetallics during CO_2ER are preferable and used to understand the results obtained from the relationship between reduction parameters and XAS analysis directly. The formation mechanism of several bimetallic nanoparticles have been investigated by in situ/ *operando* XAS, which provides useful information to guide the design and synthesis of bimetallic nanocatalysts with various structures for targeted reactions like CO_2ER.[36,87,91]

Operando, in situ even ex situ characterization of Cu based bimetallics in CO_2ER has not been investigated and studied sufficiently so far. In the future, many researchers will focus on the gap for in-depth analysis and to propose catalytic mechanisms of bimetallic electrocatalysts of CO_2ER.

3.2. Structural Models for Cu–M Bimetallic Nanocatalysts Established by XAS

Qualitatively atoms in bimetallic/alloy can exist in various ways of structural models such as cluster-in-cluster, core-shell structure, alloy with an intermetallic compound type, random alloy, etc. In addition to qualitative analysis, Hwang et al.[35] have investigated the atomic distribution of each atom using XAS in alloy, which is denoted as A-B by estimating the number of coordination number of each atom (i.e., A in terms of B and B in terms of A) compared to total number of coordination.[35,92,93] Formulating structural parameter of XAS is a powerful way to determine distribution of atoms, i.e., extent of alloying (J_A and J_B) in AB system. Therefore, using the structural parameters the following mathematical expressions are applicable

$$P_{observed} = \frac{N_{A\text{-}B}}{\sum N_{A-i}} \tag{10}$$

$$R_{observed} = \frac{N_{B-A}}{\sum N_{B-i}} \tag{11}$$

$$J_A = \frac{P_{observed}}{P_{random}} \times 100\% \tag{12}$$

$$N_{Pt\text{-}Ru} = \frac{X_{Ru}}{X_{Pt}} N_{Ru-Pt} \tag{13}$$

where $N_{A\text{-}B}$ is ratio of scattering atoms B coordination number around absorbing A atom; N_{B-A} is ratio of scattering atoms A coordination number around absorbing B atom; $\sum N_{A-i}$ is the total coordination number of absorbing atom A; $\sum N_{B-i}$ is the total coordination number of absorbing atom B; $P_{random} = R_{random} = 0.5$ for ideal alloy in the ratio of A-B (1:1); and J_A and J_B are extent or distribution of alloying for atoms A and B respectively in alloy A–B.

Suppose, if the ratio of an alloy A–B is perfectly (1:2) then, $P_{random} = 0.67$ and $R_{random} = 0.33$, while $2N_{A-A} = N_{A-B}$, $N_{B-B} = 2N_{B-A}$, which is calculated using the above formulae. Therefore, the structural models can be proposed based on the structural parameters obtained from XAS (EXAFS) and extent of alloying, which is computed using Equations (11)–(14).
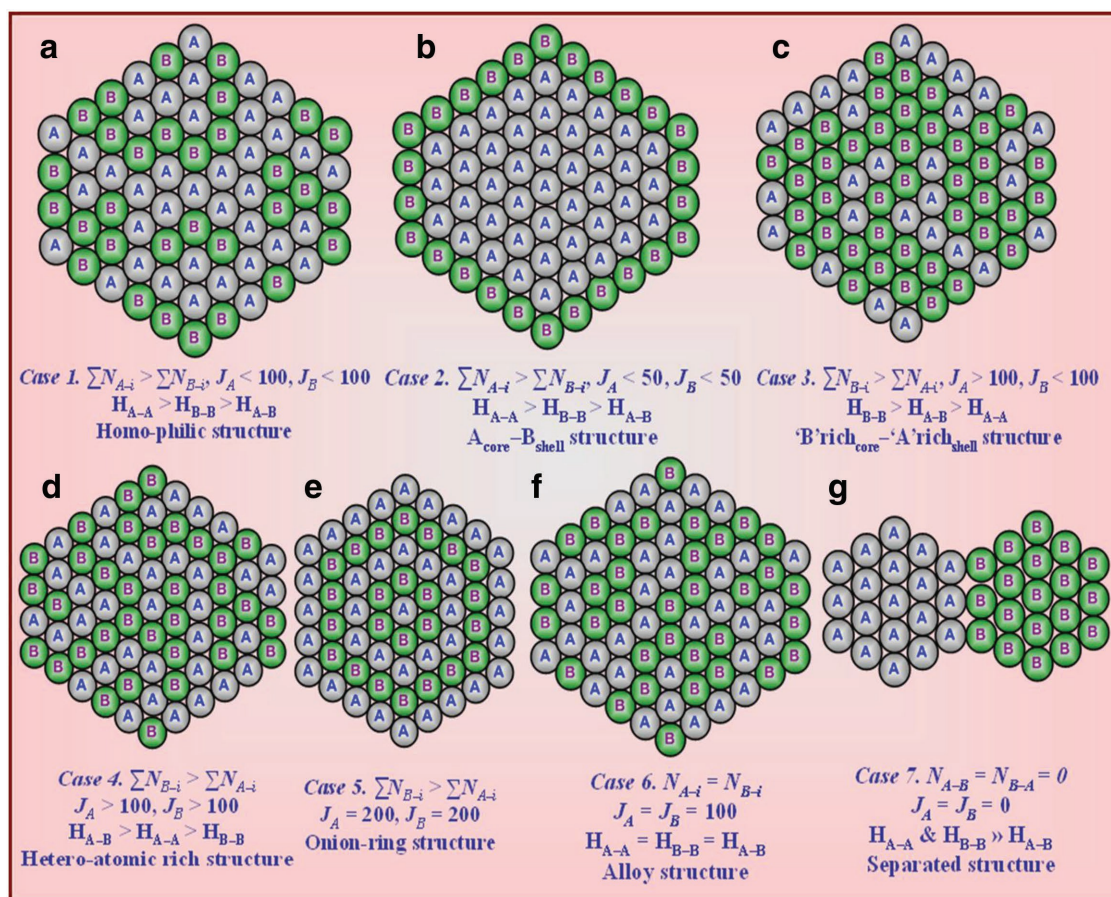
Figure 13. Illustrations of structural models of alloy/bimetallic nanoparticles at different extent of alloying or degree of alloying in terms of each case. Reproduced with permission.[35] Copyright 2005, American Chemical Society.

Accordingly, the specified cases, there are seven possible structural models indicated in **Figure 13**, but it is possible to establish unlimited possible cases regarding the extent of alloying based on real parameter/conditions. The seven possible cases are indicated below and each model is concisely shown under the figure.

All structural models influence the catalytic activity due to alterations of physic-chemical properties of nanoparticles. By considering extent of A and B in alloying, the nature of metallic interactions is an important scenario in equilibrium state. The other cases of metallic interactions are: $H_{A–A}$ (homoatomic interaction of atom A), $H_{B–B}$ (homoatomic interaction of atom B), $H_{A–B}$ or $H_{B–A}$ (heteroatomic interaction of A and B). Therefore, by considering all the above-mentioned parameters and information it is possible to clarify the seven cases one by one.[35,92,94]

✓ **Case 1**: $J_A = J_B = 0$, indicates atoms A and B do not involve in alloy formation, instead they form an independent or phase-separated cluster (Figure 13a).
✓ **Case 2**: $J_A = J_B = 100\%$, implies both A and B are fully participated in alloy formation (Figure 13b).
✓ **Case 3**: $J_A < 100\%$ and $J_B < 100\%$. In this case homoatomic interaction is more preferable than heteroatomic interactions (Figure 13c).
✓ **Case 4**: $J_A > 100\%$ and $J_B < 100\%$, this pointed out that both A and B prefer atom B than A (Figure 13d), implies segregation
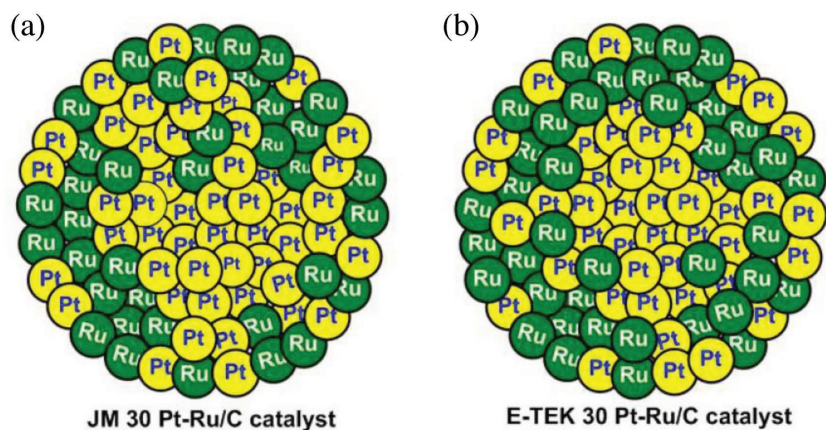
of B is dominant, and vice versa will happen if $J_B > 100\%$ and $J_A < 100\%$.
✓ **Case 5**: $J_A > 100\%$ and $J_B > 100\%$, this specifies that heteroatomic interactions (A–B) are more preferable than homoatomic (A–A) or (B–B), which means enhancement of distributions of both atoms (Figure 13e).
✓ **Case 6**: $J_A < 50\%$ and $J_B < 50\%$, in this case atom A can act as a core while B is a shell also implies that the total coordination number of atom A is higher than that of B (Figure 13f).
✓ **Case 7**: $J_A = 200\%$ and $J_B = 200\%$, tells that atom A prefers B or atom B prefers A, which results in an onion ring like structure model of an alloy (Figure 13g).

According to the cases mentioned, Hwang's team has compared the extent of alloying of his established structural model to the actual prepared bimetallic alloys such as Pd–Au, Pd–Pt, and Cu–Pd, which are selected from other literatures.[36,87,88,91,95,96] The structural model offers an applicable and experimentally agreeable approach to correlate the actual electrocatalytic performance with the coordination numbers and alloying extent of bimetallic elements in bimetallic nanoparticles.

Hwang et al.[35] have also studied the alloying extent of Pt–Ru (1:1) including qualitative and quantitative analysis of an alloy via EXAFS of Pt L3-edge and Ru K-edge based on the model structure established by the group (**Figure 14**a), also they compared

ADVANCED
SCIENCE NEWS
www.advancedsciencenews.com

ADVANCED
MATERIALS
INTERFACES
www.advmatinterfaces.de

(a)

JM 30 Pt-Ru/C catalyst

(b)

E-TEK 30 Pt-Ru/C catalyst

Figure 14. Structural models for Pt–Ru/C catalysts based on XAS parameters: a) a 20% Pt/10% Ru supplied by Johnson-Matthey (JM 30), and b) a 20% Pt/10% Ru supplied by E-TEK (E-TEK 30). Reproduced with permission.[35] Copyright 2005, American Chemical Society.

the parameters to literatures or references. From JM30 Pt–Ru/C catalyst, the calculated coordination numbers of Pt and Ru around Pt were 5.6 ± 0.3 and 1.4 ± 0.1 respectively with total coordination number of Pt 7, while the coordination number of Ru and Pt around Ru were 3.4 ± 0.2 and 2.2 ± 0.3 respectively with total coordination number of Ru 5.6. Furthermore, the calculated $P_{observed}$ and $R_{observed}$ of JM30 Pt–Ru/C were 0.2 and 0.39, respectively, and its J_{Pt} and J_{Ru} were calculated and were 40 and 78%, respectively. Additionally, the same type of computations with different values of all parameters obtained for the catalyst E-TEK 30 Pt–Ru/C (Figure 14b). In this composition the coordination numbers of Pt and Ru around Pt are 6.2 ± 0.3 and 0.9 ± 0.1 respectively with total coordination number of Pt 7.1, while coordination numbers of Pt and Ru around Ru were 3.7 ± 0.2 and 1.2 ± 0.2 respectively with total coordination number of Ru 4.9, and its J_{Pt} and J_{Ru} were 26 and 48% respectively. Since the total coordination number of Pt in both catalyst is higher than that of Ru, and $J_{Ru} > J_{Pt}$ indicates catalysts were Pt rich in the core and Ru rich in the shell structure as clearly shown in Figure 14. Increased J_{Pt} and J_{Ru} in JM 30 catalyst compared to E-TEK 30 indicates that it has facilitated atomic distribution in the alloy and confirms enhancement of homogeneity of nanoparticles (Pt and Ru) and its catalytic ability than E-TEK 30 Pt–Ru/C.

This scenario is assured by analyzing oxidation of methanol and CO stripping voltammetry on both bimetallics, which results JM 30 can oxidize CO at low onset potential and also generate higher current density at the same potential via chronoamperometry than E-TEK 30 catalyst.[35,36] In short, according to the above results it is possible to say the catalyst JM 30 Pt–Ru/C is electrocatalytically better than E-TEK 30 Pt–Ru/C. The implication is JM 30 is a superior tendency for oxidation process. It is also expected that the alloying extent or atomic distribution in bimetallic nanocatalysts will also play important role in CO_2ER.

3.3. Surface Composition and Characterization of Bimetallic Electrocatalysts

In addition to the alloying extent and structure, knowledge of both the surface composition of bimetallic nanoparticles

(bi-MNPs) is also important in catalysis; and understanding of the phenomena occurring at the particle's surface is crucial. Several theoretical approaches using thermodynamic models, or first-principles calculations, have been used to predict the surface composition of bi-MNPs. As the surface composition of bi-MNPs depends on their size, structure, bulk composition, substrate interaction, and preparation conditions it is very difficult to theoretically predict the surface composition of bi-MNPs. Although several experimental methods have been developed, determining the surface compositions of bi-MNPs (and even bulk alloys) remains problematic. Surface-sensitive techniques such as electron spectroscopy for chemical analysis, secondary ion mass spectrometry (SIMS), ion scattering spectroscopy, X-ray photoelectron spectroscopy (XPS), and Auger electron spectroscopy (AES) have given reasonably good estimates of the surface compositions of bulk or thin- film alloys. However, these techniques have severe limitations when used to analyze the surface compositions of bi-MNPs. For example, due to the escape depth of the Auger electrons and photoelectrons, the application of AES and XPS to particles with diameters of 30 nm is restricted. Although SIMS offers depth information in the range of 10 to 20 nm, it does not provide the spatial resolution of electron beam techniques such as SEM and TEM. In addition, these techniques are destructive, thus the nanoparticle's surface composition or structure may be changed during analysis. Infrared spectroscopy and selective chemisorption can be employed to determine the surface compositions of some specific bi-MNPs. Moreover, it is hard to extend these two techniques to other bi-MNPs systems due to lack of system specific adsorbates. Hwang's group recently proposed a general methodology by combining extended EXAFS analyses and modeling calculations. The proposed methodology enables us to deduce the surface composition of bi-MNPs from experimental data directly and to estimate the surface composition under real conditions. The ability of the present approach makes it a unique tool in our quest to understand the physical and chemical properties of NPs.[35,36,87,96]

By knowing only the basic crystal structure (fcc, bcc, etc.) it is possible to write the equations for the surface compositions of bi-MNPs in terms of measurable quantities. The methodology was demonstrated using bi-MNPs with an fcc structure. The equations for surface composition (X^s_A, X^s_B) of an A-B bi-MNPs system with an fcc structure can be given as follows

$$X_A^s = \frac{x\left(\sum N_{A-i} - 12\right)}{x\left(\sum N_{A-i} - 12\right) + (1-x)\left(\sum N_{B-i} - 12\right)} \tag{14}$$

$$X_B^s = \frac{(1-x)\left(\sum N_{B-i} - 12\right)}{(1-x)\left(\sum N_{B-i} - 12\right) + x\left(\sum N_{A-i} - 12\right)} \tag{15}$$

**ADVANCED
SCIENCE NEWS**

www.advancedsciencenews.com

**ADVANCED
MATERIALS
INTERFACES**

www.advmatinterfaces.de

where $\sum N_{A-i}$ and $\sum N_{B-i}$ represent the total coordination numbers around absorbing atoms A and B, respectively. We can determine the total coordination numbers of A and B, $\sum N_{A-i}$, and $\sum N_{B-i}$, from EXAFS measurements, and the bulk composition (x) from the edge jump in XANES measurements. In order to obtain the sample's precise surface composition, it is necessary to ensure that it is free from secondary phases such as oxides during XAS measurements. Once $\sum N_{A-i}$ and $\sum N_{B-i}$ are determined, the surface composition of the nanoparticles can be obtained from Equations (15) and (16). The developed methodology has been successfully demonstrated in various systems. The method can be not only used to characterize the surface compositions of various bi-MNPs under reaction conditions but also be extended to ternary nanoparticles.[35,36] By harmonizing those principles, it is predicted and expected that the above alloying extent and surface composition analyzed by XAS are also applicable to other bimetallic such Cu-based electrocatalysts for CO_2ER.

For analysis of Cu and Cu-based bimetallic electrocatalyst, XRD can clarify the characteristic pattern of each atom in alloy or as monometallic crystal phase while EDX and XPS can reveal the composition of nanoparticles with further information of electronic property obtained from XPS.[8,36,97] There are lots of types of characterizations that can provide information about the structure and order-disorder transformation scenario. Yang et al. have synthesized and investigated ordered and disordered arrangements of AuCu nanoparticles using high-angle annular dark field (HAADF)-scanning transmission electron microscopy (STEM) for the purpose of CO_2 reduction. It is identified that in the ordered arrangement of the alloy, layer of three atoms of gold in the ordered lattice are obtained in addition to the whole ordered phase crystal structure throughout the intermetallic surface (**Figure 15**a–e). The intensity profiles of Au and Cu have also shown in HAADF-STEM images (Figure 15f,g).[36]

Yang et al. in their another research topic they studied to know the structure of ordered and disordered AuCu nanoparticle using EXAFS by analyzing Cu K-edge and Au L3-edge (Figure 15h,i).[34] Both Cu K-edge and Au edge revealed the ordered structure have larger amplitude at the first shell scattering than the disordered one.[34] Interestingly, at 3rd and 4th shell scattering of Cu K-edge, which is indicated in the radial distance between 4–6 Å detected clearly and that shows the unique property of multiple scattering on Cu metal. This
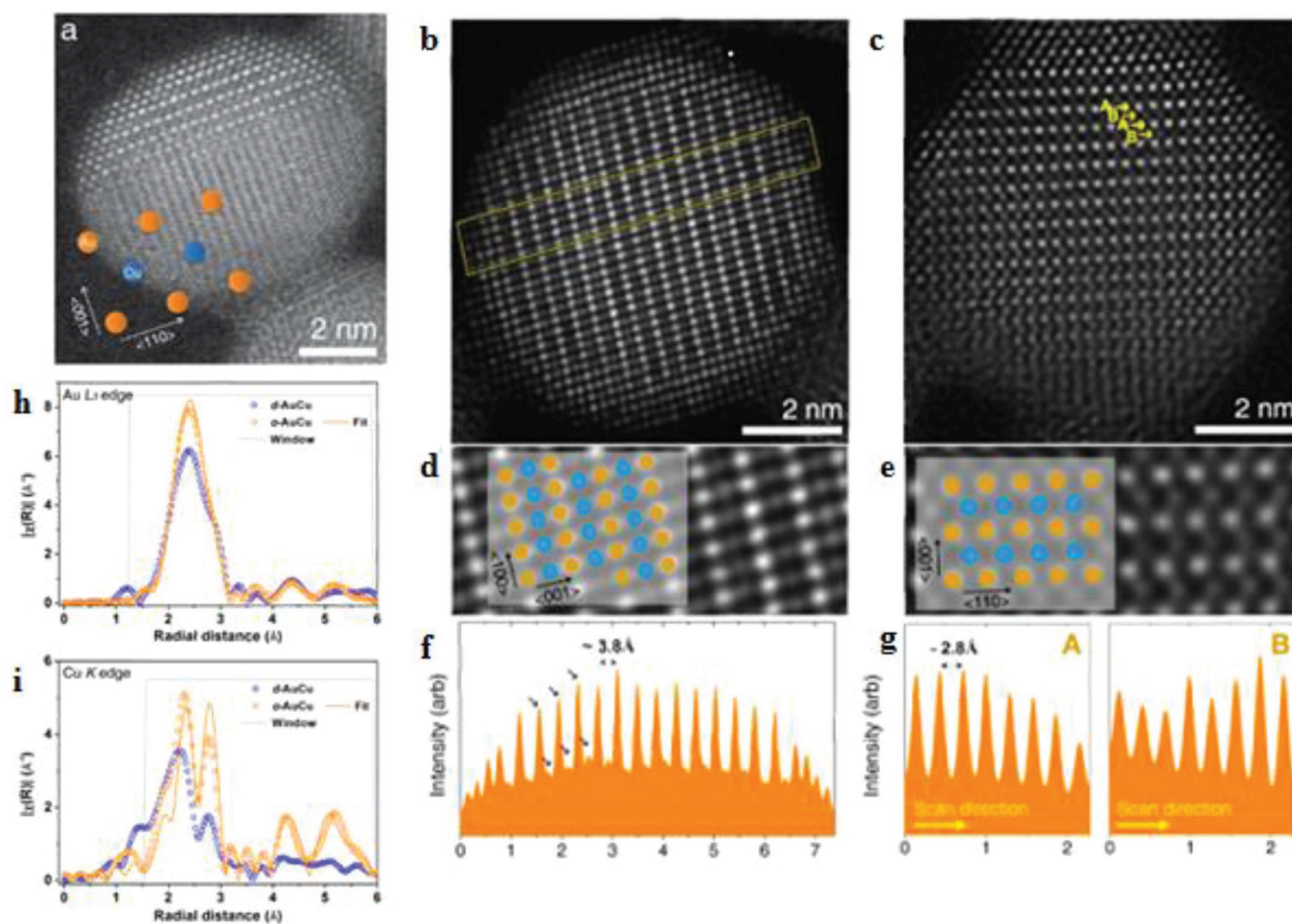
Figure 15. Aberration-corrected HAADF-STEM a) images of single lattice of ordered AuCu, b,c) wide images of ordered AuCu using HAADF-STEM projections, d,e) magnified from (b) and (c) images, f) intensity profile from image a indicates the larger intensity is Au while small one is Cu, g) average intensity profile from the inner to outer surface indicated at image (b) for arrows A and B, and the gap between separation between strong intensity refers to Au. h,i) Cu K-edge and Au L3-edge from peak XAS (EXAFS) of ordered and disordered AuCu NPs. Reproduced with permission.[34] Copyright 2017, American Chemical Society.

**ADVANCED
SCIENCE NEWS**
www.advancedsciencenews.com

**ADVANCED
MATERIALS
INTERFACES**
www.advmatinterfaces.de

property might be the possible reason for reduction of CO_2 into various types of products on AuCu NPs. Disordered structure of each edge on AuCu was characterized by small amplitude, destructive interference and multiples of scattering paths at different lengths. Therefore, the final findings for analysis of ordered AuCu by XAS and HAADF-STEM leads to the coordination environment surrounding both atoms (Au and Cu), which indicates that Au has less coordination number (relatively uncoordinated) than Cu at each lattice.[34,87,98] This implies that ordered AuCu has high coverage of Au atoms and easily exposed for reduction of CO_2 and results in better catalytic ability than the disordered alloy. Therefore, structural arrangement of atoms in electrocatalysts has a great role in selectivity and activity in CO_2ER.

Ma et al. have investigated Cu and Pd distribution using EXAFS and XANES in bimetallic of both $Pd_{85}Cu_{15}$ and $Pd_{56}Cu_{44}$ compositions, which are prepared for selective CO_2ER into CO (**Figure 16**). In XANES spectra of Pd K-edge both Pd foil and Pd atoms from both bimetallic have similar features (Figure 16a), which indicate that the dominant amount of Pd atoms in both bimetallic compositions. However, Cu K-edge (Figure 16b) in XANES spectra depicts there is an oxidation of Cu into CuO and Cu_2O. This is because Cu NP is susceptible for oxidation in air or in aqueous media. The degree of oxidation is significant at $Pd_{56}Cu_{44}$ due to higher amount Cu existed in $Pd_{56}Cu_{44}$ than $Pd_{85}Cu_{15}$. To be familiar with the structure of PdCu

bimetallic in both compositions, EXAFS spectra at Pd K-edge (Figure 16c,e) and Cu-K edge (Figure 16d,f) are essential. In the first coordination shells of both bimetallic compositions Pd can be influenced by scatterings of Pd—O while Cu is influenced by Cu—O. According to this result one can predict and perceive that the absence of Pd—O bond on $Pd_{85}Cu_{15}$ would probably due to less amount of Cu leads to less susceptible to oxygen to form copper oxides implies insignificant impact on Pd to form PdO. However, in case of $Pd_{56}Cu_{44}$ there is more Cu, potentially it forms significant amount of Cu—O, which contributes to form a bond with Pd for the formation of Pd—O.

EXAFS peaks confirm that Pd atom are enrich in the environment due to the higher amount of ratio of $N_{Pd–Pd}/N_{Pd–Cu}$ and $N_{Pd–Cu}/N_{Cu–Cu}$ than composition of Pd/Cu due to some amount Cu is occupied with oxygen. When the composition of Cu increases the scattering of Pd–Cu and Cu–Cu is higher. The selectivity of CO_2 reduction to CO using Pd was 16%, but the selectivity drastically increases to 86 and 73% using $Pd_{56}Cu_{44}$ and $Pd_{85}Cu_{15}$ respectively at −0.89V versus RHE. This scenario helps to explain why bimetallic are highly selective electrocatalyst in CO_2ER than monometallic catalysts at specified potential in which the expected and interested reduction product is formed.[56,91]

Camilo et al. have studied in situ XAS analysis of XANES and EXAFS spectrum of Cu K-edge for the electrocatalysts of Cu_2O–Cu/C and Cu_4Sn/C for the aim of selective CO_2ER into
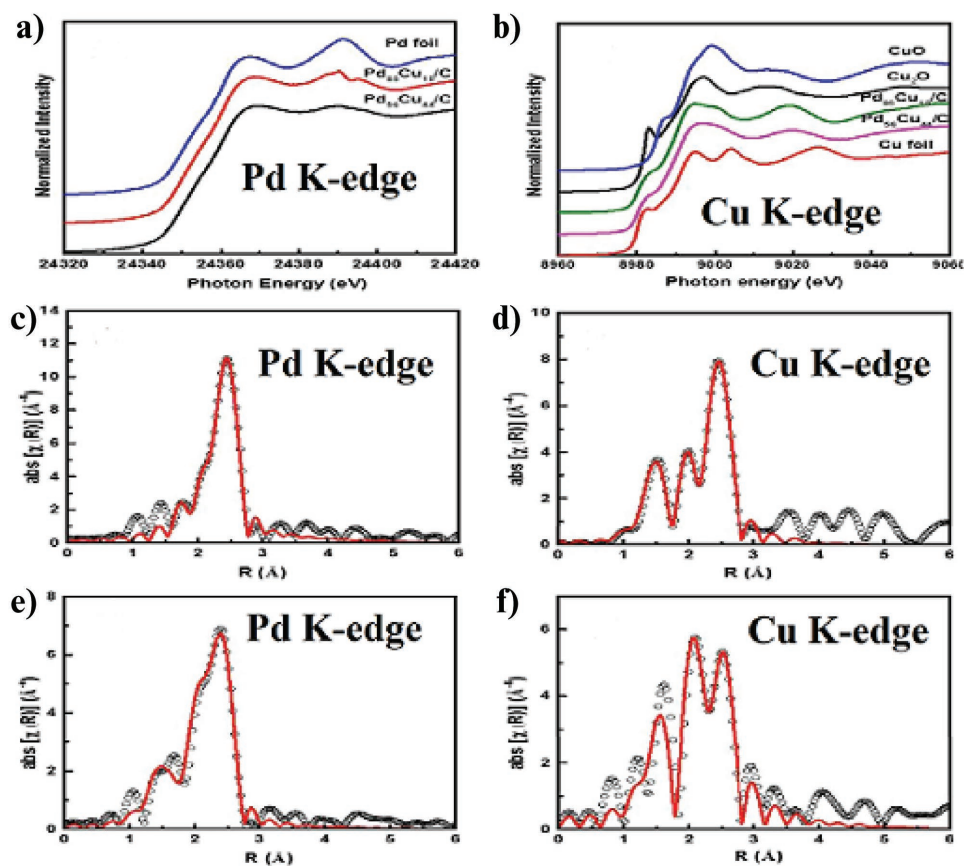
Figure 16. XANES spectra of a) Pd K-edge, b) Cu K-edge in $Pd_{56}Cu_{44}$ and $Pd_{85}Cu_{15}$ bimetallic compositions after heat treatment with H_2, c) Pd K-edge, d) Cu K-edge of $Pd_{85}Cu_{15}$, e) Pd K-edge, and f) Cu K-edge of $Pd_{56}Cu_{44}$ from EXAFS peaks. Reproduced with permission.[91] Copyright 2016, Elsevier Ltd.
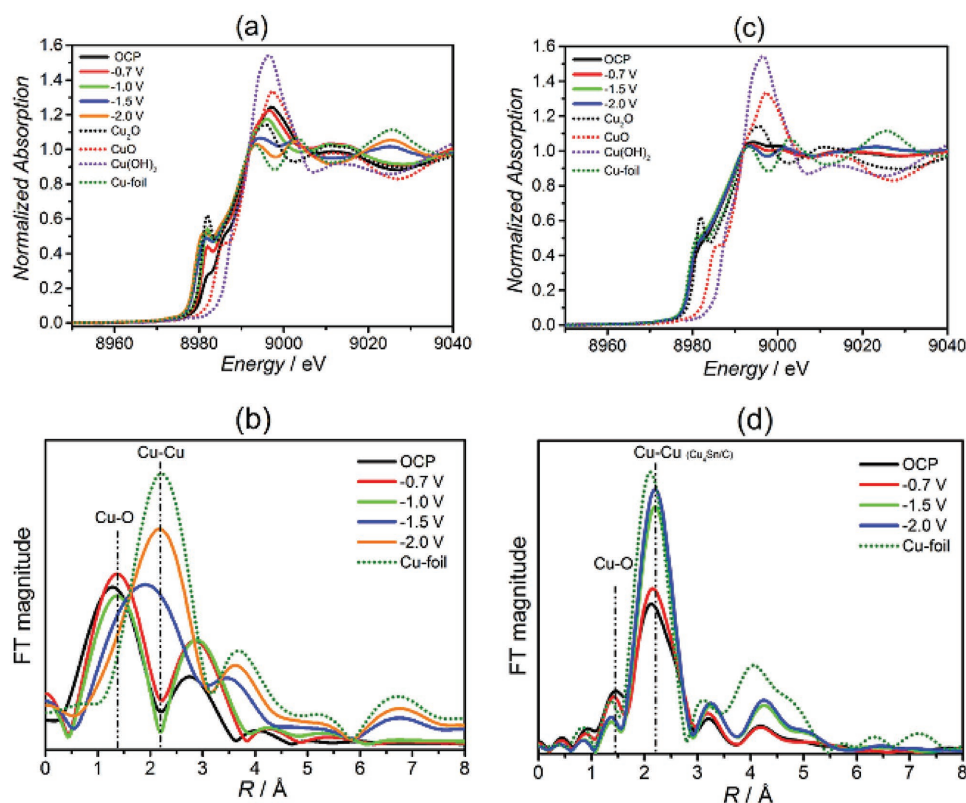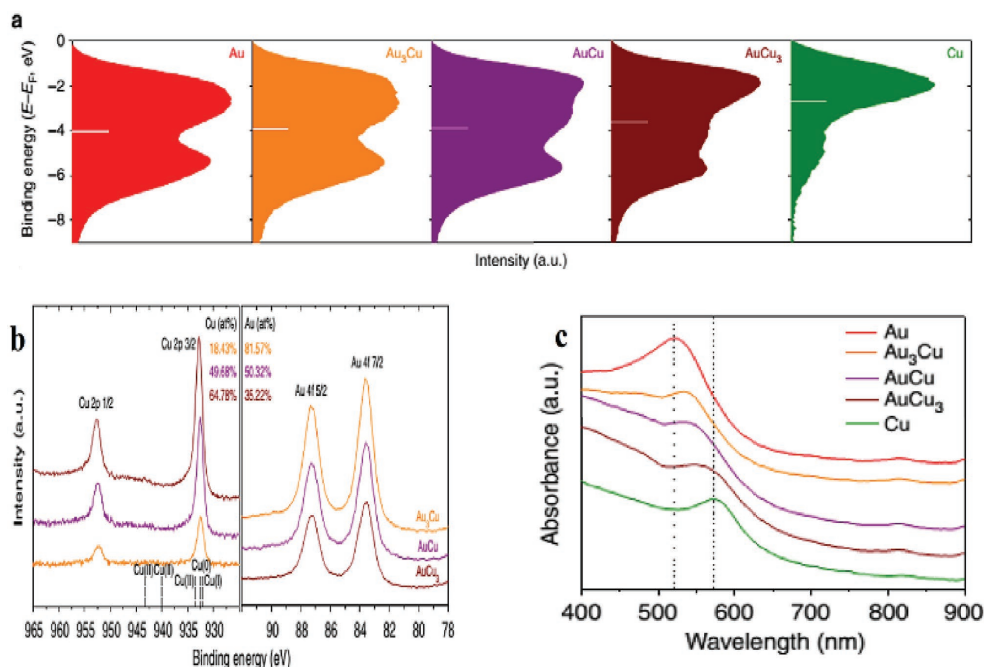
Figure 17. In situ XAS analysis of a,b) Cu K-edges of XANES and EXAFS spectra from Cu2O–Cu/C, and c,d) Cu K-edge XANES and EXAFS spectra of Cu4Sn. Reproduced with permission.[96] Copyright 2017, Sociedade Brasileira de Química

CO. During in situ analysis, CuO, Cu_2O and $Cu(OH)_2$ are used as references materials (**Figure 17**). From XANES peak depicted in Figure 17a, it is reported that at open circuit potential (OCP) the prepared electrocatalyst (Cu_2O–Cu/C) is similar to Cu_2O, but when the potential swift from OCP to −2 V there is alteration of Cu_2O into Cu metallic state and becomes similar to the reference materials. The same pattern appears at EXAFS (Figure 17b) confirms the transformation of Cu−O bond to Cu−Cu metallic bond upon the potential change. This transformation of electronic states of Cu from the as-prepared Cu_2O to Cu metallic form indicates there was CO_2 reduction during in situ XAS process with in specified potentials because metallic form of Cu can reduce CO_2 easily than Cu oxides. Significant change was not observed in the XANES of Cu K-edge for Cu_4Sn (Figure 17c). However, in the EXAFS of Cu K-edge intensity of Cu−O bond is too low and the bond length of Cu−Cu from Cu_4Sn is shifted slightly to higher value compared to the bond length of Cu−Cu from Cu-foil. This indicates there is a tensile strain at Cu−Cu bond from Cu_4Sn, which is an important scenario causing strain by inserting Sn atoms. Another interesting scenario in Figure 17d depicted decreased intensity of Cu−O and increased Cu−Cu intensity when the potential was increasing from OCP to −2V. The observation indicates that initially the as-prepared Cu_4Sn was covered by oxides and then gradually it was eliminating and metallic Cu and Sn were replaced (gradually Cu−O was decreased and replaced with Cu and Sn) with alterations of applied potentials via in situ XAS process in CO_2ER at OCP, −0.7, −1, −1.5 and, −2 V.[96]

Highfield et al. have prepared RuCu bimetallics via variation of annealing temperature for the purpose of CO_2ER and characterized the alloy by XAS. Among three prepared compositions ($Ru_{22}Cu_7$, $Ru_{17}Cu_{12.5}$, and $Ru_{10}Cu_{20}$), which is analyzed by XANES of Cu K-edge the level of oxidation of Cu is significant at $Ru_{22}Cu_7$, which implies that majority of Cu can exist in the form of Cu(I) oxidation state, i.e., it resembles the reference of Cu_2O. Upon increasing annealing temperature with H_2 the oxidation state decreases due to the reduction of Cu_2O into Cu metallic state. Ru K-edge (not shown here) explains the degree of oxidation of Ru at $Ru_{10}Cu_{20}$ is slightly higher than $Ru_{22}Cu_7$, but the effect of annealing temperature is insignificant for variation of oxidation state of Ru.[95]

UV–visible spectroscopy is also an important analytical tool to characterize alloy nanoparticles with surface plasmonic characteristics. From research of Yang et al. it is revealed that binding energy of each bimetallic and monometallic compositions (**Figure 18**a) a characteristic XPS peaks (Figure 18b) and characteristic plasmon resonance peaks at specified wave length, i.e., ≈523 and ≈570 nm (Figure 18c) for confirmation of each atom in all compositions and to understand change of binding ability through variation of compositions of atoms. Absorbance peaks of UV-visible spectroscopy for bimetallic (Au_3Cu, AuCu, and AuC_3) are in between Au and Cu monometallic electrocatalysts. While changing compositions of atoms in monometallic and bimetallic, the appearance and disappearance of absorbance peaks indicates that each composition has a characteristic UV-visible spectrum peak.[8]

ADVANCED
SCIENCE NEWS

www.advancedsciencenews.com

ADVANCED
MATERIALS
INTERFACES

www.advmatinterfaces.de

Figure 18. a) Binding energy taken from Surface valence band photoemission spectra of all types of compositions of (Au, Au$_3$Cu, AuCu, AuCu$_3$, and Cu) with respect to center of gravity shown the white line it reveals binding ability of electrocatalysts, b) XPS spectra, and c) UV–visible absorbance peak of all bimetallic and monometallic atoms of Au and Cu. Reproduced with permission.[8] Copyright 2014, Springer Nature.

4. Reduction Mechanisms of CO$_2$ER
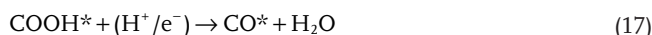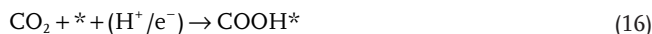
4.1. Overview of Reduction Mechanism

Even though there are plenty of mechanisms of CO$_2$ electroreduction, which have been proposed by various researchers, we have concisely compiled in this review the most interested, recent and reasonable ideas that agree to experimental approach using Cu and its bimetallic.

Investigations of CO$_2$ER mechanism via metal electrocatalysts specially on Cu surface is so far in infancy stage, however, it has been proposed numerous possible reduction steps and pathways better than other metal electrocatalysts. Consequently, intensive theoretical and experimental studies must be performed to discover the most appropriate, acceptable and reasonable reaction mechanisms. Many researchers have been predicted the possible mechanisms based on their experimental/theoretical views and DFT calculations. However, the reaction mechanisms are still under in controversial and debate due to different proposed ideas by various researchers.[17,49,51,99]

Some researchers have tried to explain the type of products obtained corresponding to each electrocatalyst including adequate description for the relationship between reduction intermediates and final products in CO$_2$ER. Variation of reduction products is mainly due to the binding strength between intermediates and the catalyst, which can be determined or proposed with or without DFT calculations that depends on the argument or the hypothesis of the researcher related to the whole processes of the experimental activity and the findings.[10,26,100]

4.2. Proposed Reductions Mechanisms from Selected Literatures

Ren et al.[10] have explained the reaction mechanism for conversion of CO$_2$ into C$_2$H$_4$ and C$_2$H$_5$OH upon enhanced coupling of C$-$C bond formation from combination of C1 species on the surface of Cu through electron transfer, hydrogenation, adsorption in the form of CO and eventually the adsorbed CO further reduced to CH$_4$ and C$_2$H$_x$O$_2$ intermediates to obtain the final product (C$_2$H$_4$ and C$_2$H$_5$OH). Peterson et al.[101] have newly investigated many different reaction paths via density functional theory by identifying the common reaction intermediates by selecting the low energy electrochemical conversion of CO$_2$ to CH$_4$ on Cu(211) surface, which are mentioned in Equations (17)–(24)

$$CO_2 + * + (H^+/e^-) \rightarrow COOH* \tag{16}$$

$$COOH* + (H^+/e^-) \rightarrow CO* + H_2O \tag{17}$$

$$CO* + (H^+/e^-) \rightarrow CHO* \tag{18}$$

$$CHO* + (H^+/e^-) \rightarrow CH_2O* \tag{19}$$

$$CH_2O* + (H^+/e^-) \rightarrow CH_3O* \tag{20}$$

$$CH_3O + (H^+/e^-) \rightarrow O* + CH_4 \tag{21}$$

$$O* + (H^+/e^-) \rightarrow OH* \tag{22}$$

$$OH* + (H^+/e^-) \rightarrow * + H_2O \tag{23}$$

**ADVANCED
SCIENCE NEWS**

www.advancedsciencenews.com

**ADVANCED
MATERIALS
INTERFACES**

www.advmatinterfaces.de

The * refers to the adsorbed intermediate or active site of the electrocatalyst surface, which is represented as $C_xH_yO_z$* where $x = 0$ or 1, $y = 0$–4, $z = 0$–2. Among all reaction steps mentioned above, the third one (Equation (19)), which requires high positive change of free energy, is confirmed as a step that needs large overpotentials for electroreduction of CO_2 and is indicated as a rate determining step.[101,102] Therefore, understanding of the nature of adsorption, change of binding energy through analysis of electronic structure in terms of charge density, local density of states, atomic charge, etc., in the absence or presence of adsorbates helps to predict the reaction mechanism of CO_2 reduction.

Hirunsit et al. and others,[102–104] have also investigated electroreduction of CO_2 on copper based alloys (Cu_3Ag, Cu_3Co, Cu_3Ir, Cu_3Pt, Cu_3Rh, Cu_3Pd, Cu_3Au, and Cu_3Ni) into methane and methanol with brief reaction steps and paths by DFT calculations. In general, their DFT calculations have shown the protonation of CO_2 to form HOCO*, then HCOOH is obtained from protonation of HOCO* or CO* in aqueous media. In other way, the conversion of CO* to HCO*/COH* is conducted and eventually the formation of methane and methanol from these intermediates can be carried out. Other research investigations revealed by DFT calculation of the kinetic barrier of CO_2 reduction that shows the selectivity step for methane versus methanol on Cu(111) occurs with hydrogenation of CO* to COH*, which yields either CH_4 or C_2H_4 while CHO* produces CH_3OH. In other research views and understanding, once COH* is formed, and then reduced to C*, and finally converted to CH_4 and C_2H_4 through dimerization of C—C coupling without electron transfer.[51,102,103,105–107]

Lu et al. have studied types of products obtained in CO_2 reduction corresponding to each transition metal catalyst mainly

in the formation of formic acid. They proposed (**Figure 19**) the general reaction paths using different metal catalysts required for each reduction products with brief identification of reaction intermediates.[43,100,103]

Furthermore, other researchers also describe based on DFT calculations in which the reduction of CH_2* to CH_3* is a potential barrier for the formation of ethylene. On the other hand, selective formation of CH_4 and C_2H_4 depends on morphology (crystalline structure) of copper metals.[85,107,108] Others depicted that production of both CH_4 and C_2H_4 is kinetically and thermodynamically favorable from CH_2* intermediate via Cu(211) surface by considering CH_4 is a favorable product.[51,53,103,105,106] Therefore, from many investigations CH_2* is a common reaction intermediate for the formation of both CH_4 and C_2H_4.

Xie et al. have investigated the reduction mechanism of CO_2 into CH_4 and then C_2H_4 is formed through two steps. Initially, CO is formed before obtaining CH_4 and eventually converted into C_2H_4 by the help of dimerization.[109] Among many intermediates and products, formic acid is one of the common products of CO_2 reduction on Cu surface. However, many studies have investigated that formic acid cannot be reduced to other products, suggesting that the reduction pathway toward formic acid is thus different from hydrocarbon formation pathway.[44,53,108,110,111]

Hori et al. explained some parameters that affect CO_2ER during the formation of methane and ethylene. The formation of CH_4 from CO is pH-dependent. In addition, the formation of ethylene is more favorable at less negative potential without simultaneous formation of CH_4 on copper surfaces. Independent experimental studies and DFT calculations by Hori et al. and Kortlever et al. proposed the reduction mechanisms
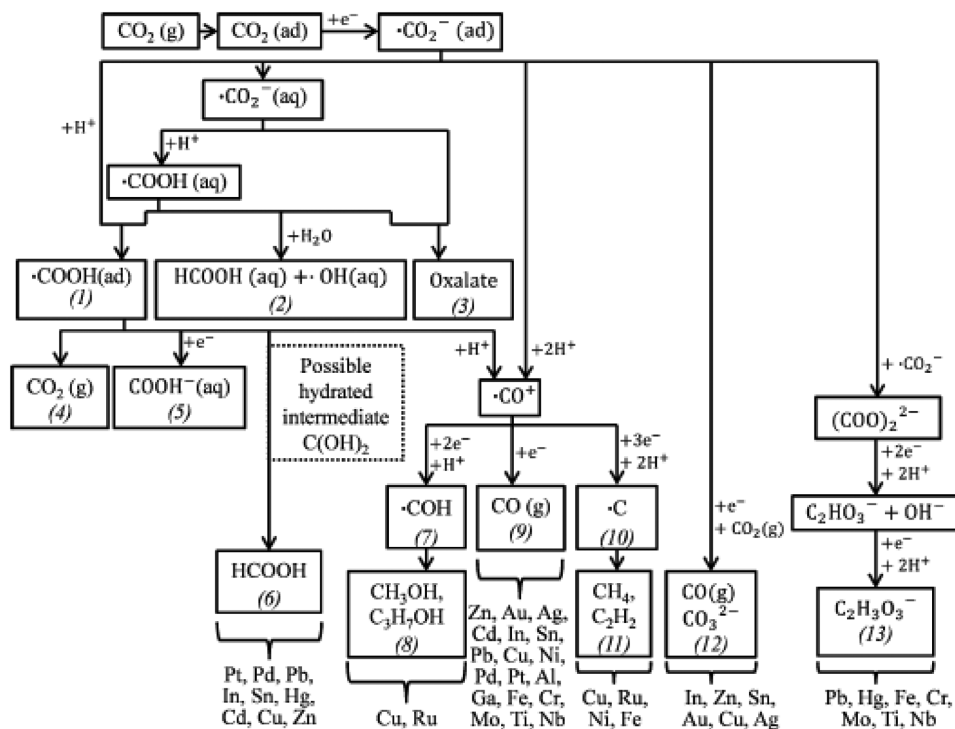

Figure 19. Reduction pathways of electrochemical reduction of CO_2 on various types of electrocatalyst for the corresponding, reduction products and reaction intermediates. Reproduced with permission.[100] Copyright 2014, John Wiley and Sons.

of CO_2 to the perspective products like methane, ethylene, methanol, formate and ethanol, which are shown schematically in **Figure 20**.[110,112] Nie et al. have also proposed the general reaction mechanism of CO_2 reduction on Cu(111) into COOH, CO, CH_3OH, CH_4, and C_2H_4 via the formation of COH* and CHO* intermediate both originated from CO*.[51]

Kuhl et al. have revealed the formation of the possible C1, C2, and C3 hydrocarbons and its derivatives with predicted reduction mechanism of CO_2ER on Cu surface. Plausible reaction mechanism (not indicated the graph) has been proposed to perceive the formation of C2 and C3 compounds and also to understand which species are involved to establish C−C bond to produce those C2 and C3 molecules such as ethylene and propylene in the reduction process. In each electrochemical reaction step there is protonation of $2H^+$ and transfer of two

electrons to replace hydroxyl group by hydrogen for further reduction of reaction intermediate species. However, it is not clear which C1 or C2 species is responsible to form C−C coupling for the formation of C2 or C3 compounds.[17,102,113]

Peterson et al.[102] have established an elegant method based on the computational hydrogen electrode (CHE) model integrated with DFT calculations to answer how copper catalyzes uniquely to generate various reduction products from CO_2. Why copper need a large over potential to reduce CO_2? Other questions were also addressed in this investigation. Using the above model techniques, pathways of electrochemical reaction, the potential requirement and estimation of free energy for each intermediate state have been manipulated. The CHE model was applicable for many different intermediates on Cu(211) surface through the reduction process of CO_2 in which
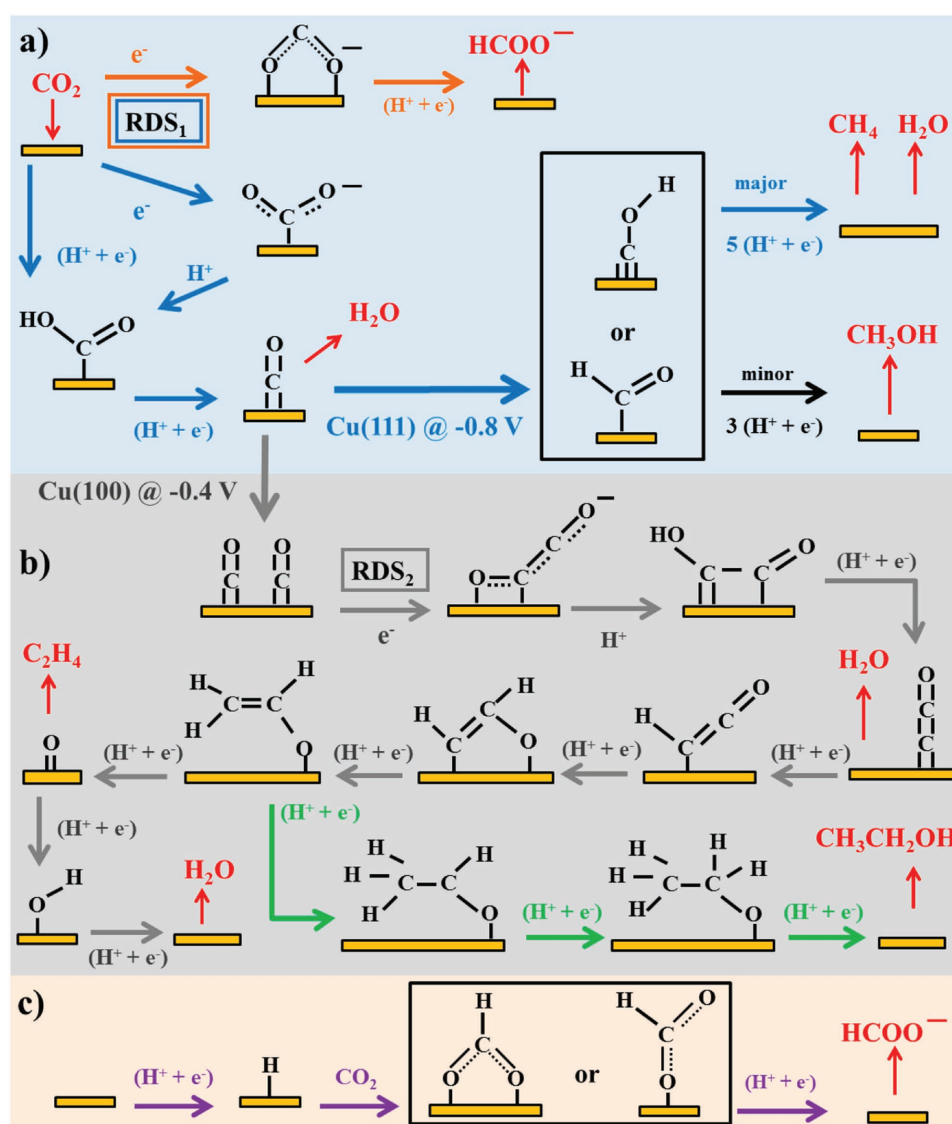
Figure 20. Electrochemical reduction mechanisms of CO_2 on Cu electrocatalysts: a) formation of CO and CH_4 indicated by the blue arrow while formate is by orange color; b) formation of C_2H_4 and ethanol from CO_2ER indicated by gray and green arrow, respectively; c) formation of formate via insertion of CO_2 into metal-H, which is indicated by purple color. The red and black color species indicate reactants (products) and adsorbates respectively in CO_2ER. Reproduced with permission.[110] Copyright 2015, American Chemical Society.

it is confirmed that the possible and lowest energy pathways are detected for major products (CO, HCOOH, CH_4, and C_2H_4) with respect to the applied potentials. The smallest negative over potential for the formation of each product in the reaction pathway is assumed as exergonic or downhill in free energy, which is considered as the limiting potential, i.e., the first estimate of the onset potential for each intermediate or product. In this modeling technique transfer of proton and electrons are carried out for each electrochemical step.[17,53,102,113]

Other research investigations supported by DFT calculation of the kinetic barrier of CO_2 reduction that results the selectivity step for methane versus methanol on Cu(111) occurs with hydrogenation of CO* to COH*, which yields either CH_4 or C_2H_4 while CHO* produces CH_3OH. In other research views and understanding, once COH* is formed then it further reduced to C*, and finally converted to CH_4 and C_2H_4. The reduction of CO* to COH* or CHO* depends on the formation of O−H and C−H bond respectively on the surface of Cu. Another proposed reaction path revealed by another research group differs from the previous reaction mechanisms for the formation of methane which is obtained through CH_2O* and CH_3O* reaction intermediates.[51,102,103,105–107]

Studies revealed that mechanism and speed of generation of CHO* with respect to COH* mainly depends on structure of Cu surface and solvation models of water (water solvated model or H-shuttling model), but the role of water is different during the formation of C−H and O−H bond for methanol and methane production through further reduction of CO,[105] as depicted in **Figure 21**. For all reduction reactions the possible participation of water molecule in hydrogenation process is revealed by water solvated and H-shuttling steps (Figure 21a,b). In water-solvated model, water molecule is available to solvate the conditions or states through the reaction path, however, the

H-shuttling reaction occurs through direct transfer of surface H* to B* (reduction intermediate). The establishment of polar O−H bond is stabilized via electron transfer by the help of proton shuttling process obtained from water (Figure 21b). In this step H-shuttling process has less activation energy. However, the C−H bond, which is classified as weak polarity and, this phenomenon leads the barrier of activation increased by H-shuttling (Figure 21a). This C−H bond needs direct surface contact and interaction with carbon and hydrogen on transition state. The following point is to describe how methanol and methane are formed from the corresponding intermediates. In the transition state, the formation of methanol is accompanied by the principle of H-shuttling assisted model (Figure 21c), while the formation of methane via water solvated model (Figure 21d). Accordingly research findings formation of methanol can also conducted via reduction of methanediol, which results from the reduction of CO_2 and it is considered as the hydrated form of aldehydes specifically formaldehyde.[51,105,106] Recent investigations also showed that the selective reduction mechanisms of CO_2 to C_1 and C_2 products like CH_4 or C_2H_4 is still a little vague to understand well, however, it is clear that these compounds are formed at higher potential than the potential needed to produce CO and others.[51,103,107]
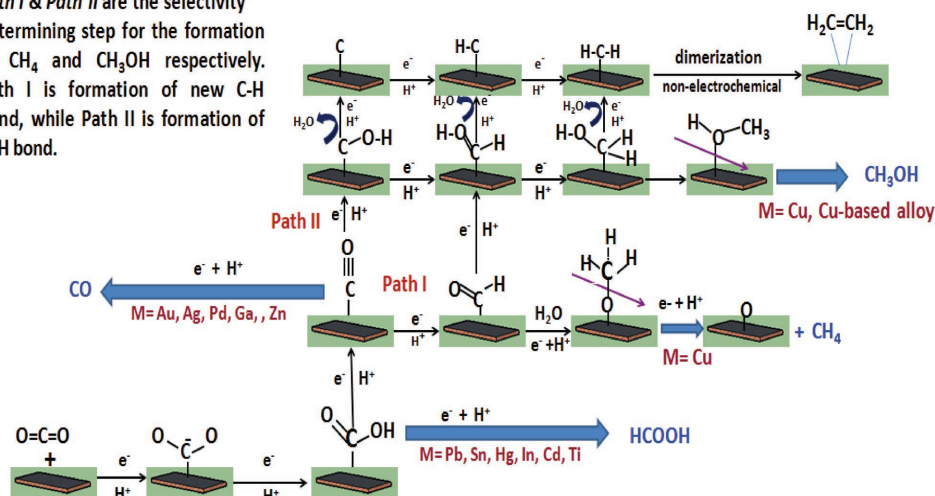
Considering various mechanisms from different research articles and papers we have compiled the general, brief and meaningful paths of reaction mechanism (**Figure 22**) of the above reduction products of CO_2 (CO, HCOOH, CH_4, CH_3OH, HCHO, and C_2H_4) on Cu and other metals surface from various literatures without considering density functional theory calculations. From our general and concise proposed reaction mechanism or scheme, formate and CO are produced initially when binding between intermediate and electrocatalyst surface is not strong enough while in the case of strong binding
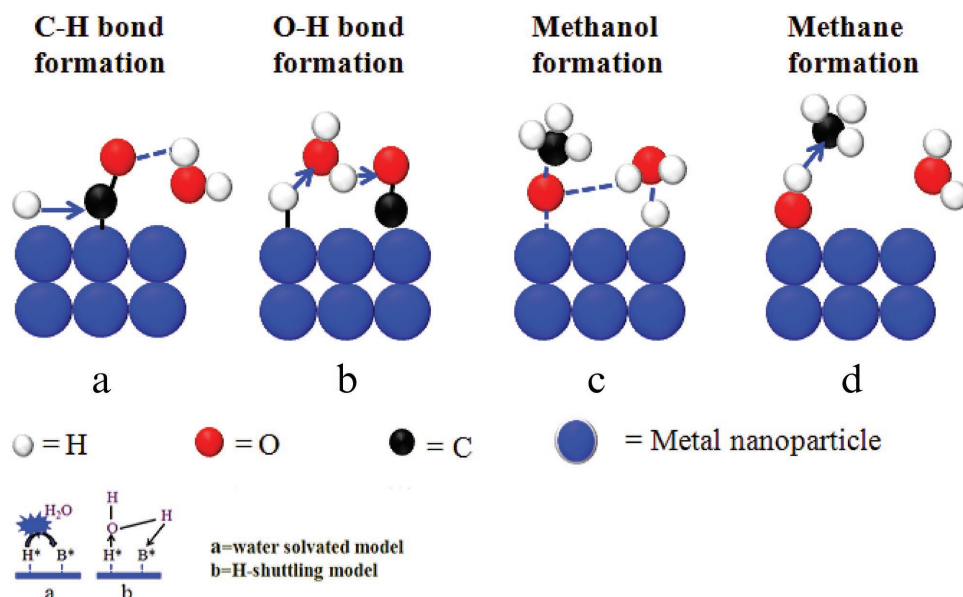
Figure 21. Formation of C−H and O−H bond via hydrogenation process and H shuttling through water on the surface of metal catalyst respectively. a) reduction of CO to CHO via C−H bond formation, b) reduction of CO to COH via O−H bond formation. Reduction of methoxy intermediates for c) the formation of methanol via H-shuttling model and d) formation of methane via water solvated model, (a) and (b) depict water solvated and H-shuttling models respectively with reaction intermediate (B*).

ADVANCED
SCIENCE NEWS
www.advancedsciencenews.com

ADVANCED
MATERIALS
INTERFACES
www.advmatinterfaces.de

Figure 22. General proposed reaction mechanism of electrochemical reduction of CO_2 on metal electrodes in aqueous solutions and the formation paths for main C1 products during the reduction process. M refers to metal catalyst, and blue color represents reduction products.

interaction the intermediate retains on the surface for a longer time and leads to further reduction undergone to convert into alcohols and hydrocarbons. There are two paths due to the formation of OCH* (path I) and COH* (path II) intermediates, which represent formation of methane and methanol respectively, as shown in the schematic Figure 22.[17,49]

5. Selected Reduction Products in CO2ER on Cu and Its Bimetallic

5.1. Cu as Monometallic Catalyst

As we have been mentioned before Cu is one of the cost-effective electrocatalysts that have versatile forms, such as nanoparticle, Cu-foil, Cu alloy, nanowire, nanofoam, unmodified bare Cu, Cu mesocrystals, modified Cu which can be performed via processes such as oxidation, ultrasonic treating, plasma activation, electrochemical deposition of Cu on substrates and many other techniques. Cu NP is one of the most common and can be prepared and/or treated using different techniques including colloidal routes, spray pyrolysis, vapor deposition, laser ablation, hydrothermal routes, chemical reduction, co-precipitation, impregnation reduction, redeposition, sputtering, electropolishing, anodization, and photodeposition techniques.[41,63,80,114,115] Electroredeposition is another technique to realize the stability of Cu+ oxidation state at high negative potential, which is preferable for enhanced catalytic activity of CO2ER for the formation of hydrocarbons specifically ethylene.[115] The formation of its bimetallic with other transition metals is a common technique for modification of Cu and its derivatives to prepare new forms of catalyst species such as Sn–Cu, Ni–Cu, Pd–Cu, Au–Cu, etc., which can catalyzes CO_2 better than individual atoms.[17,18,38,116]

Recently, Zhou et al.[115] have investigated intensively in new insight through modification of the local environment of Cu by doping boron to tune the oxidation state of Cu. The modified Cu electrocatalyst shows an excellent site activity and stability

($\approx$40 h) for CO2ER and results in the maximum faradaic efficiency (77–81%) recorded so far for the formation C2 hydrocarbons by suppressing C1 and liquid products. The simulations revealed that the capability of tuning the oxidation state of Cu is an important scenario to control over CO adsorption and also dimerization of two C1 products to form C2 hydrocarbons (specifically ethylene).

In the reduction process of CO_2 on Cu-based electrocatalyst the amount of reduction product is highly dependent on overpotential. In general perspective at high potential (>−1.0 V vs RHE) HER and formations hydrocarbons are dominant compared to formation of others main products. However, from different researchers' results it is revealed that the formation of CO and HCOOH is decreasing when the overpotential is higher and higher. Production of alcohols starts around −0.8 V versus RHE and the efficiency becomes low at higher potential (>−1.2 V vs RHE). Although activity of HER at high overpotential is dominant, it is also the predominance product at the lowest overpotential before the formation of CO and formate begins.[8,17,46,102,113] Therefore, to minimize the competitive reaction of CO2ER like HER, it is recommended that the applied potential should be as small as possible by maintaining the efficiency and effectiveness of an electrocatalyst regarding the reduction activity.

The reduction products, applied potential and electrolyte solutions used in CO2ER on Cu surface in different forms and using different supporters of electrocatalyst are summarized in **Table 1**. Even though H_2 is considered as a side reaction product, which is competing against the reduction process of CO_2, its faradaic efficiency is included in the table to identify better selectivity from various electrocatalysts. The identification is very important for future researchers to select the right way of preparation of Cu electrocatalysts based on the product required from the reduction process.

From the above table we can understand that the selectivity and FE of products of electrochemical reduction of CO_2 depend on the modification method and supports used during the preparation of Cu nanoparticles. Generally, hydrocarbons and

Table 1. CO_2ER on different forms of monocatalyst Cu with FE% of products and electrolyte solution at specified applied potential.

S.N.	Catalyst	Applied Potential	Electrolyte	Reduction Product (FE%)	Ref.
1.	Cu NPs	−1.25 V vs RHE	0.1 M $NaHCO_3$	CH_4(≈77%), H_2(25%)	[71]
2.	Cu(NPs)	−1.1 V vs RHE	0.5 M $KClO_4$	CO(≈36%), H_2(≈30%), CH_4(≈2%), C_2H_4(≈35%)	[77]
3.	Cu NPs (<15 nm)	−1.1 V vs RHE	0.1 M $KHCO_3$	H_2(≈65%), CO(≈25%), CH_4(≈15%) & C_2H_4(≈5%)	[64]
4.	Cu NPs	−2 V vs Ag/AgCl	0.1 M $KHCO_3$	H_2(≈20%), CH_4(≈5%), CO(≈5%)	[20]
5.	Cu NPs	−2 V vs RHE	0.1 M $KHCO_3$	H_2(≈5%), CO(≈10%), CH_4(≈12%)	
6.	Cu (15.3 nm)	−0.6 V vs RHE	0.5 M $KHCO_3$	CO(≈40%), H_2(≈12%), C_2H_4(≈45%), C_2H_5OH(≈13%)	[117]
7.	Cu (12.3 nm)	−0.6 V vs RHE	0.5 M $KHCO_3$	CO(≈50%), H_2(≈10%), C_2H_4(≈27%), C_2H_5OH(≈7%)	
8.	Cu(7.9 nm)	−0.6 V vs RHE	0.5 M $KHCO_3$	CO(≈42%), H_2(≈10%), C_2H_4(≈27%), C_2H_5OH(≈7%)	
9.	Cu (12.5 nm)	−0.6 V vs RHE	0.5 M $KHCO_3$	CO(≈50%), H_2(≈8%), C_2H_4(≈25%), C_2H_5OH(≈10%)	
10.	Cu NPs/Si	−1.38 V vs RHE	0.1 M $KHCO_3$	C_2H_4(≈40%), H_2(≈20%) CO(≈5%) CH_4(≈5%)	[39]
11.	Cu NW	−0.8 V vs RHE	0.5 M $KHCO_3$	CO(≈4%)	[118]
12.	Cu NW	−0.5 to −1.0 V vs RHE	0.1 M $KHCO_3$	H_2(20–80%), formate(≈0–30%), CO(≈0–60%), C_2H_6O(≈0–15%), CH_4(nil)	[119]
13.	Cu/CNT-NW	−0.5 to 2 V vs RHE	0.5 M $KHCO_3$	Formic acid (≈28%), methanol (≈47%), acetic acid (≈24%), ethanol(≈1%), acetone(≈0.3%), isopropanol(≈0.3%)	[63]
14.	Cu NWs & NN	−0.9 to −1.3 V vs RHE	0.1 M $KHCO_3$	H_2(≈18–30%), formate (≈12–47%), CH_4(≈0–15%), C_2H_4(≈3–12%)	[73]
15.	Cu/graphite	–	proton conducting Sterion	Methanol(≈78%), acetone(≈18%), acetaldehyde(≈9%), methyl formate(nil), methane(nil)	[20]
16.	Cu/activated carbon	–	proton conducting Sterion	Methanol(≈43%), acetone(≈5%), acetaldehyde(≈50%), methyl formate(nil), methane(nil)	[120]
17.	Cu/carbon nano fiber	–	proton conducting Sterion	Methanol(nil), ethanol(nil), 2-propanol(nil), n-propanol(≈12%), CO(≈8%), acetaldehyde(≈65%), methyl formate(nil), methane(≈5%)	
18.	Cu/CNT	−1.44 V vs RHE	$KHCO_3$	CH_4(≈33%), C_2H_4(≈25%), ethanol(≈6%), propanol(≈3%), CO(1%), H_2(≈2%)	[121]
19.	Cu/CNT	−1.7 V vs SCE	0.5 M $NaHCO_3$	Methanol (≈38%)	[122]
	Cu/CNS	−1.2 V vs RHE	0.1 M $KHCO_3$	C_2H_5OH(≈65%), H_2(≈10%), CO(≈5%), CH_4(≈5%)	[123]
20.	Cu/CNT-IMR	−0.5 to 2 V vs RHE	0.5 M $KHCO_3$	Formic acid (≈13%), methanol (≈23%), acetic acid (≈62%), acetone(≈1%),	[63]
21.	Cu-NFs	−1.6 V vs RHE	0.1 M $KHCO_3$	HCOOH(≈50%), H_2(≈25%), CH_4(≈5%), C_2H_4(≈15%)	[111]
22.	Cu-PANI	−1.1 V vs RHE	0.5 M H_2SO_4	Formic acid (≈10%), methanol (≈5%)	[124]
23.	Cu-PANI + Pd-PANI	−1.1 V vs RHE	0.5 M H_2SO_4	Formic acid (≈13%), methanol(≈4%)	
24.	PANI/Cu_2O	−0.3 V vs SCE	0.1 M tetrabutyl ammonium perchlorate	Formic acid(≈30%), acetic acid(≈63.0%)	[125]
25.	Cu/Cu foil	−1.2 V vs RHE	0.1 M $KHCO_3$	H_2(≈20%) CH_4(≈40%), C_2H_4(≈5%), CO(≈2%)	
26.	Cu/Ni	−1.2 V vs RHE	0.1 M $KHCO_3$	H_2(≈40%), CH_4(≈30%), C_2H_4(≈5%), CO(≈2%)	[75]
27.	Cu/Ti	−1.2 V vs RHE	0.1 M $KHCO_3$	H_2(≈50%), CH_4(≈15%), C_2H_4(3%), CO(5%)	
28.	Cu/TiO_2	−1.5 V vs RHE)	0.2 M KI	Ethanol (≈27%), propanol(≈7%)	[117]
29.	Cu(100)	−0.9 V vs RHE	0.1 M $KHCO_3$	CH_4(≈5%), C_2H_4(≈20%), H_2(≈60%), CO(≈4%), ethanol(≈7%), formate(≈10%), acetone(≈2%)	[126]
30.	Cu(111)	−0.9 V vs RHE	0.1 M $KHCO_3$	CH_4 (nil), C_2H_4(nil), H_2(≈70%), CO(≈10%), formate(≈20%)	
31.	Cu(110)	−0.9 V vs RHE	0.1 M $KHCO_3$	CH_4 (≈5%), C_2H_4(≈5%), H_2(≈70%), CO(≈6%), formate(≈24%)	
32.	Cu bare	−1.2 V vs RHE	0.1 M $KHCO_3$	H_2 (≈25%), CH_4(≈40%), C_2H_4(≈2%), CO(≈2%)	[75]
33.	Cu mesopore	−1.7 V vs RHE	M $KHCO_3$	CH_4 (≈45%), C_2H_6(≈45%), C_2H_4(≈40%), CO(≈10%)	[127]
34.	Cu foam	−0.73 V vs RHE	0.1 M KOH	CO(≈5%)	[118]
35.	Cu(Polycrystalline)	−0.8 V vs RHE	0.5 M $KHCO_3$	CO(≈19%)	[118]
36.	Cu(polycrystalline)	−1 V vs RHE	0.1 M $KHCO_3$	CO (≈15%), H_2(≈45%), other(≈36%)	[128]
37.	Cu plate	−1.8 V vs Ag/AgCl	0.1 M $KHCO_3$	Formate (≈20%)	[129]
38.	Cu	−1.1 to −0.7 V vs RHE	0.1 M $KHCO_3$	CO (≈4%), H_2(≈40%), HCOOH(≈2%), ethanol(≈4%), CH_4(nil), ethylene(≈4.5%), acetone(≈1.5%), acetone(≈1%)	[8]

ADVANCED
SCIENCE NEWS
www.advancedsciencenews.com

ADVANCED
MATERIALS
INTERFACES
www.advmatinterfaces.de

Table 1. Continued.

S.N.	Catalyst	Applied Potential	Electrolyte	Reduction Product (FE%)	Ref.
	Cu-foil	−1.6 V vs RHE	0.1 M KHCO$_3$	HCOOH (≈15%), H$_2$(≈45%), CH$_4$(≈38%), C$_2$H$_4$(≈5%)	[111]
39.	Cu foil	−1.9 V vs RHE	0.1 M KHCO$_3$	CH$_4$ (≈20%), C$_2$H$_4$(≈10%)	[130]
40.	Cu foil + glycerine	−1.9 V vs RHE	0.1 M KHCO$_3$	CH$_4$(≈35%), C$_2$H$_4$(≈25%)	
41.	OD-Cu	−0.6 V vs RHE	0.1 M KHCO$_3$	CO(≈40%), COOH(≈35%), H$_2$(≈25%)	[131]
42.	Cu sponge (electropolished)	−1 V vs RHE	0.5 M NaHCO$_3$	H$_2$(≈65%), CO(≈2%), formate(≈25%), C$_2$H$_4$(≈2%), C$_2$H$_6$(nil), total C$_2$H$_6$(nil)	[132]
43.	Cu sponge (annealed)	−1 V vs RHE	0.5 M NaHCO$_3$	H$_2$(≈60%), CO(≈5%), formate(≈18%), C$_2$H$_4$(≈15%), C$_2$H$_6$(≈8%), total C2(≈23%)	
44.	Cu sponge (electro-deposited)	−1 V vs RHE	0.5 M NaHCO$_3$	H$_2$(≈65%), CO(≈3%), formate(≈5%), C$_2$H$_4$(≈12%), C$_2$H$_6$(≈16%), total C$_2$H$_6$(≈28%)	
45.	Cu(electro-polished)	−1.1 V vs RHE	0.5 M KClO$_4$	CO(≈17%),H$_2$(≈38%),CH$_4$(≈6%), C$_2$H$_4$(≈15%)	[77]
46.	Cu (sputtered)	−1.1 V vs RHE	0.5 M KClO$_4$	CO(≈22%),H$_2$(≈26%),CH$_4$(≈8%),C$_2$H$_4$(≈24%)	
47.	CuO	−1.5 V vs Ag/AgCl	0.5 M KHCO$_3$	H$_2$(≈40%), HCOOH(≈38%), CO(≈20%)	[47]
48.	Cu/Cu$_2$O	−2 V vs Fc+/Fc	CO$_2$ saturated DMF/H$_2$O (97:3, v/v)	H$_2$(≈28%), CO(≈2%), formate (≈53%)	[133]
49.	Cu/Cu$_2$O-addition of different organic additives	−2 V vs Fc+/Fc	CO$_2$ saturated DMF/H$_2$O (97:3, v/v)	H$_2$(≈30–58%), CO(≈1–4%), formate(≈47–64%)	
50.	Cu$_x$O	−0.5 V vs RHE	0.5 M KHCO$_3$	Formic acid(≈59%)	[134]
51.	Cu$_2$O-derived Cu	−0.9 V vs RHE	0.1 M HCO$_3$	CH$_4$(nil), C$_2$H$_4$(≈20%), H$_2$(≈40%), CO(≈4%), ethanol(≈10%), formate(≈12%), propanol(≈5%), acetone(≈1%)	[126]
52.	Cu$_2$O film (0.2 µm thick)	−0.99 V vs RHE	0.1 M KHCO$_3$	CO(≈2%), CH$_4$(≈10%), C$_2$H$_4$(≈33%), C$_2$H$_5$OH(≈6%), C$_2$H$_6$(ND), HCOO$^−$(≈13%),H$_2$(≈26%)	[10]
53.	Cu$_2$O film (3.6 µm thick)	−0.99 V vs RHE	0.1 M KHCO$_3$	CO(≈0.4%), CH$_4$(≈0.3%), C$_2$H$_4$(≈34%), C$_2$H$_5$OH(≈16%), C$_2$H$_6$(≈0.2%), HCOO$^−$(≈4%),H$_2$(≈39%)	

NPs, nanoparticles; NN, nanoneedle; CNT, Carbon nano tube; Cu-NFs, cupper nano flowers; CNS, Carbon nano spike prepared from N-doped grapheme; OD, oxide-derived; IMP, impregnation; NW, nanowire; RDs, rhombic dodecahedrons; NCs, nanocubes; PANI, polyaniline; ND, not detected; HSA-Bi, high surface area Bi.

HER are the dominant products at higher potential including many other diversified reduction products using Cu.

5.2. Cu–M Bimetallic Catalysts

As it is indicated in the previous sections alloying forms of Cu electrocatalysts with other metals are better options for electrochemical reduction of CO$_2$ compared to Cu monocatalysts. Because bimetallics have advantages over monocatalysts due to it can catalyze CO$_2$ with less overpotential, obtain many types of products and also can generate enhanced current density and faradaic efficiency. Among many of alloy electrocatalysts including, Cu–Au, Cu–Ni, Cu–Sn, Cu–Pb, Cu–Pd, Cu–Zn, Cu–Cd, Cu–Ag, etc., have been experimentally analyzed for reduction of CO$_2$ to CO, formate and other products. Alloy electrocatalysts have a tendency for capable of turning the binding strength of key intermediates, so that the selectivity and product formation can be manipulated.[5,8,17,47]

In case of Cu bimetallic nanoparticles, the synergistic (electronic and geometric) effect are able to enhance and tune its catalytic activity to achieve high selectivity of products from CO$_2$ reduction, and it is expected to mitigate the proton–catalyst interaction (to suppress HER) and at the same time optimize the binding strength of the common intermediates (COOH*

and CO*) in the pathway by using both effects. Some studies mentioned that based on surface valence band spectra, geometric effects rather than electronic effects seem to be significant in determining the selectivity of bimetallic catalysts such as Cu–Pd.[5,8,17,32,103]

According to different research articles,[8,34,49] reduction of CO$_2$ using AuCu bimetallic alloys the major products is CO in which the amount of CO was directly proportional to the amount of Au content with high current density but formation of small amounts of hydrocarbons and formate. Yang et al. have well studied electrochemical reduction of CO$_2$ using monometallic catalysts (Au and Cu) and bimetallic (AuCu, Au$_3$Cu, and AuCu$_3$) monolayer electrocatalysts, which are all prepared under the same conditions. HER becomes dominant with increasing composition of Cu with respect to Au, while the amount of CO is higher when the composition of Cu is lower than Au.[8]

Among all electrocatalysts studied by Yang et al., pure Cu nanoparticle showed the least activity in terms of current density and faradaic efficiency of products, while increasing the Au content enhances the activity with better stability. However, the composition of Au$_3$Cu shows the highest catalytic activity from all catalysts (Au, Cu, AuCu$_3$, and AuCu). They also pointed out that the overall current density also includes the current from HER, so it is difficult to determine which catalyst is effective and selective for CO$_2$ reduction by considering only the value

**ADVANCED
SCIENCE NEWS**
www.advancedsciencenews.com

**ADVANCED
MATERIALS
INTERFACES**
www.advmatinterfaces.de

of current density. For this reason, determination of FE of each reduction product are performed and analyzed to compare the selectivity of each composition.[8,45,77,113,135] To compare electrochemical reduction of CO_2 using each electrocatalyst in terms of its specific active site for the formation of CO was evaluated by analyzing its TOR at −0.73 V versus RHE. Therefore, it is reported that TOR value of Au_3Cu was the highest one, which is 93.1 times that of the TOR values of Cu electrocatalyst, while Au and AuCu were the 2nd and 3rd, which are 83.7 and 40.4 times that of TOR of Cu respectively. According to their investigations, at the beginning CO_2 is adsorbed onto the surface of electrocatalysts in the form of COOH and eventually reduced to CO. For this reason, the binding energies of COOH and CO have significant impacts on TOR of product CO.[8,136,135]

Electronic, geometric, strain and other effects have a potential to tune the selectivity, reduction activity and faradaic efficiency of products in CO_2ER. Kortlever et al. and other studies revealed that Au–Cu alloy can reduce CO_2 selectively into CO. The production of CO was manipulated by effect of geometric and electronic properties between alloys or reduction intermediates and the electrocatalyst surface.[8,26,110,138,139] Studies pointed out that selective production of hydrocarbons was performed using Cu overlayer on Pt in which the reduction product is tuned by differences in the surface strain. Relief from strain is also an effect in selectivity and activity in CO_2ER.[10,110,138] In case of film electrocatalysts, strain effect could appear due to volume changes of the film during the reduction process of CO_2.[10]

The reason why Au_xCu_y alloy shows a better production ability of CO than individual Cu and Au alone is that the alloy catalyst has a tendency to stabilize COOH in CO_2ER. This implies that CO_2 can be easily activated into COOH, which further transforms in the form of CO on the surface of bimetallic catalyst. However, such types of properties are almost not favorable using monometallic catalysts.[8,138] Therefore, use of bimetallic catalysts is ideal for the fulfillment of the above requirement due to the formation of additional bonds, which arises from oxophilic properties of metals from bimetallic catalysts.

Electronic effect can be described as the charge transfer among alloying elements and the adsorbates, so the binding strength of reduction intermediates will be affected and the effects can be evaluated using various surface compositions. The geometric effect is the local atomic arrangement of bimetallic catalysts at the active sites where the reduction is carried out. The change in the electronic structure of a catalyst becomes a cause for electronic effect on the binding strength of reaction intermediates for further reduction. For d-block metals their binding ability with reaction products or intermediates are determined by the mechanism of d-band interacting with the adsorbate that significantly affect the selectivity of products of CO_2 reduction.[8,136,140]

Rasul et al.[131] have studied electrochemical reduction of CO_2 using copper indium (Cu–In) bimetallic with showing high selectivity of CO at moderate overpotential and good stability. The investigation revealed Cu–In alloy is able to reduce CO_2 to CO with

high faradaic efficiency near to 95% and insignificant amount of H_2 indicates it has high selectivity for the desired product. Hoffman et al. have also studied CO_2ER using Cu–In alloy to produce CO with faradaic efficiency around 70% within −0.4 to −0.7 V versus RHE. In this alloy of Cu–In, it is investigated due to the inherent ability of In to suppress the HER. Even at high cathodic potentials, the electrocatalyst is capable of producing significant amounts of formate and CO. High conductive nature with various composition of each atom in Cu–In to the dendrite formation drives to be selective towards formate and syngas production by suppressing hydrogen generation in CO_2ER.[131,141–143]

Guo et al. have studied the formation of CH_4 from reduction of CO_2 using CuPt bimetallic electrocatalysts using the composition ratio of $CuPt_2$, CuPt, Cu_2Pt, Cu_3Pt, and Cu_5Pt.[144] The reduction scheme is shown in **Figure 23**. The catalyst containing Cu_3Pt generated the highest faradaic efficiency of CO while CuPt produces the least one but the highest competitive reaction (HER). It is known that Pt is a good electro-catalytic for HER due to its unique tendency for affinity of H^+, which leads to facilitate the protonation of adsorbed CO* and eventually further reduce CO into CH_4. Therefore, in addition to the unique ability of Pt, the synergetic effect between Pt and Cu has a significant contribution for effective conversion of CO_2 to CH_4.[105,144,145]

Li et al. studied CO_2ER using CuPd bimetallic at optimized Cu to Pd ratio of 3:7 (Cu_3Pd_7) with good selectivity to produce CO with approximate 80% FE at −0.8V versus RHE. The reason for the selectivity is the electronic and geometric effects of Cu and Pd bimetallic proposed from DFT calculations. Cu is changing the electronic structure of the bimetallic environment, i.e., Pd and it provides the electrocatalyst by adjusting the atomic arrangement of Pd reactive site to be selective for CO in CO_2 reduction.[30]

Sarfraz et al. have studied CO_2ER using Cu–Sn bimetallic, which is prepared by depositing Sn on Cu sheet and produces above 95% of FE of CO at −0.5 V versus RHE. Individual Sn and Cu are able to generate significant amount of HER rather than CO, however, by making an alloy of Cu–Sn it becomes highly selective towards CO in the reduction process. The study reveals optimized ratio of Sn deposited on the Cu is very important to suppress production of H_2. DFT calculation describes when Sn replaces Cu the adsorption of hydrogen decreases,
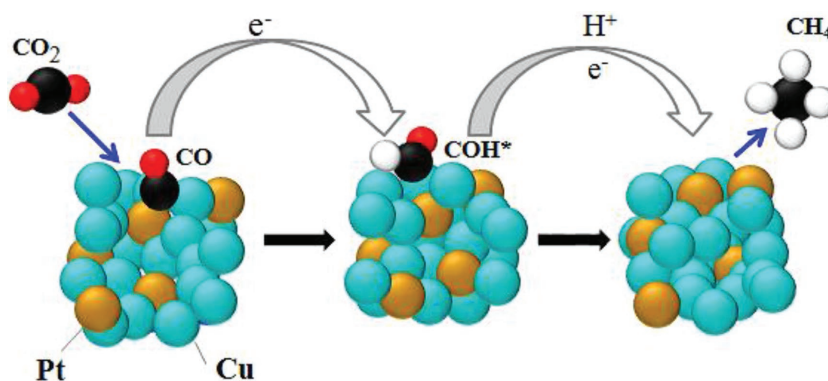
Figure 23. A proposed mechanism illustrating the steps of CO_2 electroreduction and CH_4 formation occurring at the Cu_3Pt NCs catalyst.

**ADVANCED
SCIENCE NEWS**

www.advancedsciencenews.com

**ADVANCED
MATERIALS
INTERFACES**

www.advmatinterfaces.de

which is an important scenario for low selectivity of H_2 and enhanced selectivity of CO.[146]

In multimetallic or bimetallic electrocatalysts, the effect of composition (ratio of each metals), elemental arrangements (ordered, disordered, phase-separated) and mixing pattern have major role in selectivity, faradaic efficiency and catalytic ability in CO_2 reduction.[5,8,17] **Table 2** describes the products, potential applied, main products and electrolyte solutions used in

Table 2. Copper based electrocatalyst for CO_2ER, which is compiled from various literatures including type of catalysts, concentration of electrolyte solution, the potential required and FE% of each reduction product.

S.N	Catalyst	Potential Applied	Electrolyte	Major product (FE%)	Ref.
1.	Cu–Au	−0.9 V vs RHE	0.1 M $KHCO_3$	CO($\approx$50%), H_2($\approx$40%), HCOOH($\approx$3%), ethanol($\approx$0.5%), CH_4(nil)	[8]
2.	Cu_3Au	−0.9 V vs RHE	0.1 M $KHCO_3$	CO($\approx$32%), H_2($\approx$45%), HCOOH($\approx$5%), ethanol($\approx$1.5%), CH_4($\approx$4.5%), acetate($\approx$1%), ethylene($\approx$0.5%)	
3.	$CuAu_3$	−0.8 V vs RHE	0.1 M $KHCO_3$	CO($\approx$60%), H_2($\approx$45%), formate($\approx$5%)	
4.	Cu–Au (disordered)	−0.77 V vs RHE	0.1 M $KHCO_3$	CO($\approx$37%), H_2($\approx$60%)	[34]
5.	Cu–Au (ordered)	−0.77 V vs RHE	0.1 M $KHCO_3$	CO($\approx$80%), H_2($\approx$17%)	
6.	Cu_3Ag/Cu	−1.05 V vs Ag/AgCl	0.1 M $KHCO_3$	C_2H_4($\approx$20%), C_2H_5OH($\approx$13%)	[147]
7.	CuAg/Cu	−1.05 V vs Ag/AgCl	0.1 M $KHCO_3$	C_2H_4($\approx$18%), C_2H_5OH($\approx$13%)	
8.	$CuAg_6$/Cu	−1.05 V vs Ag/AgCl	0.1 M $KHCO_3$	C_2H_5OH($\approx$15%), C_2H_4($\approx$14%)	
9.	Cu–Pd	−1.8 V vs $Ag/AgNO_3$	0.1 M $TBAPF_6$/CH_3CN	CH_4($\approx$35%)	[148]
10.	Cu_3Pd	−1.8 V vs $Ag/AgNO_3$	0.1 M $TBAPF_6$/CH_3CN	CH_4($\approx$36%)	
11.	Cu_2Pd	−1.8 V vs $Ag/AgNO_3$	0.1 M $TBAPF_6$/CH_3 CN	CH_4($\approx$50%)	
12.	$CuPd_2$	−1.8 V vs $Ag/AgNO_3$	0.1 M $TBAPF_6$/CH_3CN	CH_4($\approx$30%)	
13.	Cu–Pd (ordered)	−0.7 V vs RHE	1 M KOH	CO($\approx$77%), CH_4($\approx$2%), C_2H_4($\approx$1%), C_2H_5OH(nil)	[5]
14.	Cu–Pd (disordered)	−0.7 V vs RHE	1 M KOH	CO($\approx$50%), CH_4($\approx$3%), C_2H_4($\approx$6%), C_2H_5OH($\approx$4%)	
15.	Cu–Pd (phase separated)	−0.7 V vs RHE	1 M KOH	CO($\approx$20%), CH_4($\approx$0.5%), C_2H_4($\approx$47%), C_2H_5OH($\approx$15%)	
16.	Cu_3Pd	−0.7 V vs RHE	1 M KOH	CO($\approx$65%), CH_4(nil), C_2H_4($\approx$25%), C_2H_5OH($\approx$7%)	
17.	$CuPd_3$	−0.7 V vs RHE	1 M KOH	CO($\approx$98%), CH_4(nil), C_2H_4(nil)	
18.	$Cu_{56}Pd_{44}$	−0.89 V vs RHE	0.1 M $KHCO_3$	CO ($\approx$86%)	[91]
19.	$Cu_{85}Pd_{15}$	−0.89 V vs RHE	0.1 M $KHCO_3$	CO ($\approx$73%)	
20.	$CuPt_2$	−1.6 V vs SCE	0.5 M $KHCO_3$	CH_4($\approx$5%), H_2($\approx$18%)	[144]
21.	Cu–Pt	−1.6 V vs SCE	0.5 M $KHCO_3$	CH_4($\approx$15%), H_2($\approx$12%)	
22.	Cu_2Pt	−1.6 V vs SCE	0.5 M $KHCO_3$	CH_4($\approx$17%), H_2($\approx$11%)	
23.	Cu_3Pt	−1.6 V vs SCE	0.5 M $KHCO_3$	CH_4($\approx$23%), H_2($\approx$10%)	
24.	Cu_5Pt	−1.6 V vs SCE	0.5 M $KHCO_3$	CH_4($\approx$13%), H_2($\approx$8%)	
25.	Cu/Pt(211)	−1.3 V vs RHE	0.1 M $KHCO_3$	H_2($\approx$84%), CH_4($\approx$5%)	[139]
26.	Cu/Pt(111)	−1.3 V vs RHE	0.1 M $KHCO_3$	H_2($\approx$80%), CH_4($\approx$7%)	
27.	Cu–In	−0.6 V vs RHE	0.1 M $KHCO_3$	CO($\approx$90%), H_2($\approx$10%)	[141]
		−0.8 V vs RHE	0.1 M $KHCO_3$	Formate($\approx$40%), CO($\approx$35%), H_2($\approx$30%)	
		−0.9 V vs RHE	0.1 M $KHCO_3$	Formate($\approx$50%), CO($\approx$30%), H_2($\approx$25%)	
		−1.0 V vs RHE	0.1 M $KHCO_3$	Formate($\approx$50%), CO($\approx$15%), H_2($\approx$35%)	
		−1.1 V vs RHE	0.1 M $KHCO_3$	Formate($\approx$35%),	
28.	Cu–Sn	−0.6 V vs RHE	0.1 M $KHCO_3$	CO($\approx$95%), H2($\approx$5%), HCOOH($\approx$1%)	[149]
29.	$CuInO_2$	−0.6 V vs RHE	0.1 M $KHCO_3$	CO($\approx$50%), HCOOH($\approx$10%), H_2($\approx$25%)	[143]
30.	$Cu/In(OH)_3$	−0.6 V vs RHE	0.1 M $KHCO_3$	CO($\approx$58%), H_2($\approx$23%), HCOOH($\approx$2%)	
31.	Cu/I_2O_3	−0.6 V vs RHE	0.1 M $KHCO_3$	CO($\approx$45%), H_2($\approx$20%), HCOOH($\approx$15%)	
32.	Cu_5Zn_8 (electrochemical)	−1.4 V vs Ag/AgCl	–	HCOOH($\approx$71%)	[150]
33.	Cu_5Zn_8 (photoelectrochemical)	−1.4 V vs Ag/AgCl	–	HCOOH($\approx$79%)	
34.	Cu_4ZnO/Cu	−1.05 V vs Ag/AgCl	0.1 M $KHCO_3$	C_2H_5OH($\approx$25%), H_2($\approx$50%), C_2H_4($\approx$10%), CO($\approx$10%)	[147]
35.	CuO/Cu	−1.05 V vs Ag/AgCl	0.1 M $KHCO_3$	C_2H_4($\approx$30%), C_2H_5OH($\approx$10%)	
36.	$Cu_{3.5}Ni$/Cu	−1.05 V vs Ag/AgCl	0.1 M $KHCO_3$	C_2H_4($\approx$12%), C_2H_5OH($\approx$3%),	

electrochemical reduction of CO_2. All information compiled in the table are used to identify and select the best bimetallic electrocatalyst in terms of selectivity, applied potential and faradaic efficiency (FE) for future researchers.

From the reduction products of CO_2 in Table 2, one can understand that ordered or advanced modified structure of bimetallic electrocatalysts are selective for production of CO with generation of small amount of hydrogen. At higher potential, the formation of hydrocarbons and hydrogen is dominant than CO. However, CO and formate can be produced at lower potential.

According to the value of %FE of CO, formate and hydrocarbons of CO_2ER using selected Cu bimetallic and Cu alone electrocatalysts from previous tables (Table 1 and 2) it is summarized concisely in **Table 3**. From this summarized table one can understand that the FE of CO and formate are significantly higher than FE of hydrocarbons and alcohols in any type of electrocatalyst. This scenario tells that there is limitation to obtain selective electrocatalyst for hydrocarbons and alcohols proportionally or nearly to that of an electrocatalyst selective to CO and formate, even though Cu is the unique electrocatalyst for production of hydrocarbons. Although Cu is the best electrocatalyst to reduce CO_2 into hydrocarbons, the %FE can

exceed above 50% so far. This is very important to easily identify the type of catalysts that are able to generate higher FE of the reduction products at specific reduction product and electrocatalyst, as it is compiled in the table.

6. Summary and Outlook

In order to motivate and stimulate future scientists to harmonize in new and advanced research era of CO_2ER, findings, ideas and recommendations are summarized here cohesively and coherently. We have described important points concisely and forwarded our outlooks based on the latest research outputs and investigations of its electrochemical reduction in the context of advantages, identification of intrinsic factors during the reduction, characterizations of Cu and its bimetallic electrocatalysts, types of reduction products and many other perspectives in the reduction process. Most of researchers have reported their results by mixing up site activity and overall activity of electrocatalysts. In this review we have tried to differentiate and recommend for future researchers to identify the site activity from electrocatalysts and relate to the activity of CO_2 reduction.

- The choice of electrocatalysts and its preparation technique including the modification methods play a great role in selectivity, efficiency and stability of catalysts. The ultimate goal of this surface engineering is to enhance surface area and reproduce active sites into the system for CO_2ER with better catalytic efficiency and selectivity. Generally, all electrocatalyst metals do not produce the same type of reduction products. Some categories are able to produce CO dominantly and others might be selective to formate, hydrocarbons, alcohols etc., which depend on their electronic and structural properties of atoms in electrocatalysts. In another way some categories of transition metals are prone to HER and make CO_2 reduction selectivity too difficult. Size, arrangement and structural properties of atoms in electrocatalyst surface and its morphology have a huge impact on catalytic ability. High number of active sites created on the surface leads to enhance selectivity and faradaic efficiency of reduction products. Size of nanoparticle is directly related to the active electrochemical surface area (number of active sites) and the coordination number of each nanoparticle. Smaller nanoparticle contains higher surface area leading to less coordination number to the neighboring atoms and exposes easily to CO_2.

- Rough and smooth surface morphology of Cu and Cu-based electrocatalysts show different catalytic abilities since the number of active sites created are different in number and type of active site. Rough surface has significant edges, steps and defects, which contribute for better catalytic performance than smooth surface. Regarding to arrangement of atoms in alloys, ordered structure of nanoparticles are selective to CO by suppressing the competitive HER, when compared to disordered and phase-segregating arrangements. For these reason, one should know and familiar the size and atomic arrangement of nanoparticles and morphology of active surface of an electrocatalyst if it is interested to determine the types of reduction products and reduction mechanism as well. Surface modification of electrocatalysts like doping

Table 3. Summary of FE of CO, formate and hydrocarbons with the corresponding electrocatalysts.

Reduction product	FE	Cu bimetallic or monocatalysts
CO	>70%	$Pd_{56}Cu_{44}$, $Pd_{85}Cu_{15}$, $CuPd_3$, Au–Cu (ordered), Cu–Pd (ordered), Cu–In, Cu–Sn
	50–70%	AuCu(disordered), Au_3Cu(disordered), Cu–Pd (disordered), Cu_3Pd, $CuInO_2$, Cu/In(OH)$_3$
	30–49%	$AuCu_3$(disordered), Cu/I_2O_3, Cu NW, OD–Cu, Pd@Cu, NCs, Cu(12.5 nm), Cu(12.3 nm), Cu(7.9 nm), Cu(15.3 nm), Cu(NPs)
	10–30%	Cu_4ZnO/Cu, Cu–Pd (phase separated), Cu NPs(<15 nm), Cu mesopore, CuO, Cu(Polycrystalline), Pd@Cu RDs, Cu(electro-polished), Cu(sputtered)
Formate	>70%	Cu_5Zn_8, Sn/Cu, Sn/Cu foil, Bi/Cu
	50–70%	Cu–In, Cu/Cu_2O, Cu_xO, Cu-NFs
	10–49%	Cu/I_2O_3, $CuInO_2$, $CuInO_2$, Cu–In, CuO, Cu plate, Cu NW, Cu-foil, PANI/Cu_2O, Cu/CNT-NW, Cu(111), Cu(110)
Alcohols (ethanol or methanol)	>50%	Cu/CNS, Cu/graphite
	20–50%	Cu/activated carbon, Cu/CNT-IMR, Cu/CNT-NW, Cu/TiO_2, Cu_4ZnO/Cu
Hydrocarbons	30–50%	CuO/Cu, Cu-Pd (phase separated), Cu polycrystalline, Cu bare, Cu/Ni, Cu/Cu foil, Cu NPs/Si, Cu mesopore, Cu-foil, Pd@Cu NCs, Pd@Cu RDs, 0.2 μm Cu_2O film
	5–30%	Cu/Pt(111), $CuPt_2$, CuPt, Cu_2Pt, Cu_3Pt, Cu_5Pt & Cu/Pt(211), Cu_3Pd, Cu–Pd (disordered), Cu_4ZnO/Cu, $Cu_{3.5}Ni/Cu$, Cu_3Ag/Cu
H_2	>50%	Cu/Ti, Cu/CNT, Cu NW, Cu(100), Cu(110), Cu(111), Cu_4ZnO/Cu, Cu_2Pd, Cu–In, Cu/Pt(211), Cu/Pt(111)

other element, oxidation of the surface, electrodeposition of metal over the other, ordering of atoms in case of bimetallics, surface etching, alloying, etc., are common ways to increase surface activity of Cu and Cu based electrocatalysts. The binding tendency of reaction intermediates with catalyst surface significantly affects the product distribution, selectivity and faradaic efficiency. Bimetallic or alloy compositions of metals generally show better catalytic activity and selectivity than monometallic catalysts. The catalytically active surface sites of bimetallics vary according to the alloying composition and extent.

- The composition of electrocatalysts has an effect in selectivity, efficiency, stability and product distribution of CO_2 reduction. Alloying extent of Cu–M induces electronic and/or geometric changes that provide a synergistic effect and create better active sites for reduction activity, as seen in the examples of CuAu, CuPd, or CuPt bimetallics. Electronic state, properties and structures of the bimetallic electrocatalyst is directly linked to binding strength of intermediates to the catalyst surface and thus influence the reaction mechanism and pathway. In addition, geometric structural variation or distribution also affects the local atomic arrangement on the active site, which can alter the reaction pathway as well. Electronic and geometric properties of Cu and its derivative electrocatalysts can be investigated and revealed by experimental results such as XANES, EXAFS, etc. Specifically, geometric arrangement prominently plays a significant role when reduction products are complicated and involving many electrons such as formation of CH_4 and C_2H_4. This might be the reaction mechanisms are not well understood, specially in case of several electron transfer. Therefore, researchers should consider not only the compositions of Cu based bimetallics but also give more attention to atomic distribution and arrangement and their coordination environments.

- Detection of active sites in CO_2ER is a big challenge. Therefore, we understand and suggest that well defined nanocatalyst is an important task to identify active sites from the surface of electrocatalysts. Detailed investigations of structural and electronic properties of electrocatalysts to the single atom level help to explore the active sites in the form of synergistic effect, defects, d-band vacancy, etc. Operando, in-situ and ex-situ characterization of electrocatalyst is a crucial task before reduction catalysis is performed to understand the reaction mechanism and to predict types of products obtained. For Cu bimetallic catalysts, XAS analysis is an interesting and promising characterization tool to understand all electronic and geometric nature of the metal together with surrounding or local environments of central metals. Using XAS it is possible to determine quantitatively the structural parameters of Cu alloy, surface and bulk compositions of each atom, to evaluate atomic distribution or surface composition of the bimetallic nanoparticles and alloying extent. In generals, it is agreed that the distribution of atoms has a great impact in physicochemical properties of bimetallic electrocatalysts that influence the CO_2ER significantly.

- Electrochemical reduction of CO_2 faces plenty of challenges and limitations. To cleave bonds of the stable CO_2 molecule during CO_2ER, it requires high overpotential, which is considered as one of the big challenge in the reduction

process. The low solubility of CO_2 in water during reduction process results in low mass transfer and adsorption rate leads to affect FE, current density and selectivity of products. The difference between reduction potential of each product is too small and this imposes huge difficulties on selectivity and separation of those reduction products. HER and CO_2 reduction occur in similar potential domains and this leads to competition between the two events on Cu surface, which in return decreases the efficiency of CO_2 reduction. Another challenge is the demand of high costs and skilled personnel because it requires advanced analytical instruments for detection and separation of products. Consequently, the complexity of the reduction process ahead future researchers to predict and investigate various mechanisms and reaction paths with identification of different intermediates to know the final reduction product. However, the exact reduction mechanisms of CO_2ER are not well understood. This is a big assignment for the next researchers to disclose the issue via theoretical and experimental investigations.

Therefore, the existence of challenges of CO_2 reduction are the driving forces to attract and highly inspire future researchers hope that the emerging technology (CO_2ER) for production of essential chemicals by utilization of green (renewable) energy to minimize anthropogenic CO_2 emission is real, effective and efficient using economically feasible Cu based electrocatalysts.

7. Conclusion

In this review we can concluded that CO_2ER is one of the most essential technologies to mitigate the emitting CO_2 into the atmosphere and simultaneously to converts into usable and essential chemicals containing high energy density such as hydrocarbons, carbon monoxide, alcohols and other products. For the electroreduction process Cu and Cu-based electrocatalysts are widely used because the abundant materials have unique electronic and structural properties and versatile morphology to produce wide range of products. Based on numerous modification methods of Cu and Cu bimetallics or alloys, selective reduction products can be obtained by tuning number of active sites, shapes, sizes, morphology, oxidation state, arrangement of atoms (order-disorder), surface area, composition, etc., of nanocatalysts. Cu is the only electrocatalyst that can convert CO_2 into hydrocarbons specifically into methane and ethylene. In the periodic table Cu is found in group IB, which is characterized as a filled d band. It is understood that when Cu forms an alloy with incomplete filled d band metal (M), suppose group VIIIB transition metals. the substitution of M atom by Cu in the metal lattice adds extra electrons to the lattice. Therefore, by tuning the compositions of the bimetallic proportion one can to control or vary the degree of filling of the d band electrons. Thus, Cu bimetallics compared to Cu alone offer great potential and flexibility to enhance the activity and tune the selectivity of CO_2ER. The big challenge in CO_2ER using Cu electrocatalyst is the competing reaction from HER, especially at higher negative potentials and requirement for high onset potential. Cu-based bimetallics are enhanced electrocatalysts compared to their monometallic counterpart

because of the advantages gained through synergistic, strain and alloying effects in terms of selectivity, stability and activity in the electrocatalytic reduction process. Advanced characterization of Cu and its derivative surfaces offers new routes to identify the site activity and to predict and propose reduction mechanisms for the required product. Doping foreign material on Cu surface is able to tune its oxidation state, which is closely related to the adsorption of intermediates on the surface and could dimerize C1 products into C2 hydrocarbons. Therefore, tuning required parameters during the preparation of Cu-based electrocatalyst is a critical step to improve catalytic activity, selectivity, and stability of electrocatalysts in CO_2ER.

Conflict of Interest

The authors declare no conflict of interest.

[1] H. B. Yang, S.-F. Hung, S. Liu, K. Yuan, S. Miao, L. Zhang, X. Huang, H.-Y. Wang, W. Cai, R. Chen, *Nat. Energy* **2018**, *3*, 140.

[2] G. O. Larrazábal, T. Shinagawa, A. J. Martín, J. Pérez-Ramírez, *Nat. Commun.* **2018**, *9*, 1477.

[3] S. Gao, Y. Lin, X. Jiao, Y. Sun, Q. Luo, W. Zhang, D. Li, J. Yang, Y. Xie, *Nature* **2016**, *529*, 68.

[4] J. Qiao, Y. Liu, F. Hong, J. Zhang, *Chem. Soc. Rev.* **2014**, *43*, 631.

[5] S. Ma, M. Sadakiyo, M. Heima, R. Luo, R. T. Haasch, J. I. Gold, M. Yamauchi, P. J. Kenis, *J. Am. Chem. Soc.* **2016**, *139*, 47.

[6] a) N. S. Lewis, D. G. Nocera, *Proc. Natl. Acad. Sci. USA* **2006**, *103*, 15729; b) M. Dresselhaus, I. Thomas, *Nature* **2001**, *414*, 332.

[7] B.-X. Dong, L.-Z. Wang, L. Song, J. Zhao, Y.-L. Teng, *Energy Fuels* **2016**, *30*, 6620.

[8] D. Kim, J. Resasco, Y. Yu, A. M. Asiri, P. Yang, *Nat. Commun.* **2014**, *5*, 4948.

[9] a) I. Ganesh, *Renewable Sustainable Energy Rev.* **2014**, *31*, 221; b) M. Asadi, K. Kim, C. Liu, A. V. Addepalli, P. Abbasi, P. Yasaei, P. Phillips, A. Behranginia, J. M. Cerrato, R. Haasch, *Science* **2016**, *353*, 467.

[10] D. Ren, Y. Deng, A. D. Handoko, C. S. Chen, S. Malkhandi, B. S. Yeo, *ACS Catal.* **2015**, *5*, 2814.

[11] K. J. P. Schouten, Z. Qin, E. P. R. Gallent, M. T. Koper, *J. Am. Chem. Soc.* **2012**, *134*, 9864.

[12] a) I. Tsiropoulos, R. Hoefnagels, M. Broek, M. K. Patel, A. P. Faaij, *GCB Bioenergy* **2017**, *9*, 1489; b) S. Bajracharya, K. Vanbroekhoven, C. J. Buisman, D. P. Strik, D. Pant, *Faraday Discuss.* **2017**, *202*, 433; c) E. T. Kho, T. H. Tan, E. Lovell, R. J. Wong, J. Scott, R. Amal, *Green Energy Environ.* **2017**, *2*, 204; d) K. S. Rawat, A. Mahata, B. Pathak, *J. Catal.* **2017**, *349*, 118; e) J. T. Feaster, C. Shi, E. R. Cave, T. Hatsukade, D. N. Abram, K. P. Kuhl, C. Hahn, J. K. Nørskov, T. F. Jaramillo, *ACS Catal.* **2017**, *7*, 4822; f) S. Ma, P. J. Kenis, *Curr. Opin. Chem. Eng.* **2013**, *2*, 191; g) J. L. White, M. F. Baruch, J. E. Pander III, Y. Hu, I. C. Fortmeyer, J. E. Park, T. Zhang, K. Liao, J. Gu, Y. Yan, *Chem. Rev.* **2015**, *115*, 12888.

[13] H.-Y. Kim, I. Choi, S. H. Ahn, S. J. Hwang, S. J. Yoo, J. Han, J. Kim, H. Park, J. H. Jang, S.-K. Kim, *Int. J. Hydrogen Energy* **2014**, *39*, 16506.

[14] X. Zhang, Z. Wu, X. Zhang, L. Li, Y. Li, H. Xu, X. Li, X. Yu, Z. Zhang, Y. Liang, *Nat. Commun.* **2017**, *8*, 14675.

[15] C. Costentin, M. Robert, J.-M. Savéant, *Chem. Soc. Rev.* **2013**, *42*, 2423.

[16] D. T. Whipple, P. J. Kenis, *J. Phys. Chem. Lett.* **2010**, *1*, 3451.

[17] D. D. Zhu, J. L. Liu, S. Z. Qiao, *Adv. Mater.* **2016**, *28*, 3423.

[18] G. Keerthiga, R. Chetty, *J. Electrochem. Soc.* **2017**, *164*, H164.

[19] M. R. Singh, E. L. Clark, A. T. Bell, *Phys. Chem. Chem. Phys.* **2015**, *17*, 18924.

[20] I. Merino-Garcia, E. Alvarez-Guerra, J. Albo, A. Irabien, *Chem. Eng. J.* **2016**, *305*, 104.

[21] S. Zhao, R. Jin, R. Jin, *ACS Energy Lett.* **2018**, *3*, 452.

[22] J. He, N. J. Johnson, A. Huang, C. P. Berlinguette, *ChemSusChem* **2018**, *11*, 48.

[23] C. W. Li, J. Ciston, M. W. Kanan, *Nature* **2014**, *508*, 504.

[24] A. M. Appel, J. E. Bercaw, A. B. Bocarsly, H. Dobbek, D. L. DuBois, M. Dupuis, J. G. Ferry, E. Fujita, R. Hille, P. J. Kenis, *Chem. Rev.* **2013**, *113*, 6621.

[25] S. Verma, B. Kim, H. R. Jhong, S. Ma, P. J. Kenis, *ChemSusChem* **2016**, *9*, 1972.

[26] M. Liu, Y. Pang, B. Zhang, P. De Luna, O. Voznyy, J. Xu, X. Zheng, C. T. Dinh, F. Fan, C. Cao, *Nature* **2016**, *537*, 382.

[27] a) Q. Lu, J. Rosen, F. Jiao, *ChemCatChem* **2015**, *7*, 38; b) J. J. Spivey, A. Egbebi, *Chem. Soc. Rev.* **2007**, *36*, 1514; c) P. C. Munasinghe, S. K. Khanal, *Bioresour. Technol.* **2010**, *101*, 5013; d) K. A. Magrini-Bair, W. S. Jablonski, Y. O. Parent, M. M. Yung, *Top. Catal.* **2012**, *55*, 209.

[28] Y. Chen, C. W. Li, M. W. Kanan, *J. Am. Chem. Soc.* **2012**, *134*, 19969.

[29] W. Ju, A. Bagger, G.-P. Hao, A. S. Varela, I. Sinev, V. Bon, B. R. Cuenya, S. Kaskel, J. Rossmeisl, P. Strasser, *Nat. Commun.* **2017**, *8*, 944.

[30] M. Li, J. Wang, P. Li, K. Chang, C. Li, T. Wang, B. Jiang, H. Zhang, H. Liu, Y. Yamauchi, *J. Mater. Chem. A* **2016**, *4*, 4776.

[31] a) S. Y. Choi, S. K. Jeong, H. J. Kim, I.-H. Baek, K. T. Park, *ACS Sustainable Chem. Eng.* **2016**, *4*, 1311; b) S. S. Itkulova, K. Zhunusova, G. Zakumbaeva, *Appl. Organomet. Chem.* **2000**, *14*, 850; c) S. Ishimaru, R. Shiratsuchi, G. Nogami, *J. Electrochem. Soc.* **2000**, *147*, 1864; d) R. Shiratsuchf, S. Ishimaru, G. Nogami, in *Studies in Surface Science and Catalysis*, Vol. 114, Elsevier, Kyoto, Japan **1998**, p. 573; e) R. Schrebler, P. Cury, C. Suarez, E. Munoz, H. Gomez, R. Cordova, *J. Electroanal. Chem.* **2002**, *533*, 167; f) N. Lebedeva, V. Rosca, G. Janssen, *Electrochim. Acta* **2010**, *55*, 7659; g) L. Chen, C. Bock, P. Mercier, B. MacDougall, *Electrochim. Acta* **2012**, *77*, 212; h) F. Jia, X. Yu, L. Zhang, *J. Power Sources* **2014**, *252*, 85; i) F.-x. Shen, J. Shi, T.-y. Chen, F. Shi, Q.-y. Li, J.-z. Zhen, Y.-f. Li, Y.-n. Dai, B. Yang, T. Qu, *J. Power Sources* **2018**, *378*, 555; j) T. Szumełda, A. Drelinkiewicz, E. Lalik, R. Kosydar, D. Duraczyńska, J. Gurgul, *Appl. Catal., B* **2018**, *221*, 393.

**ADVANCED
SCIENCE NEWS**
www.advancedsciencenews.com

**ADVANCED
MATERIALS
INTERFACES**
www.advmatinterfaces.de

[32] M. Watanabe, M. Shibata, A. Kato, M. Azuma, T. Sakata, *J. Electrochem. Soc.* **1991**, *138*, 3382.

[33] Q. Lu, J. Rosen, Y. Zhou, G. S. Hutchings, Y. C. Kimmel, J. G. Chen, F. Jiao, *Nat. Commun.* **2014**, *5*, 3242.

[34] D. Kim, C. Xie, N. Becknell, Y. Yu, M. Karamad, K. Chan, E. J. Crumlin, J. K. Nørskov, P. Yang, *J. Am. Chem. Soc.* **2017**, *139*, 8329.

[35] B.-J. Hwang, L. S. Sarma, J.-M. Chen, C.-H. Chen, S.-C. Shih, G.-R. Wang, D.-G. Liu, J.-F. Lee, M.-T. Tang, *J. Am. Chem. Soc.* **2005**, *127*, 11140.

[36] C. H. Chen, C. J. Pan, W. N. Su, L. S. Sarma, C. C. A. Andra, H. S. Sheu, D. G. Liu, J. F. Lee, B. J. Hwang, *ChemNanoMat* **2016**, *2*, 117.

[37] a) S. Sun, C. B. Murray, D. Weller, L. Folks, A. Moser, *Science* **2000**, *287*, 1989; b) J.-I. Park, M. G. Kim, Y.-w. Jun, J. S. Lee, W.-r. Lee, J. Cheon, *J. Am. Chem. Soc.* **2004**, *126*, 9072; c) P. Lu, J. Dong, N. Toshima, *Langmuir* **1999**, *15*, 7980.

[38] K. P. Kuhl, T. Hatsukade, E. R. Cave, D. N. Abram, J. Kibsgaard, T. F. Jaramillo, *J. Am. Chem. Soc.* **2014**, *136*, 14107.

[39] M. Padilla, O. Baturina, J. P. Gordon, K. Artyushkova, P. Atanassov, A. Serov, *J. CO2 Util.* **2017**, *19*, 137.

[40] a) A. Januszewska, R. Jurczakowski, P. J. Kulesza, *Langmuir* **2014**, *30*, 14314; b) W. Zhu, R. Michalsky, Ö. Metin, H. Lv, S. Guo, C. J. Wright, X. Sun, A. A. Peterson, S. Sun, *J. Am. Chem. Soc.* **2013**, *135*, 16833; c) X. Zhang, Z. Wu, X. Zhang, L. Li, Y. Li, H. Xu, X. Li, X. Yu, Z. Zhang, Y. Liang, *Nat. Commun.* **2017**, *8*, 14675; d) C. Kim, H. S. Jeon, T. Eom, M. S. Jee, H. Kim, C. M. Friend, B. K. Min, Y. J. Hwang, *J. Am. Chem. Soc.* **2015**, *137*, 13844.

[41] P. De Luna, R. Quintero-Bermudez, C.-T. Dinh, M. B. Ross, O. S. Bushuyev, P. Todorović, T. Regier, S. O. Kelley, P. Yang, E. H. Sargent, *Nat. Catal.* **2018**, *1*, 103.

[42] a) Y. Hori, K. Kikuchi, S. Suzuki, *Chem. Lett.* **1985**, *14*, 1695; b) M. Azuma, K. Hashimoto, M. Hiramoto, M. Watanabe, T. Sakata, *J. Electroanal. Chem. Interfacial Electrochem.* **1989**, *260*, 441; c) Y. Hori, K. Kikuchi, A. Murata, S. Suzuki, *Chem. Lett.* **1986**, *15*, 897; d) R. Holze, *J. Solid State Electrochem.* **2008**, *12*, 1521; e) N. Gupta, M. Gattrell, B. MacDougall, *J. Appl. Electrochem.* **2006**, *36*, 161; f) K. Hara, A. Tsuneto, A. Kudo, T. Sakata, *J. Electrochem. Soc.* **1994**, *141*, 2097; g) O. Scialdone, A. Galia, G. L. Nero, F. Proietto, S. Sabatino, B. Schiavo, *Electrochim. Acta* **2016**, *199*, 332.

[43] M. Azuma, K. Hashimoto, M. Hiramoto, M. Watanabe, T. Sakata, *J. Electrochem. Soc.* **1990**, *137*, 1772.

[44] Y. Chen, M. W. Kanan, *J. Am. Chem. Soc.* **2012**, *134*, 1986.

[45] Y. Hori, A. Murata, R. Takahashi, *J. Chem. Soc., Faraday Trans. 1* **1989**, *85*, 2309.

[46] Y. Hori, H. Wakebe, T. Tsukamoto, O. Koga, *Electrochim. Acta* **1994**, *39*, 1833.

[47] P. Huang, S. Ci, G. Wang, J. Jia, J. Xu, Z. Wen, *J. CO2 Util.* **2017**, *20*, 27.

[48] a) K. Udupa, G. Subramanian, H. Udupa, *Electrochim. Acta* **1971**, *16*, 1593; b) J. Ryu, T. Andersen, H. Eyring, *J. Phys. Chem.* **1972**, *76*, 3278; c) W. Paik, T. Andersen, H. Eyring, *Electrochim. Acta* **1969**, *14*, 1217; d) A. Gennaro, A. A. Isse, J.-M. Savéant, M.-G. Severin, E. Vianello, *J. Am. Chem. Soc.* **1996**, *118*, 7190.

[49] L. Zhang, Z. J. Zhao, J. Gong, *Angew. Chem., Int. Ed.* **2017**, *56*, 11326.

[50] K. J. P. Schouten, Z. Qin, E. Pérez Gallent, M. T. Koper, *J. Am. Chem. Soc.* **2012**, *134*, 9864.

[51] X. Nie, W. Luo, M. J. Janik, A. Asthagiri, *J. Catal.* **2014**, *312*, 108.

[52] Y. Hori, H. Konishi, T. Futamura, A. Murata, O. Koga, H. Sakurai, K. Oguma, *Electrochim. Acta* **2005**, *50*, 5354.

[53] F. Calle-Vallejo, M. Koper, *Angew. Chem.* **2013**, *125*, 7423.

[54] a) C. C. McCrory, S. Jung, I. M. Ferrer, S. M. Chatman, J. C. Peters, T. F. Jaramillo, *J. Am. Chem. Soc.* **2015**, *137*, 4347; b) H.-K. Lim, H. Shin, W. A. Goddard III, Y. J. Hwang, B. K. Min, H. Kim, *J. Am. Chem. Soc.* **2014**, *136*, 11355.

[55] a) M. Gangeri, S. Perathoner, S. Caudo, G. Centi, J. Amadou, D. Begin, C. Pham-Huu, M. J. Ledoux, J.-P. Tessonnier, D. S. Su, *Catal. Today* **2009**, *143*, 57; b) Y.-J. Zhang, V. Sethuraman, R. Michalsky, A. A. Peterson, *ACS Catal.* **2014**, *4*, 3742.

[56] D. Gao, H. Zhou, J. Wang, S. Miao, F. Yang, G. Wang, J. Wang, X. Bao, *J. Am. Chem. Soc.* **2015**, *137*, 4288.

[57] Z. Weng, Y. Wu, M. Wang, J. Jiang, K. Yang, S. Huo, X.-F. Wang, Q. Ma, G. W. Brudvig, V. S. Batista, *Nat. Commun.* **2018**, *9*, 415.

[58] a) J. Liu, *ACS Catal.* **2016**, *7*, 34; b) C. Zhao, X. Dai, T. Yao, W. Chen, X. Wang, J. Wang, J. Yang, S. Wei, Y. Wu, Y. Li, *J. Am. Chem. Soc.* **2017**, *139*, 8078; c) Q. Jia, N. Ramaswamy, H. Hafiz, U. Tylus, K. Strickland, G. Wu, B. Barbiellini, A. Bansil, E. F. Holby, P. Zelenay, *ACS Nano* **2015**, *9*, 12496.

[59] M. Cho, J. T. Song, S. Back, Y. Jung, J. Oh, *ACS Catal.* **2018**, *8*, 1178.

[60] C. Shi, H. A. Hansen, A. C. Lausche, J. K. Nørskov, *Phys. Chem. Chem. Phys.* **2014**, *16*, 4720.

[61] J. K. Nørskov, T. Bligaard, A. Logadottir, J. Kitchin, J. G. Chen, S. Pandelov, U. Stimming, *J. Electrochem. Soc.* **2005**, *152*, J23.

[62] J. Xie, Y. Huang, H. Yu, *Front. Environ. Sci. Eng.* **2014**, *9*, 861.

[63] B. C. Marepally, C. Ampelli, C. Genovese, F. Tavella, L. Veyre, E. A. Quadrelli, S. Perathoner, G. Centi, *J. CO2 Util.* **2017**, *21*, 534.

[64] R. Reske, H. Mistry, F. Behafarid, B. Roldan Cuenya, P. Strasser, *J. Am. Chem. Soc.* **2014**, *136*, 6978.

[65] H. A. Gasteiger, S. S. Kocha, B. Sompalli, F. T. Wagner, *Appl. Catal., B* **2005**, *56*, 9.

[66] S. Mukerjee, *J. Appl. Electrochem.* **1990**, *20*, 537.

[67] a) L. Li, A. H. Larsen, N. A. Romero, V. A. Morozov, C. Glinsvad, F. Abild-Pedersen, J. Greeley, K. W. Jacobsen, J. K. Nørskov, *J. Phys. Chem. Lett.* **2012**, *4*, 222; b) J. Kleis, J. Greeley, N. Romero, V. Morozov, H. Falsig, A. H. Larsen, J. Lu, J. J. Mortensen, M. Dułak, K. S. Thygesen, *Catal. Lett.* **2011**, *141*, 1067; c) G. L. Bezemer, J. H. Bitter, H. P. Kuipers, H. Oosterbeek, J. E. Holewijn, X. Xu, F. Kapteijn, A. J. van Dillen, K. P. de Jong, *J. Am. Chem. Soc.* **2006**, *128*, 3956; d) J. Den Breejen, P. Radstake, G. Bezemer, J. Bitter, V. Frøseth, A. Holmen, K. d. Jong, *J. Am. Chem. Soc.* **2009**, *131*, 7197; e) A. Moshfegh, *J. Phys. D: Appl. Phys.* **2009**, *42*, 233001.

[68] G. Tritsaris, J. Greeley, J. Rossmeisl, J. K. Nørskov, *Catal. Lett.* **2011**, *141*, 909.

[69] H. Mistry, R. Reske, Z. Zeng, Z.-J. Zhao, J. Greeley, P. Strasser, B. R. Cuenya, *J. Am. Chem. Soc.* **2014**, *136*, 16473.

[70] a) A. M. Argo, J. F. Odzak, B. C. Gates, *J. Am. Chem. Soc.* **2003**, *125*, 7107; b) B. R. Cuenya, S.-H. Baeck, T. F. Jaramillo, E. W. McFarland, *J. Am. Chem. Soc.* **2003**, *125*, 12928; c) F. Behafarid, L. Ono, S. Mostafa, J. Croy, G. Shafai, S. Hong, T. Rahman, S. R. Bare, B. R. Cuenya, *Phys. Chem. Chem. Phys.* **2012**, *14*, 11766.

[71] K. Manthiram, B. J. Beberwyck, A. P. Alivisatos, *J. Am. Chem. Soc.* **2014**, *136*, 13319.

[72] a) W. Lv, J. Zhou, F. Kong, H. Fang, W. Wang, *Int. J. Hydrogen Energy* **2016**, *41*, 1585; b) E. Liu, L. Qi, J. Bian, Y. Chen, X. Hu, J. Fan, H. Liu, C. Zhu, Q. Wang, *Mater. Res. Bull.* **2015**, *68*, 203.

[73] J. Xie, Y. Huang, H. Yu, *Front. Environ. Sci. Eng.* **2015**, *9*, 861.

[74] Z. Wang, G. Yang, Z. Zhang, M. Jin, Y. Yin, *ACS Nano* **2016**, *10*, 4559.

[75] A. N. Karaiskakis, E. J. Biddinger, *Energy Technol.* **2017**, *5*, 901.

[76] I. Takahashi, O. Koga, N. Hoshi, Y. Hori, *J. Electroanal. Chem.* **2002**, *533*, 135.

[77] W. Tang, A. A. Peterson, A. S. Varela, Z. P. Jovanov, L. Bech, W. J. Durand, S. Dahl, J. K. Nørskov, I. Chorkendorff, *Phys. Chem. Chem. Phys.* **2012**, *14*, 76.

[78] a) G. S. Prakash, F. A. Viva, G. A. Olah, *J. Power Sources* **2013**, *223*, 68; b) Y. Hori, I. Takahashi, O. Koga, N. Hoshi, *J. Mol. Catal. A: Chem.* **2003**, *199*, 39; c) J. Qiao, P. Jiang, J. Liu, J. Zhang, *Electrochem. Commun.* **2014**, *38*, 8.

[79] R. Kas, R. Kortlever, A. Milbrat, M. T. Koper, G. Mul, J. Baltrusaitis, *Phys. Chem. Chem. Phys.* **2014**, *16*, 12194.

[80] C. S. Chen, A. D. Handoko, J. H. Wan, L. Ma, D. Ren, B. S. Yeo, *Catal. Sci. Technol.* **2015**, *5*, 161.

[81] a) A. B. Shah, S. T. Sivapalan, B. M. DeVetter, T. K. Yang, J. Wen, R. Bhargava, C. J. Murphy, J.-M. Zuo, *Nano Lett.* **2013**, *13*, 1840; b) Y. Xia, Y. Xiong, B. Lim, S. E. Skrabalak, *Angew. Chem., Int. Ed.* **2009**, *48*, 60; c) A. R. Tao, S. Habas, P. Yang, *Small* **2008**, *4*, 310; d) H. L. Skriver, N. Rosengaard, *Phys. Rev. B* **1992**, *46*, 7157.

[82] S. Zhu, M. Shao, *J. Solid State Electrochem.* **2016**, *20*, 861.

[83] J. H. Sinfelt, *Acc. Chem. Res.* **1977**, *10*, 15.

[84] A. S. Varela, N. Ranjbar Sahraie, J. Steinberg, W. Ju, H. S. Oh, P. Strasser, *Angew. Chem., Int. Ed.* **2015**, *54*, 10758.

[85] S. Zhang, P. Kang, S. Ubnoske, M. K. Brennaman, N. Song, R. L. House, J. T. Glass, T. J. Meyer, *J. Am. Chem. Soc.* **2014**, *136*, 7845.

[86] a) B. Kumar, M. Asadi, D. Pisasale, S. Sinha-Ray, B. A. Rosen, R. Haasch, J. Abiade, A. L. Yarin, A. Salehi-Khojin, *Nat. Commun.* **2013**, *4*, 2819; b) V. Tripkovic, M. Vanin, M. Karamad, M. r. E. Björketun, K. W. Jacobsen, K. S. Thygesen, J. Rossmeisl, *J. Phys. Chem. C* **2013**, *117*, 9187.

[87] J. Sinfelt, G. Via, F. Lytle, *J. Chem. Phys.* **1980**, *72*, 4832.

[88] B. J. Hwang, C.-H. Chen, L. S. Sarma, J.-M. Chen, G.-R. Wang, M.-T. Tang, D.-G. Liu, J.-F. Lee, *J. Phys. Chem. B* **2006**, *110*, 6475.

[89] a) K. Asakura, *X-ray Absorption Fine Structure for Catalysts and Surfaces*, World Scientific, University of Tokyo, Japan **1996**, p. 33; b) N. Becknell, Y. Kang, C. Chen, J. Resasco, N. Kornienko, J. Guo, N. M. Markovic, G. A. Somorjai, V. R. Stamenkovic, P. Yang, *J. Am. Chem. Soc.* **2015**, *137*, 15817.

[90] a) Z. Feng, W. T. Hong, D. D. Fong, Y.-L. Lee, Y. Yacoby, D. Morgan, Y. Shao-Horn, *Acc. Chem. Res.* **2016**, *49*, 966; b) X. Liu, W. Yang, Z. Liu, *Adv. Mater.* **2014**, *26*, 7710; c) K. A. Stoerzinger, W. T. Hong, E. J. Crumlin, H. Bluhm, Y. Shao-Horn, *Acc. Chem. Res.* **2015**, *48*, 2976; d) Z. Feng, J. Lu, H. Feng, P. C. Stair, J. W. Elam, M. J. Bedzyk, *J. Phys. Chem. Lett.* **2013**, *4*, 285.

[91] Z. Yin, D. Gao, S. Yao, B. Zhao, F. Cai, L. Lin, P. Tang, P. Zhai, G. Wang, D. Ma, *Nano Energy* **2016**, *27*, 35.

[92] C.-R. Bian, S. Suzuki, K. Asakura, L. Ping, N. Toshima, *J. Phys. Chem. B* **2002**, *106*, 8587.

[93] N. Toshima, T. Yonezawa, *New J. Chem.* **1998**, *22*, 1179.

[94] a) N. Toshima, M. Harada, Y. Yamazaki, K. Asakura, *J. Phys. Chem.* **1992**, *96*, 9927; b) N. Toshima, M. Harada, T. Yonezawa, K. Kushihashi, K. Asakura, *J. Phys. Chem.* **1991**, *95*, 7448.

[95] J. Highfield, T. Liu, Y. S. Loo, B. Grushko, A. Borgna, *Phys. Chem. Chem. Phys.* **2009**, *11*, 1196.

[96] M. R. Camilo, W. O. Silva, F. H. Lima, *J. Braz. Chem. Soc.* **2017**, *28*, 1803.

[97] a) L. I. Hung, C. K. Tsung, W. Huang, P. Yang, *Adv. Mater.* **2010**, *22*, 1910; b) A. K. Sra, T. D. Ewers, R. E. Schaak, *Chem. Mater.* **2005**, *17*, 758.

[98] A. Knauer, A. Eisenhardt, S. Krischok, J. M. Koehler, *Nanoscale* **2014**, *6*, 5230.

[99] T. Cheng, H. Xiao, W. A. Goddard III, *J. Am. Chem. Soc.* **2016**, *138*, 13802.

[100] X. Lu, D. Y. Leung, H. Wang, M. K. Leung, J. Xuan, *ChemElectroChem* **2014**, *1*, 836.

[101] T. Adit Maark, B. Nanda, *J. Phys. Chem. C* **2016**, *120*, 8781.

[102] A. A. Peterson, F. Abild-Pedersen, F. Studt, J. Rossmeisl, J. K. Nørskov, *Energy Environ. Sci.* **2010**, *3*, 1311.

[103] P. Hirunsit, W. Soodsawang, J. Limtrakul, *J. Phys. Chem. C* **2015**, *119*, 8238.

[104] W. J. Durand, A. A. Peterson, F. Studt, F. Abild-Pedersen, J. K. Nørskov, *Surf. Sci.* **2011**, *605*, 1354.

[105] X. Nie, M. R. Esopi, M. J. Janik, A. Asthagiri, *Angew. Chem., Int. Ed.* **2013**, *52*, 2459.

[106] H. A. Hansen, J. H. Montoya, Y.-J. Zhang, C. Shi, A. A. Peterson, J. K. Nørskov, *Catal. Lett.* **2013**, *143*, 631.

[107] K. Schouten, Y. Kwon, C. Van der Ham, Z. Qin, M. Koper, *Chem. Sci.* **2011**, *2*, 1902.

[108] J. H. Montoya, C. Shi, K. Chan, J. K. Nørskov, *J. Phys. Chem. Lett.* **2015**, *6*, 2032.

[109] J.-F. Xie, Y.-X. Huang, W.-W. Li, X.-N. Song, L. Xiong, H.-Q. Yu, *Electrochim. Acta* **2014**, *139*, 137.

[110] R. Kortlever, J. Shen, K. J. P. Schouten, F. Calle-Vallejo, M. T. Koper, *J. Phys. Chem. Lett.* **2015**, *6*, 4073.

[111] J. E. McMurry, M. P. Fleming, *J. Am. Chem. Soc.* **1974**, *96*, 4708.

[112] a) Y. Hori, I. Takahashi, O. Koga, N. Hoshi, *J. Phys. Chem. B* **2002**, *106*, 15; b) Y. Hori, R. Takahashi, Y. Yoshinami, A. Murata, *J. Phys. Chem. B* **1997**, *101*, 7075.

[113] K. P. Kuhl, E. R. Cave, D. N. Abram, T. F. Jaramillo, *Energy Environ. Sci.* **2012**, *5*, 7050.

[114] a) A. A. Ponce, K. J. Klabunde, *J. Mol. Catal. A: Chem.* **2005**, *225*, 1; b) A. G. Nasibulin, E. I. Kauppinen, D. P. Brown, J. K. Jokiniemi, *J. Phys. Chem. B* **2001**, *105*, 11067; c) R. Tilaki, S. Mahdavi, *Appl. Phys. A* **2007**, *88*, 415; d) B. Deng, A.-W. Xu, G.-Y. Chen, R.-Q. Song, L. Chen, *J. Phys. Chem. B* **2006**, *110*, 11711.

[115] Y. Zhou, F. Che, M. Liu, C. Zou, Z. Liang, P. De Luna, H. Yuan, J. Li, Z. Wang, H. Xie, *Nat. Chem.* **2018**, *10*, 974.

[116] J. Albo, D. Vallejo, G. Beobide, O. Castillo, P. Castaño, A. Irabien, *ChemSusChem* **2017**, *10*, 1100.

[117] S. Ma, M. Sadakiyo, R. Luo, M. Heima, M. Yamauchi, P. J. Kenis, *J. Power Sources* **2016**, *301*, 219.

[118] K. Chen, X. Zhang, T. Williams, L. Bourgeois, D. R. MacFarlane, *Electrochim. Acta* **2017**, *239*, 84.

[119] D. Raciti, K. J. Livi, C. Wang, *Nano Lett.* **2015**, *15*, 6829.

[120] N. Gutiérrez-Guerra, L. Moreno-López, J. Serrano-Ruiz, J. Valverde, A. de Lucas-Consuegra, *Appl. Catal., B* **2016**, *188*, 272.

[121] C. Genovese, C. Ampelli, S. Perathoner, G. Centi, *J. Catal.* **2013**, *308*, 237.

[122] S. S. Hossain, S. Ahmed, *J. Nanomater.* **2014**, *2014*, 9.

[123] Y. Song, R. Peng, D. K. Hensley, P. V. Bonnesen, L. Liang, Z. Wu, H. M. Meyer, M. Chi, C. Ma, B. G. Sumpter, A. J. Rondinone, *ChemistrySelect* **2016**, *1*, 6055.

[124] W. Zheng, S. Nayak, W. Yuan, Z. Zeng, X. Hong, K. A. Vincent, S. C. E. Tsang, *Chem. Commun.* **2016**, *52*, 13901.

[125] A. N. Grace, S. Y. Choi, M. Vinoba, M. Bhagiyalakshmi, D. H. Chu, Y. Yoon, S. C. Nam, S. K. Jeong, *Appl. Energy* **2014**, *120*, 85.

[126] Y. Huang, A. D. Handoko, P. Hirunsit, B. S. Yeo, *ACS Catal.* **2017**, *7*, 1749.

[127] K. D. Yang, W. R. Ko, J. H. Lee, S. J. Kim, H. Lee, M. H. Lee, K. T. Nam, *Angew. Chem., Int. Ed.* **2017**, *56*, 796.

[128] J.-H. Kim, H. Woo, S.-W. Yun, H.-W. Jung, S. Back, Y. Jung, Y.-T. Kim, *Appl. Catal., B* **2017**, *213*, 211.

[129] W. Lv, J. Zhou, J. Bei, R. Zhang, F. Kong, W. Wang, *Int. J. Electrochem. Sci.* **2016**, *11*, 6183.

[130] M. S. Xie, B. Y. Xia, Y. Li, Y. Yan, Y. Yang, Q. Sun, S. H. Chan, A. Fisher, X. Wang, *Energy Environ. Sci.* **2016**, *9*, 1687.

[131] S. Rasul, D. H. Anjum, A. Jedidi, Y. Minenkov, L. Cavallo, K. Takanabe, *Angew. Chem.* **2015**, *127*, 2174.

[132] A. Dutta, M. Rahaman, M. Mohos, A. Zanetti, P. Broekmann, *ACS Catal.* **2017**, *7*, 5431.

[133] T. N. Huan, P. Simon, A. Benayad, L. Guetaz, V. Artero, M. Fontecave, *Chem. – Eur. J.* **2016**, *22*, 14029.

[134] M. Fan, Z. Bai, Q. Zhang, C. Ma, X.-D. Zhou, J. Qiao, *RSC Adv.* **2014**, *4*, 44583.

[135] M. Gattrell, N. Gupta, A. Co, *J. Electroanal. Chem.* **2006**, *594*, 1.

[136] A. A. Peterson, J. K. Nørskov, *J. Phys. Chem. Lett.* **2012**, *3*, 251.

[137] a) H. A. Hansen, J. B. Varley, A. A. Peterson, J. K. Nørskov, *J. Phys. Chem. Lett.* **2013**, *4*, 388; b) H. L. Skriver, H. Lengkeek, *Phys. Rev. B* **1979**, *19*, 900.

[138] R. Reske, M. Duca, M. Oezaslan, K. J. P. Schouten, M. T. Koper, P. Strasser, *J. Phys. Chem. Lett.* **2013**, *4*, 2410.

[139] A. S. Varela, C. Schlaup, Z. P. Jovanov, P. Malacrida, S. Horch, I. E. Stephens, I. Chorkendorff, *J. Phys. Chem. C* **2013**, *117*, 20500.

[140] P. Hirunsit, *J. Phys. Chem. C* **2013**, *117*, 8262.

[141] Z. B. Hoffman, T. S. Gray, K. B. Moraveck, T. B. Gunnoe, G. Zangari, *ACS Catal.* **2017**, *7*, 5381.

[142] a) A. Jedidi, S. Rasul, D. Masih, L. Cavallo, K. Takanabe, *J. Mater. Chem. A* **2015**, *3*, 19085; b) J. E. Pander III, M. F. Baruch, A. B. Bocarsly, *ACS Catal.* **2016**, *6*, 7824; c) J. N. Butler, M. Dienst, *J. Electrochem. Soc.* **1965**, *112*, 226; d) M. Metikoš-Huković, S. Omanović, *J. Electroanal. Chem.* **1998**, *455*, 181; e) M. Jitaru, D. Lowy, M. Toma, B. Toma, L. Oniciu, *J. Appl. Electrochem.* **1997**, *27*, 875.

[143] G. O. Larrazábal, A. J. Martín, S. Mitchell, R. Hauert, J. Pérez-Ramírez, *ACS Catal.* **2016**, *6*, 6265.

[144] X. Guo, Y. Zhang, C. Deng, X. Li, Y. Xue, Y.-M. Yan, K. Sun, *Chem. Commun.* **2015**, *51*, 1345.

[145] M. Nakamura, T. Kobayashi, N. Hoshi, *Surf. Sci.* **2011**, *605*, 1462.

[146] S. Sarfraz, A. T. Garcia-Esparza, A. Jedidi, L. Cavallo, K. Takanabe, *ACS Catal.* **2016**, *6*, 2842.

[147] D. Ren, B. S.-H. Ang, B. S. Yeo, *ACS Catal.* **2016**, *6*, 8239.

[148] S. Zhang, P. Kang, M. Bakir, A. M. Lapides, C. J. Dares, T. J. Meyer, *Proc. Natl. Acad. Sci. USA* **2015**, *112*, 15809.

[149] X. Zhang, Z. Wu, X. Zhang, L. Li, Y. Li, H. Xu, X. Li, X. Yu, Z. Zhang, Y. Liang, H. Wang, *Nat. Commun.* **2017**, *8*, 14675.

[150] G. Yin, H. Abe, R. Kodiyath, S. Ueda, N. Srinivasan, A. Yamaguchi, M. Miyauchi, *J. Mater. Chem. A* **2017**, *5*, 12113.